

Grid resilience enhancement by implementing Smart Microgrids.

Master Thesis Project

David Gómez de Segura Balerdi

Technische Universiteit Delft

Grid resilience enhancement by implementing Smart Microgrids.

Master Thesis Project

by

David Gómez de Segura Balerdi

Student number: **4706110**

in partial fulfillment of the requirements for the

Industrial Engineering Master
at UPNA (Public University of Navarre)

conducted at the Delft University of Technology,
to be defended publicly on Friday June 18st, 2018 at 9:30 AM.

Supervisor:	Prof. Dr. ir. J.L. Jose Rueda Torres	
Thesis committee:	Prof. Dr. P. Palensky,	TU Delft
	Prof. Dr. ir. J.L. Rueda Torres,	TU Delft
	Prof. Dr. ir. Mohamad Ghaffarian Niasar,	TU Delft

An electronic version of this thesis is available at <http://repository.tudelft.nl/>.

Abstract

The electrical power industry is undergoing rapid transformation, and Smart Grids technologies can facilitate the growing penetration of renewable energies, as well as the necessity of providing flexibility to variable generation. Furthermore, their widespread installation results in a modernization of the electric grid, opening up new operation possibilities. This Master Thesis Project is formulated to study the resilience enhancements that can be achieved in the electric grid, by means of integrating distributed generation within Smart Microgrids.

Several guidelines that should lead the design of microgrids in order to improve the survivability and restoration capacities of the system are provided in this project. Optimization of current features such island mode of operation and advanced metering infrastructure are studied. In addition, the concept of a meshed set of loop-based microgrids and self-healing procedures are proposed.

Furthermore, a versatile RSCAD microgrid model has been developed, implementing the aforementioned resilience-related guidelines. It accounts for a microgrid with diverse distributed generation, which integrates a number of city facilities modelled as loads. Making use of the RTDS simulator, several simulations have been run on the model, validating its normal functioning and testing the response given to critical situations.

Acknowledgements

This thesis is the culmination of several months of intensive work, which have allowed me to transform a vague idea into a fulfilling project. I have learned a great deal in the process, and I finish with the hope that my contribution to this field can help building a better future.

I would like to thank Prof. dr. Peter Palensky for introducing me to the Intelligent Electrical Power Grids research group, and for giving me the first orientation on my research topic. Also, I have to acknowledge my daily supervisor, Dr. ir. Jose Luis Rueda, who, despite having a busy schedule, was always there for counselling me throughout the process.

Finally, a **big thanks** goes to my family and friends for always being there, giving me motivation and support. I must say, 1100 kilometers feel like walking-distance when you are lucky enough to be surrounded by such wonderful people.

*David Gómez de Segura Balerdi
Delft, May 2018*

Contents

List of Figures	ix
List of Tables	xiii
1 Introduction	1
1.1 Research theme	1
1.2 Project description & Research Questions	3
1.3 Contributions	3
2 Theoretical background	5
2.1 Microgrid	5
2.2 Mesh networking	6
2.3 Smart Grids	6
2.4 Reliability vs Survivability vs Resilience	8
2.4.1 Reliability	8
2.4.2 Survivability	8
2.4.3 Resilience	9
3 Fields of improvement	11
3.1 Island mode of operation	11
3.1.1 System restoration	12
3.1.2 Real life situations	13
3.2 N+X redundancy	15
3.3 Topology	17
3.4 Advanced metering infrastructure (AMI)	21
3.5 Self-healing	24
3.5.1 Fault location, isolation and service restoration (FLISR)	24
3.5.2 Implementation	25
4 Microgrid model	27
4.1 General overview of the system	27
4.1.1 The microgrid	28
4.1.2 Introduction to the modelling	32
4.2 Photovoltaic system	33
4.2.1 PV Modelling	33
4.2.2 PV control system	37
4.3 Battery energy storage system (BESS)	41
4.3.1 BESS modelling	41
4.3.2 BESS control	43
4.4 Wind energy system	45
4.4.1 Wind energy system modelling	45
4.4.2 Wind energy system control	47
4.5 Diesel generator	49
4.6 Loads	51
4.7 Cable calculations	52
4.7.1 Material selection	52
4.7.2 Electrical calculations	54

5	RSCAD implementation	59
5.1	Modelling tool	59
5.2	General overview of the model	61
5.3	Photovoltaic system	65
5.3.1	Solar cell parameters	65
5.3.2	Grid-connected PV system Draft overview	67
5.3.3	PV control system	72
5.4	Battery energy storage system (BESS)	77
5.4.1	Battery parameters	77
5.4.2	BESS Draft overview	78
5.4.3	BESS control system	79
5.5	Wind energy system	85
5.5.1	Wind energy system Draft overview	85
5.5.2	Wind turbine and multimass	87
5.6	Diesel generator	90
5.6.1	Diesel generator Draft overview	90
5.6.2	Diesel generator control	92
5.7	Loads	94
5.8	Implementation of lines	95
6	Microgrid simulations	99
6.1	Graphical User Interface	99
6.2	Microgrid operation	102
6.3	Simulating weather events during islanded mode of operation	107
6.3.1	Load shedding	109
6.3.2	Failure in transmission lines	110
6.4	Meshed set of loop-based microgrids	114
7	Conclusions	115
	Appendices	117
A	PV system control	119
B	BESS control	123
C	User Manual	127
C.1	Compiling the circuit	127
C.2	RunTime canvas	128
C.3	Simulations	132
	Bibliography	135

List of Figures

1.1	Forecast of the evolution of global electricity production by generation type.	1
1.2	Electric customers disrupted by <i>NERC</i> ⁰ -reported electric transmission outages by cause (2000-2014).	2
2.1	Total mesh topology among different microgrids.	6
2.2	AMI system structure.	7
2.3	Example of a performance chart with a pre-defined threshold.	9
3.1	Microgrid-based load restoration process.	13
3.2	Radial-based microgrid facing failure in transmission lines.	17
3.3	Loop-based topology microgrid facing failure in transmission lines.	18
3.4	Conceptual draft of a meshed set of loop-based Smart microgrids (M#n).	20
3.5	Improvement of the pinging procedure by means of the meshed cluster of microgrids.	22
3.6	Fault location, isolation and service restoration, provided by [1]	24
4.1	Satellite image of the layout of the microgrid.	29
4.2	Numbered sections of connection lines.	30
4.3	High-voltage grid map, provided by Tennet.	31
4.4	Satellite view of the Rijkswijk Wateringen Substation.	32
4.5	Evolution of solar PV installation, provided by IEA PVSP.	33
4.6	Equivalent circuit of an ideal solar cell.	33
4.7	Equivalent circuit of the single diode, five parameter model.	34
4.8	Current-Voltage curve depending on solar irradiance.	36
4.9	Power-Voltage curve depending on solar irradiance.	36
4.10	Three-phase to direct-quadrature-zero transformation of voltages and currents.	37
4.11	Decoupled dq current control.	38
4.12	DC bus voltage control for the d-axis current reference.	39
4.13	AC bus voltage control for q-axis current reference.	39
4.14	SPWM for VSC firing pulses.	40
4.15	Electrical equivalent circuit of the Min/Rincon-Mora model.	42
4.16	Grid-connected and islanded-mode control differentiation.	44
4.17	Configuration of a Double Fed Induction Generator.	46
4.18	Price of commercial copper, given by <i>LME</i> ¹	53
4.19	Price of commercial aluminum, given by <i>LME</i>	53
4.20	Maximum admissible currents (A) in permanent regime.	54
4.21	Equivalent circuit of a short transmission line.	55
4.22	Vector diagram of the short transmission line equivalent circuit.	56
5.1	Draft circuitry of the microgrid's connection to the main grid.	61
5.2	Block parameters of the three-phase breaker.	62
5.3	Configuration parameters of the transformer.	63
5.4	Configuration parameters of the transformer.	63
5.5	Draft circuitry of the complete microgrid.	64
5.6	Data-sheet of the electrical characteristics under STC.	65
5.7	Temperature ratings for the PV 300W module.	66
5.8	Mechanical data of the 300W PV module.	67
5.9	Grid-connected PV system Draft overview.	67
5.10	Configuration window of the PV array model block.	68
5.11	Module data and configuration window of the PV array model block.	70

5.12	Array configuration window of the PV array model block.	70
5.13	Configuration window of the transformer modelled in the PV system.	72
5.14	General view of the PV control schema.	73
5.15	Outer loop calculation of i_{dref} and i_{qref}	74
5.16	Inner loop dq current control.	74
5.17	Protection logic applied to the PV system.	75
5.18	Average Control of Voltages and Currents.	76
5.19	Grid-connected BESS system Draft overview.	78
5.20	Configuration window of the Li-ion battery block.	78
5.21	Parameters window of the Li-ion battery block.	79
5.22	General view of the BESS control schema.	79
5.23	Outer loop calculation of i_{dref} and i_{qref} in the grid-connected scenario.	80
5.24	Inner loop calculation of the modulation voltages.	81
5.25	Outer loop for islanded mode of operation voltage control.	82
5.26	Obtainment of control signals needed for the VSC.	83
5.27	Protection&Start Up block implemented in the BESS control.	84
5.28	Microgrid-connected wind energy system Draft overview.	85
5.29	Induction Machine configuration window.	86
5.30	Induction Machine's motor electrical parameters window.	87
5.31	Circuitry deployed to implement the Wind Turbine and Multimass model.	88
5.32	Wind Turbine model implementation.	89
5.33	Microgrid-connected diesel generator Draft overview.	90
5.34	Electric machine model's definition of parameters.	91
5.35	Circuitry implemented in the PSS block.	92
5.36	Circuitry implemented in the Excitation System block.	92
5.37	Circuitry implemented in the Speed Governor block.	93
5.38	Parameters window of the dynamic load model.	94
5.39	Description of the tlines provided in the .tlo file.	96
5.40	Conductor data section in the Tline tool.	97
5.41	PI section parameters in the Draft block.	98
6.1	Graphical User Interface designed in the RunTime tool.	100
6.2	Active power contribution of each DER and main grid during a normal-day simulation.	103
6.3	Switch of mode of operation to islanded mode.	104
6.4	Synchronization block in the RunTime canvas.	105
6.5	Re-connection to the main grid.	106
6.6	Synchronization block during re-connection procedure.	107
6.7	Microgrid's response to varying meteorological conditions under islanded mode of operation.	108
6.8	BESS support to microgrid's islanded mode of operation.	109
6.9	Load shedding applied during hurricane-like meteorological conditions.	110
6.10	Single failure in transmission lines.	111
6.11	Division of the microgrid in two separated sub-microgrids.	112
6.12	Response of the system to the second line failure.	113
6.13	RunTime canvas after performing the second simulation.	114
A.1	Phase Lock Loop circuitry (A).	119
A.2	Phase Lock Loop circuitry (B).	120
A.3	Outer loop PI control (VAC) circuitry.	120
A.4	Outer loop PI control Q circuitry.	121
A.5	Inner loop PI control for i_d circuitry.	121
A.6	Inner loop PI control for i_q circuitry.	122
B.1	BESS PI control for active power (P) circuitry.	123
B.2	BESS PI control for reactive power (Q) circuitry.	124
B.3	BESS PI control (VAC) for q axis reference circuitry.	124
B.4	BESS PI control (VAC) for islanded mode of operation circuitry.	125

C.1	Draft compiling process.	127
C.2	RunTime canvas functionality.	128
C.3	Diesel generator sub-block.	129
C.4	PV system sub-block.	129
C.5	Battery energy storage system sub-block.	130
C.6	Wind system sub-block.	131
C.7	Loads' P and Q sliders.	131
C.8	Simulation block in the Draft module.	132
C.9	Simulation block in the RunTime module.	133
C.10	Sequencer block component types.	133
C.11	Scheduler implementation in the PV system.	134

List of Tables

4.1	Specific location and coordinates of the DERs implemented in the microgrid.	29
4.2	Loads supplied by the designed microgrid.	30
4.3	Distance measurements between nodes.	31
4.4	Parameters of the diesel generator model.	49
4.5	Material <i>properties</i> ¹ of aluminum and copper.	52
4.6	Active power generated by the DERs taking part of the microgrid.	55
4.7	Data necessary for voltage drop calculation referred to aluminum cables.	57
5.1	Electrical data of the chosen 300W version.	65
5.2	Withstanding of challenging environmental conditions.	67
5.3	Main parameters of the chosen lithium-ion battery.	77
5.4	Electrical parameters of the induction machine model.	86
5.5	Values obtained from the .tlo file.	97
5.6	Final PI section values.	98
6.1	Solar irradiance and wind speed inputs.	102
6.2	Synchronization criteria.	105

1

Introduction

1.1. Research theme

The world's energy system possesses considerable inertia, such that any change or shift in the general tendency is usually slowly implemented. Nevertheless, within the framework of the Paris Agreement and given the unsustainability of our actual fossil-predominant energy mix, we are experimenting an ongoing energy transition. According to [2], solar photovoltaic (PV), onshore wind, hydropower, and offshore wind, in that order, will account for 85% of global electricity production in 2050. Along these lines, electric vehicles (EVs) are also called to experiment a broader user adoption in the upcoming years, contributing to higher levels of generation and distribution system capacity utilization.

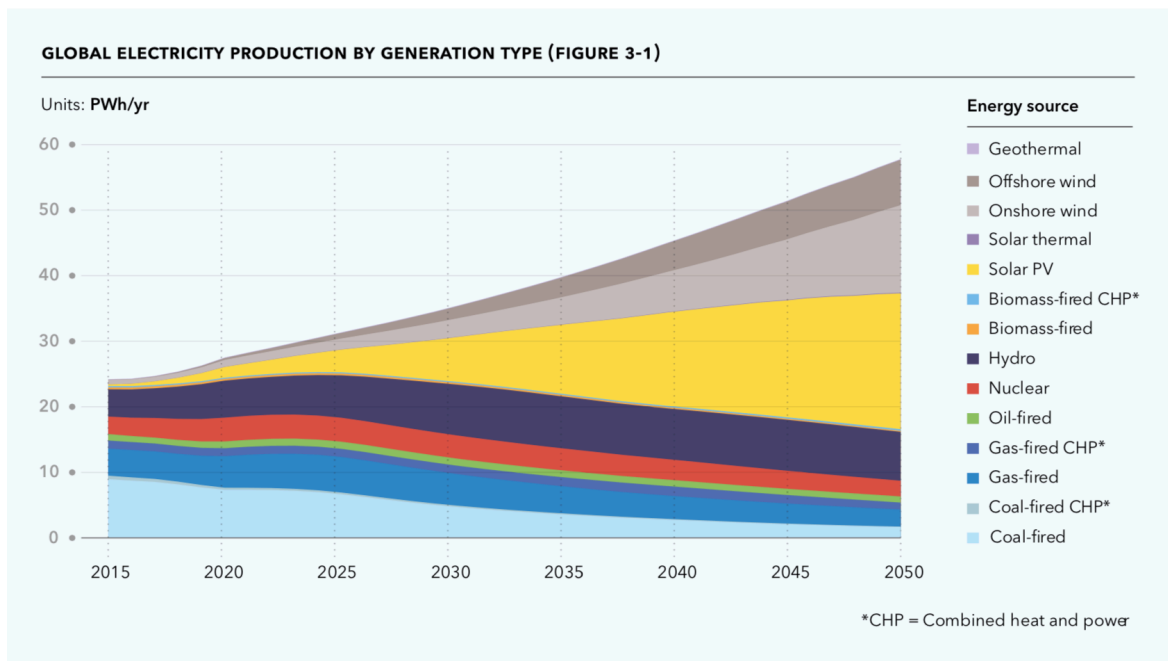


Figure 1.1: Forecast of the evolution of global electricity production by generation type.

This vast penetration of renewables implies a replacement of thermal generators with converter-connected sources of power, which leads to stability in response to disturbances becoming an issue. Furthermore, other problems like the intermittency of generation from renewable sources and the lack of dispatch ability arise.

These energy sources are weather driven and obey no schedule, thus new operational procedures are required. Here is where the smart grid features prove to be beneficial, since through cooperation, this

technology can provide the flexibility needed to integrate variable generation [3] [4] [5]. In addition, the deployment of EVs in the energy market, together with the support of smart grids, can compensate for the fluctuations of the electric grid.

These valuable assets have been noticed by the scientific community and are currently under heavy research. However, smart grids constitute a relatively new concept (first formal definition was given in 2007 [6]) and its many characteristics have not yet reached technology maturity. In short, its implementation transforms the current grid into a more intelligent one that provides the aforementioned advantages [7] and:

- Facilitates better situation awareness and operator assistance.
- Improves efficiency by maximizing asset utilization.
- Creates a two-way communication between the consumer and the utility, bringing forth the prosumer role.
- Enhances resilience against component failures and natural disasters with autonomous control actions aimed to minimize the frequency and magnitude of power outages.

Enhancement of electrical resilience, understood as the restoration ability of a system after general failure, constitutes an important field of researching and is highly related to the survivability of the system. According to the Argonne National Laboratory [8], severe weather is the single leading cause of outages in the power system of the United States. This gives an idea of the importance of resilience, since when combining severe weather with natural disasters, it accounts for 64% of the total outages.

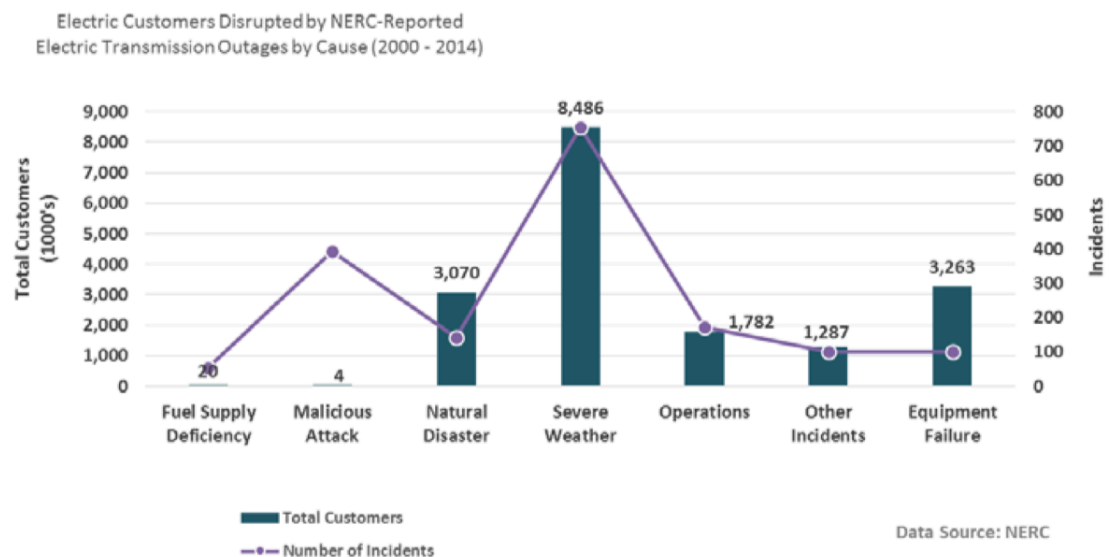


Figure 1.2: Electric customers disrupted by NERC⁰-reported electric transmission outages by cause (2000-2014).

Smart grid's capability of working grid-connected and in island mode present several opportunities and challenges regarding resilience. Other features such full awareness of the system through smart metering, meshed topology achieving optimal interconnection and distributed automation resulting in self-healing are topics that hold a promising perspective in relation with it.

From a financial perspective, weather-related outages are estimated to have cost the U.S. economy an inflation-adjusted annual average of \$18 billion to \$33 billion in the past years [9]. Any effective improvements in this field would result in tremendous benefits both economical and social related. Performing a fast recovery after a natural disaster, or the possibility of critical loads such hospitals surviving throughout the event, would result in fewer and less extended humanitarian crisis. Thus, enhancing the resilience of the electrical system with smart grids ought to be in any country's agenda, and will be the core of the research deployed in this thesis.

⁰North American Electric Reliability Corporation

1.2. Project description & Research Questions

The main goal of the thesis is the *enhancement of resilience of the system with smart grids*, which at the moment remains in the RD (Research and Development) phase, constituting a bit of a greenfield. When selecting the scope of the project, the focus has not been narrowed down to an specific, in order to obtain the bigger picture. Rather than optimizing one single aspect, we will focus on obtaining the guidelines that should be implemented when designing smart grids to achieve the desired improvement in the recovery capabilities of the system. The reason behind the chosen scope is the fairly recent implementation of smart grid technology, alongside with the novelty that suppose its study in relation with resilience, which result in the absence of an accepted framework.

Once this theoretical approach to resilience is properly studied and determined, a model of a smart grid is to be developed keeping into consideration its correlation with reality. The model is carried out using the RTDS simulator [10], which performs real time digital simulations accurately over a frequency range from DC to 3 kHz. It implements the main aforementioned resilience guidelines within its design, and every DER ¹ and load is thoroughly modelled. Finally, severe weather events will be simulated, and the response of the improved smart microgrid will be plotted and studied.

The following research questions have been formulated to address the objective:

- **What are the state-of-the-art guidelines that shall lead the design of smart microgrids in order to enhance its resilience?**
- **Considering the theoretical analysis, can we provide a versatile model in accordance with it, aiming to offer a benchmark scenario to study grid resilience by means of Smart Microgrids implementation?**
- **Once simulations are run in the model, do the results validate the model itself and the theoretical resilience-related assumptions?**

1.3. Contributions

The existing electric grids are undergoing a broad modernization which keeps seeking for a better customer service. With the purpose of making it more reliable, efficient, secure, and resilient to the external and internal cause of power outages, several studies are currently being conducted.

From a scientific perspective, the contribution of this thesis is to study and provide conscientious insights on how the implementation of smart grids can enhance this latter feature, resilience. To that mean:

- A study on the most optimal resilience-related smart grid's future design lines is to be conducted, analyzing matters such topology, redundancy, system awareness or distribution automation. Given the novelty of this field, benchmarking is necessary in order to establish the ground for future research.
- Once satisfactory guidelines are reached, those with the better future prospective and impact in the system's resilience will be implemented in the design of a city-based smart microgrid. It will consist on different distributed energy sources, representing the actual variety of distributed generation, and the loads will be modelled to represent services to the community (schools, hospitals, train stations, etc).
- This design of the smart microgrid, along with the achieved resilience-related guidelines and theoretical modelling of every DER will converge on a model of the microgrid. It will be developed and run in the RTDS simulator, keeping its parameters non-fixed so as to allow future users to tailor it to their needs.
- Simulations of different scenarios with varying weather conditions will be run on the model, collecting data of its behaviour when facing them and its posterior recovery. The necessary tools for building customized weather scenarios and studying them will be provided.

¹Distributed Energy Resource

- Data obtained from the aforementioned simulations will then be used to validate the previous study and the RTDS simulator model of a smart microgrid. The project will end with an analysis on the enhancements achieved on system resilience by means of a widespread implementation of smart microgrids.

Master Thesis outline

This section comprises a brief description of every chapter conforming the project.

- **Chapter 1: Introduction**

Constitutes the starting point of the thesis, and therefore it must present the chosen research theme and the reasons behind that choice. This is further elaborated when providing a thorough project description, which ends up with the three research questions that will be the driven-force of the entire project. The last part of this introduction chapter consists in the contributions that this thesis will provide to the scientific community.

- **Chapter 2: Theoretical background**

Once the the introduction has settled the start of the project, the reader must get familiarized with the concepts dealt within the thesis. Some of them, like resilience, present a rather subjective definition and thus, the chosen approach must be explained. The main topics of this chapter are: the microgrid concept, mesh networking, Smart Grid technologies and resilience-related terms.

- **Chapter 3: Fields of improvement**

In this chapter, and through extensive scientific literature research, we have selected the most promising topics where the relation between grid resilience and the implementation of microgrids seems to offer promising results. Based on those, five different fields which would improve the resilience and survivability of the system have been developed: island mode of operation, N+X redundancy, loop-based and meshed topology, advanced metering infrastructure (AMI) and self-healing capabilities.

- **Chapter 4: Microgrid model**

This chapter is a continuation of the previous one, given that the most feasible fields of improvements are put together to design a theoretical microgrid in the vicinity of Delft. The model consists in four different distributed energy resources (DERs) and four different loads, accounting for real-life facilities of the city. Accurate modelling of the DERs and the selected control strategies are explained and implemented within this chapter.

- **Chapter 5: RSCAD implementation**

Once the microgrid has been theoretically modelled, we make use of the RSCAD software [10] to perform its implementation. Again, this chapter is divided in subsections accounting for every microgrid's component, and thorough explanations of the followed process to come up with the final model are given.

- **Chapter 6: Microgrid simulations**

This chapter is the culmination of the thesis, given that the fields of improvement lead to the development of a theoretical model, which was then implemented in the RSCAD software to perform simulations by making use of the RTDS simulator. These simulations will test normal weather conditions on different modes of operation to validate the model, as well as extreme weather circumstances where failures happen within the microgrid.

- **Chapter 7: Conclusion**

This chapter gathers the thoughts on what have been achieved and which would be the lines of future work regarding the selected topic of the thesis.

2

Theoretical background

The purpose of this chapter involves giving a common ground from which the reader can catch up to the dissertation developed regarding the resilience in Smart Microgrids. Furthermore, this initial chapter will help narrowing the studied issues down, as specific definitions and/or explanations on the matter will be brought up.

2.1. Microgrid

First of all, a proper definition of microgrid shall be given. In order to do so, two different frameworks will be taken into consideration: the European and the American. A definition based on several EU research projects can be found in [11], stating the following,

"Microgrids comprise low voltage (LV) distribution systems with distributed energy resources (DER) (micro-turbines, fuel cells, PV, etc.) together with storage devices (flywheels, energy capacitors and batteries) and flexible loads. Such systems can be operated in a non-autonomous way, if interconnected to the grid, or in an autonomous way, if disconnected from the main grid. The operation of microsources in the network can provide distinct benefits to the overall system performance, if managed and coordinated efficiently."

By terms of this first approach, the components (DERs, storage devices and flexible loads), and operation (interconnected or disconnected from the main grid) of a standard microgrid are defined. Furthermore, the possibility of improvements for the overall system by means of a correct management and coordination is also brought up. This will be one of the main goals to work towards.

The American framework, represented here by the United States Department of Energy (DOE), gives a formal definition in [12] for microgrid,

"A group of interconnected loads and distributed energy resources within clearly defined electrical boundaries that acts as a single controllable entity with respect to the grid. A microgrid can connect and disconnect from the grid to enable it to operate in both grid-connected or island- mode."

Once both perspectives have been presented, we observe that both concur in the general aspects. Therefore we proceed to offer a simplified combined definition of what is a microgrid, which will be held as true henceforth.

"A microgrid is a set of interconnected loads, distributed energy resources and storage devices forming a single controllable entity. It operates with clearly defined electrical boundaries, and can do so interconnected to the main grid or disconnected from it (island mode)."

2.2. Mesh networking

Inquiring for a general definition, we could define it to be,

“An infrastructure in which the nodes are connected to as many other as previously designed, with the possibility to achieve a full interconnection. These links are to be direct, dynamic and there shall not exist any hierarchy in-between them.”

Several advantages related to our topic come off this approach. For instance, the double function of the nodes (transmit own data & act as a relay for others) allows the overall system to dynamically configure and organise itself. Therefore, in case of node failure, the pathing implemented provides different routes that enable the system to continue maintaining its operability.

Depending on the amount of connections implemented, two different self-explanatory topologies result: partial mesh topology (which could fit our necessities inside each microgrid) and total mesh topology (applicable to the overall system, considering each microgrid as a node).

These features will prove to be useful to our use-case, and this topic will be further studied in the following sections.

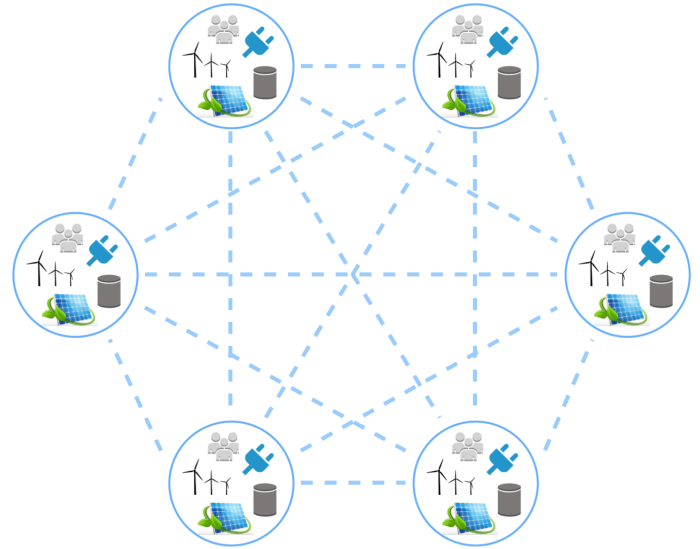


Figure 2.1: Total mesh topology among different microgrids.

2.3. Smart Grids

The Smart Grid concept is called to transform the unidirectional electric power grid by using advanced automatic control, communication techniques and other forms of information technology [13]. It aims to integrate devices, processes, energy infrastructure, information and markets as a collaborative procedure which allows energy to be generated, distributed and consumed with an increased efficiency. For the purpose of this thesis, its implementation within the microgrid network will be studied, as it constitutes one of the most promising ideas to support integrating RES¹ in future power systems.

The Smart Grids European Technology Platform [14] stated its formal definition as *an electricity network that can intelligently integrate the actions of all users connected to it - generators, consumers and those that do both - in order to efficiently deliver sustainable, economic and secure electricity supplies*. Two main ideas related to our field of investigation are to be highlighted from this definition:

- Intelligent electricity network: which accounts for the integrated communication and load control. General system awareness can be accomplished through sensing and continuous measurements, and there are promising possibilities related to power system automation.
- Secure electricity supply: has the objective of improving the quality of service provided by the grid. This rather complex purpose is to be accomplished through improvements and optimization in several fields such reliability, survivability and resilience of the system.

In short, smart grid is the collection of all technologies, concepts, topologies, and approaches that allow the silo hierarchies of generation, transmission, and distribution to be replaced with an end-to-end, organically intelligent, fully integrated environment where the processes, objectives, and needs of all stakeholders are supported by the efficient exchange of data, services and transactions [15].

¹Renewal Energy Sources

The metering side of smart grid distribution systems has made the leap from automated meter reading (AMR) to the actual advanced metering infrastructure (AMI). The AMI technology is the system and network used to measure, collect, store, analyze, and use energy usage data. It provides the ability of allowing a two-way communication to the meter, as well as the ability to modify customers' service level and perform load management. Its general structure comprises a number of technologies and applications working as an unity [16]:

- Smart Meters (SMs): are solid-state programmable devices that perform several functions. Among these, bidirectional metering and measuring (not only for electricity consumption but also for real-time electricity load, maximum demand, voltage, current, frequency, power factor, etc.), loss/restoration of power notifications, and remote turn-on or turn-off operations can prove useful when selecting strategies to enhance the resilience of the system.
- User gateways (UGs): implement protocol conversion and communications between two heterogeneous networks, like the in-home network and wide area network.
- Home (local) area networks: consists on a local area network, which interfaces with SMs, UGs, distributed energy resources, and local control devices
- Wide-area communications infrastructure: supports continuous interaction between the utility, the consumer, and the controllable electrical load. It must employ open bidirectional communication standards, yet requiring high security.
- Meter data management systems (MDMS): with an AMI head end in contact with the user side, is a database of meter data with analytic tools. It interacts with other systems of the electric power utilities, including consumer information, outage management and distribution management systems.

Figure 2.2, provided by [16], gives an accurate representation of its main components.

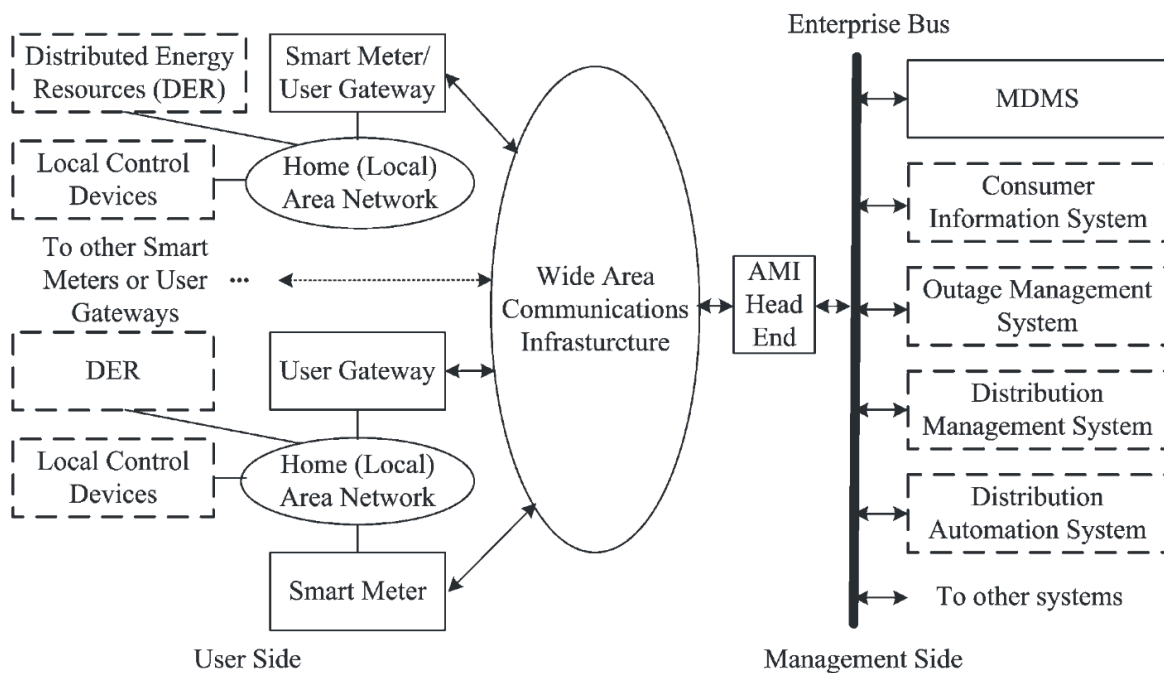


Figure 2.2: AMI system structure.

2.4. Reliability vs Survivability vs Resilience

Primarily, we consider of utmost importance to define the distinctions between these three highly-related concepts: reliability, survivability and resilience. In some cases, the boundaries are not set clear, leading to misunderstandings in the topic.

However, we believe that a previous definition of risk will set the focus of the reader in accordance with the content of the section. That is why, according to [17], we define it as *“a situation involving exposure to danger”* or more specifically as *“the possibility that something unpleasant or unwelcome will happen”*.

Nevertheless, and trying to have a more subject-related approach to it, we move to a definition in the risk analysis field [18], where it is defined as the *“effect of uncertainty on objectives”*. Then, by associating the risk to an undesired event that can happen in our system, we can express it as follows,

$$\text{Risk} = \text{consequences of the event} \times \text{likelihood of occurrence}$$

These consequences could be regarded from an economic point of view, or a functionality one, depending on the purpose of the analyser. From now on, this standpoint will be used when referring to risk.

2.4.1. Reliability

It is often misused as a term that gathers together robustness, security, resiliency and risk among others characteristics of the system. However, and narrowing it down to its basic acceptance, we could define it as the quality of the service provided by a system during a measured period of time. Basically, it accounts for its performance against potential low-impact/high-probability events.

Approaching the reliability of a system from an industry point of view, we contemplate two different angles: communication and electricity. As exposed in [19], the communication industry usually measures it by stating the fraction of the time that a particular service is available. Similarly, the electricity industry uses reliability metrics such as the System Average Interruption Frequency Index (SAIFI)² and the System Average Interruption Duration Index (SAIDI)³ for the distribution service, or the Loss of Load Expectation (LOLE)⁴ for the bulk grid level.

Finally, and analysing the concept of reliability applied to a power grid [20], we define it to be related to the respective reliabilities of its elements. This implies that it could be established as a function of the operation of both its physical components (e.g. transmission lines and generators) and its software elements (e.g. communication links).

2.4.2. Survivability

The concept of survivability is highly-related to resilience, as it takes account for the capability of a system to continue performing its activities under different disturbances. A more accurate definition is given in [21], stating that *“survivability has been defined as the capability of a system to fulfil its mission, in a timely manner, in the presence of attacks, failures, or accidents, where the term “system” is used in the broadest possible sense”*.

Applying that definition to our system, a microgrid, it is necessary to settle a minimum level of overall system operation under which the system would be defined as non-functional. To this purpose, two approaches can be taken:

- Set a number of services / functioning loads as essential, and consider the system to be functional providing that these elements are successfully working.

²SAIFI: measures the average frequency of outages per customer.

³SAIDI: measures the average duration of outages, for one customer, in a one-year-time-period.

⁴LOLE: accounts for the amount of electric energy demand that remains unserved during a specified period of time.

- Measure the system performance using a function (e.g. $P(t)$) that takes into consideration certain aspects of operation: power quality, stability parameters, etc. Then set a threshold that sets a limit under which the system is considered to be non-operational.

Every mode of operation in between the normal functioning and these limits would then be considered as a “degraded mode” and the survivability would quantify the performance of the system under these conditions.

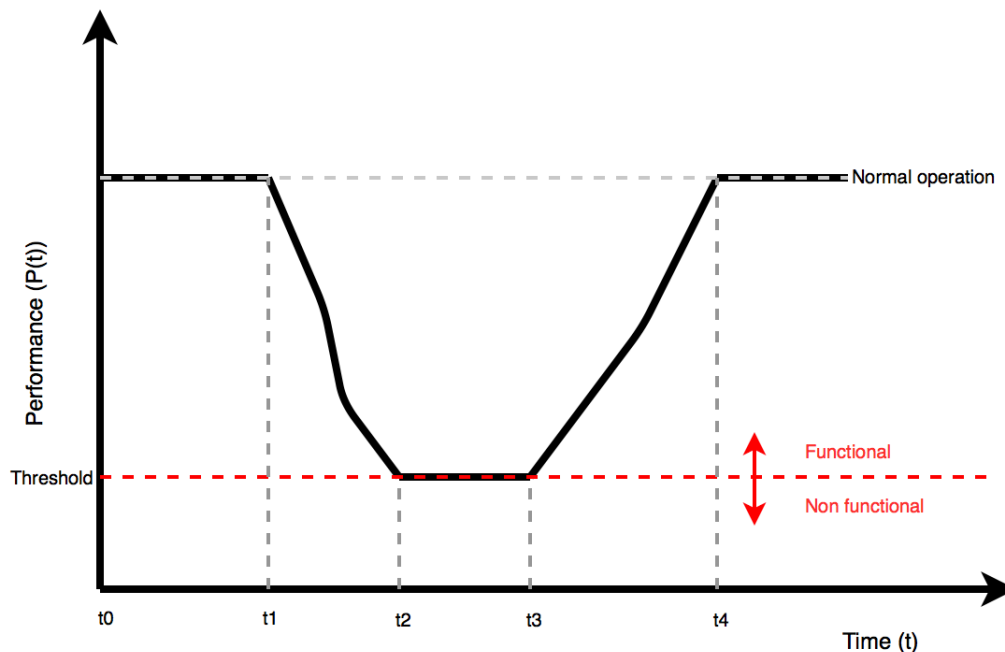


Figure 2.3: Example of a performance chart with a pre-defined threshold.

The chart shown in figure 2.3 represents the functioning of a system that experiments an unknown failure in t_1 , leading to failure in the system by the time t_2 . Then, a restoration protocol is started in t_3 , reaching normal operation again after certain time, in t_4 . Survivability would then be measured in the intervals $t_1 - t_2$ and $t_3 - t_4$, where the system is operating in a degraded way, thus its performance is below standard operation and above non-functional values.

Historically, measures taken in the electrical grid to increase survivability with respect to blackouts have included adding battery backup to streetlights at critical intersections or ensuring that emergency service providers (police, fire, hospitals) have well-maintained backup power systems. In other fields, such as IT systems, survivability typically refers to the ability of the system to provide critical services, after some portion(s) of the network has been compromised [19].

2.4.3. Resilience

As previously stated, the idea of resilience comes along with survivability and sometimes both terms are included inside the same boundaries. This concept is borrowed from material science, where it defines the amount of distortion energy (per unit volume) that can be recovered from an elastically deformed object when the force that is causing the distortion stops. Abstracting the idea, it is clear that there will be a close relation between resilience and restoration.

From a computer science perspective [22], cyber resilience entails the ability to withstand a (single, one-time, limited-duration) disruption, maintaining a minimum acceptable level of performance and recovering within an acceptable time. From this definition we can already see the double scope of the concept, although this particular discipline would only focus in the cyber-attack possibilities when

preparing a system to failure and recovery.

When studying resilience applied to the power system, we will concentrate in situations involving critical events such as severe storms, hurricanes, floodings or cyber attacks. On the basis that infallible system protection is not achievable, and preparing the microgrid against these aforementioned events, two chronological scopes of operation are chosen under resilience analysis.

The first stage would be to optimise the behaviour of the system during degraded operation, trying to avoid failure while preparing for that possibility. This phase is closely in touch with the survivability of the system, and it requires an accurate performance function to quantify the results and act in consequence.

The second stage comes when the system experiences a failure, and it comprises the restoration efforts made to achieve normal operation. This is made by human operators, thus it depends on how well they respond to these critical events. Microgrids will play an active role in order to ensure an optimised restoration, by utilising its many characteristics: change to island-mode in order to protect the integrity of their loads, use of smart meters to provide precise data regarding the specific location of the power outages, distribution of power depending on the importance of the load, and so on.

3

Fields of improvement

The aim of this chapter is to provide a series of guidelines that shall be applied when designing Smart microgrids in order to enhance their survivability and resilience. Several concepts will be reviewed from that perspective, proposing changes in current microgrid features as well as presenting new ones.

3.1. Island mode of operation

From the previously stated definition of microgrid, we can see that there are two different modes of operation: grid-connected and island mode.

- Under normal conditions, both meteorological and electrical, the microgrid performs its operation as **grid-connected**. Normally, the power flow starts in the bulk generation and reaches the end-consumer going through transmission and distribution levels. However, a grid-connected microgrid allows the power to be interchanged between the grid and the microgrid, with the peculiarity that it can be done in both directions, originating the concept of *prosumer*. According to [23], *"physically, the prosumer consists of a combination of components: energy sources, loads, and storage; and an electric grid. The prosumer also contains controls to operate its system, and a market or other economic decision making system. The prosumer has a set of functions associated with interactions to the external world such as consuming or producing energy and participating in the market. It has also two internal functions: operate its power system, and economically optimize its energy use."*
- Extreme weather events or major electrical failures can compromise the main grid proper functioning, leading in some cases to widespread outages. These abnormal conditions prompt the microgrid to disconnect itself from the main grid and switch its functioning to **island mode of operation** [24]. The situation then compels the microgrid to supply its loads with the distributed energy resources within its electrical boundaries, which can be done through voltage and frequency management, altogether with a balancing of the supply and demand.

From the perspective of survivability and resilience that characterize this study, the ability of operating in island mode provides the microgrid with great features to guarantee the partial or complete survival of the overall system, in addition to its fast restoration after a catastrophic event. While in normal conditions, the power supply for a load could be cut due to problems in the bulk, transmission or distribution level of the power system, in this case the damage had to be done directly in the microgrid to stop its functioning. The fact that we have the production and consumption of energy so geographically close allows the designer of the microgrid to provide the installations with measures against the most likely severe event to occur in that specific location. For example, when designing a microgrid in a zone prone to suffer hurricanes, subterranean DERs could be implemented in order to ensure their survival and supply to critical loads through the whole event.

Another important aspect to take into consideration is the preparedness of the microgrid to change to island mode, as the transient states constitute a complicated issue. As mentioned before, such

network would have the possibility of changing to island mode provided that there are installed power units able to feed the necessities of the system. Moreover, these sources should be equipped with the appropriate automation systems enabling island mode operation[25], such: systems distributing the generated power between particular sources, frequency controllers and network load relief systems.

Finally, the current trend of implementing renewal distributed energy resources such photovoltaic panels or wind turbines in the microgrids must be accounted. Their intermittent and weather-dependent nature cannot provide a constant power supply when switching to island mode, and therefore, they must be installed along with other DERs such battery energy storage systems (BESS) or diesel generators.

3.1.1. System restoration

An optimized design, implementation and operation of the microgrids within a power system presents the opportunity of influencing positively its resilience. Particularly, it can provide great improvements during the recovery & restoration phase after the electricity grid has presented failures [26]. Among the characteristics that allows this feature, the opportunity of switching between grid-connected and islanded mode of operation occupies an important role.

The ultimate objective of a restoration plan is to bring the loads back to normal operation, doing so in a safe and efficient way and giving precedence to critical ones such hospitals or transport facilities. Traditionally, this procedure starts at the transmission level and works towards the distribution level. As a result, load restoration constitutes the final stage of a process whose time-line can go up to days, impacting severely in the quality of service received by the consumers.

The fact that power systems are usually centralized worsens the situation, delaying even more the restoration of some loads and highlighting their noticeable weaknesses in such critical situations. In order to face these challenges, the use of microgrids so as to enhance system resilience presents itself as a promising concept. The unique characteristics that allow these improvements in system restoration can be summarize in the following two:

- **Flexibility in operation:** when undergoing violent weather conditions and depending on the status of the main grid and the microgrid itself, the master controller has the option of changing operation between grid-connected and island mode. It can also choose the optimal amount of power interchanged with the grid, in addition to selecting an ad-hoc use of local resources and adaptable settings for protection devices. On top of that, and depending on the topology implemented in the microgrid, the connections can be reconfigured on-the-go by the master controller if the situation requires it.
- **Self-supply:** when the transition to island mode is needed, the loads must be supplied with the distributed energy resources present in the microgrid. Providing that we count on different DERs, with a variety that can guarantee the continuous supply, the load restoration process will be significantly improved.

One of the main reasons why these characteristics have a profound impact in the system resilience, and more accurately, in its recovery time after a catastrophic event, is the possibility of performing self-healing. When a microgrid receives damage to a certain point where it can still operate, the master controller can perform a set of actions in order to save the endangered or damaged loads. This activity perfectly complements the traditional restoration, whose direction goes downward from the transmission to the distribution side, with this self-healing activities, that perform load restoration with an upward process starting directly in the distribution level.

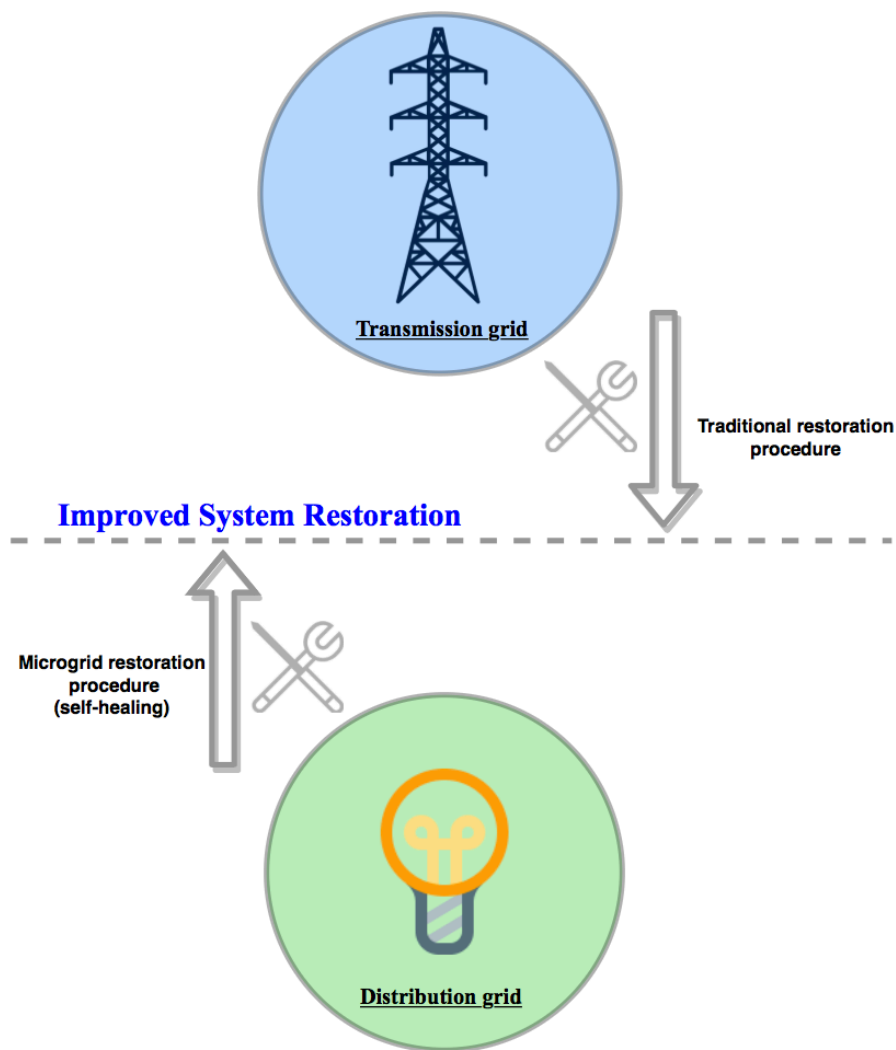


Figure 3.1: Microgrid-based load restoration process.

As a result of this strategy, full system restoration is achieved faster than in the traditional system restoration procedure. This technique, combined with a better observability of the system and thus, a more accurate gauging of failures, provides noticeable enhancements in the system's capacity of recovering after facing outages.

3.1.2. Real life situations

From a theoretical perspective, it has been studied through the previous analysis that the implementation of microgrids in our power system would result in an enhanced resilience when facing catastrophic events. The focus of this section is set on real situations where the effects / possible effects of having such networks are exposed.

Superstorm Sandy

This type of severe weather manifestations (superstorms and hurricanes) have been extensively studied in the United States, as they suffer them practically every year. Just in 2012, when Superstorm Sandy hit, the estimated cost due to its power outages was in the range of \$27 billion to \$52 billion [9]. Therefore, grid resiliency is increasing its importance, as climate change increases the frequency and intensity of severe weather.

Although an ideal island mode of operation with properly implemented battery energy storage system would be the direction to work towards, in reality this is yet to be proved as a completely viable option. Instead, microgrids that present withing its DERs natural gas-fueled sources, such fuel cells or

microturbines, have been tested to have better probabilities of remaining operational after hurricanes [27]. This is the case of the microgrid at Verizon's Garden City, New York, Central Office, consisting of seven 200 kW fuel cells, which managed to operate within its limits of normality after both the Hurricane Irene (2011) and the Superstorm Sandy (2012) took place. Nevertheless, and in order to make up for the slow dynamic response of the fuel cells, this microgrid uses diesel generators when facing grid outages so as to provide power supply. This idea will be noted down and taken into consideration when modelling our own microgrid.

Other examples include the microgrid settled at the Federal Drug Administration's White Oak Research Facility (Maryland), which was able to maintain their loads supplied through the Superstorm Sandy by means of switching its functioning to island mode of operation. This particular central utility plant microgrid has an operational capacity of 26 MW, that can go up to 55MW if needed. A study conducted between 2010 and 2013 proved its capacity to work in island mode over 70 times, remaining operational 100% of the time and avoiding interruption not only during Superstorm Sandy and Hurricane Irene, but also during an earthquake that took place the year before [28].

Evangelos Florakis Naval Base Explosion

It happened in Cyprus, on 11th July 2011, and affected a power station nearby called Vasilikos. The widespread damages suffered by this station, which was the largest and newest in the country, led to half of the population losing electricity supply immediately. Cyprus, which is an island, had no interconnections with near countries and this loss of 51% of the whole country generation capacity caused a rise of 100% in the cost of electricity to the consumer within a year. Furthermore, this abrupt drop of generation capacity precipitated the implementation of load shedding strategies for over a month, making users to experience two-hour power interruptions twice a day, until generation units were conveyed to Cyprus.

This is an example of how an electric system exceedingly dependent on a centralized power station can collapse, resulting in not only a major outage, but also bad quality of service during a prolonged elapse of time. It is safe to assume that if part of the power supply would have been dependent on geographically separated microgrids, the response offered to this unfortunate event would have had smaller repercussions in both the end-consumers and the overall electric system.

Tohoku Earthquake & Tsunami

Another real example which happened in this decade is the 9.0-magnitude earthquake that shook the north-east coast of Japan on 11th March 2011. It was the most powerful ever-recorded earthquake in the country, and it was followed by a tsunami with waves over 40 meters high. In this desperate situation, Sendai Microgrid at the Tohoku Fukushi University was able to supply several loads (which included a Hospital) during up to two days while the nearby grids were powerless [29]. This microgrid was initially developed as a demonstration project called "Experimental Study of Multi Power Quality Supply System" (MPQSS) and has several generation sources: a photovoltaic array, a phosphoric acid fuel cell and two gas engines.

3.2. N+X redundancy

The previous section was focused on how the microgrid is able to change its mode of operation when failures compromise the main grid, being able to continue supplying its loads even in extreme cases when the general power has been cut off. However, no specific examination has been done regarding the scenario where the microgrid itself presents damage. When facing these situations derived from the critical events mentioned before, component failure is sure to come up as an issue and therefore should be addressed directly. In particular, this section is focused on the potential improvements of following a N+X redundancy strategy.

With the idea of achieving an outstanding resilience and survivability, the concept of *mission critical system* is introduced. It accounts for a system that is fundamental for an organization or a business, meaning that its failure would have a great impact in the operations carried out by them. For instance, data centers, electrical power systems or spacecraft applications could fall under this category. Nevertheless, and although a microgrid most likely would not need this level of reliability (depending on the importance of the loads within its electrical boundaries), we could adapt the strategies used in these cases to our own. Here is where the N+X redundancy shines, as it is thoroughly implemented in these environments which need to ensure continuity in their services under almost any circumstance.

In this method, N takes account for the number of components that conform the system (in our case lines, DERs, transformers, etc) and X stand for the number of back up components available. The two mainly used schemes that are deployed when designing redundancy are 1+1 and N+1. The first one consists in providing a duplicate or every component of the system, in case the primary fails. However, this straightforward approach has its economical aspect as the main drawback, given that the investment necessary for the installation would be doubled. The second scheme, N+1, requires one back up additional element for N number of other components and would be more easily implemented in a microgrid.

When deciding upon the implementation of redundancy, the nature of the aforementioned backup component shall be decided, as they can be considered as standby or as active-active components.

- **Standby components:** these components do not have any active role during normal operation of the system and will therefore be purely redundant until the system is facing the failure of a component. In that situation, a failover ¹ procedure will be executed providing that the number of components presenting failure does not exceed the installed redundancy (X). This resilience strategy, although seemingly simple, requires to balance the optimal amount of redundancy installed in accordance with the economical budget, the operation practicality and the necessities of the system.
- **Active-active components:** this case, which is of higher complexity, implies using back up elements that remain active during normal operation of the system even when the primary components are completely functional. In addition to that, the system should be able to continue functioning in the event of X components experiencing faults and restore operation from that point.

To provide an understandable example of failover with this behaviour, the concept of high availability clusters is used. According to [30], "high availability is a key component of business resiliency, whose objective is to provide near-continuous application availability through both planned and unplanned outages". In computation field, this concept is applied by forming groups of computers which take advantage of their redundancy to provide continued service when a primary component fail. In order to do so, they make use of failover policies.

This concept can be abstracted to a microgrid, where the active-active connections and transmission lines would be designed so as not to operate at 100% capacity during normal operation.

¹Backup operational mode which ensures that the functions of a system component are assumed by the installed back up component when the first one becomes unavailable

With this measure, when facing failure of a component, traffic intended for the failed line could either be passed onto another one or balanced across the remaining operational ones.

Nevertheless, N+X redundancy has serious limitations, as the usual values for X (back up components) are 1 and 2. This is due to a compromise between the economical aspects of the project and the improvements in reliability and resilience obtained. Moreover, analyzing critical events that took place in the past years, we find that Superstorm Sandy (2012) [26] was a N-90 contingency. This fact, although the hurricane was one of the most powerful that have happened in the last years, clearly shows that this method alone would not have a big impact in our system's resilience. However, it can increase the range of operation under critical circumstances, achieving a better response against critical events and improving greatly the reliability indexes.

The concepts studied in this section will have an important influence in the next one, that deals with the choosing of an optimal topology for the microgrid.

3.3. Topology

In general terms, the topology of a system tells how elements/devices relate spatially and virtually to each other. The microgrid's topology has an important impact on the resilience of the system, and therefore we shall present the basic directions to which the improvements should head.

Conventional microgrid topology planning (MTP) usually works with radial distribution networks and therefore, an extensive number of research papers perform simulations based on that assumption [31] [32] [33] [34]. However, when using this distribution, any failure in the connection lines would result in every downstream distributed energy resource and/or load becoming isolated from the network. That is why this configuration becomes a bottleneck when exploiting the resilience-related benefits of a microgrid-based system.

In accordance with the previous section, the topology of the microgrid should take into consideration adding optimal redundancy to the design, improving this way the response against structural damages. Along these lines, two main options appear to fill the necessities of a microgrid:

Loop-based topology

Inquiring for a formal definition, loop topology is applicable to a network where all the components are connected serially in such a manner that the first and the last components share a path between them. From a redundancy point of view, in terms of connection between DERs and loads, the system would present $N+1$ redundancy.

This option provides several advantages in opposition to the radial configuration, as it improves the performance at power delivery points within its limits. This is due to the availability of a secondary path that ensures both the energy delivery and the fault magnitude determination upon failure of a transmission line. While when implementing a radial topology and having a failure in the network we lose awareness of the downstream part of the microgrid as well as the possibility of supplying those loads, changing the topology to a loop-based microgrid would allow us to bear through these small scale contingencies achieving a higher-reliability microgrid operation.

In the above figure 3.2 we can observe how a radial-based microgrid faces a failure in transmission lines by switching its mode of operation to islanded. However, when those conditions that prompted the outage in the transmission lines affect the microgrid itself (e.g. a tree falling on the connection lines), this radial configuration loses the possibility of supplying the end-of-line loads, as well as awareness of that part of the microgrid.

Opposite to that, figure 3.3 shows the exact same situation faced by a loop-based microgrid, which is able to maintain the loads supply throughout the event.

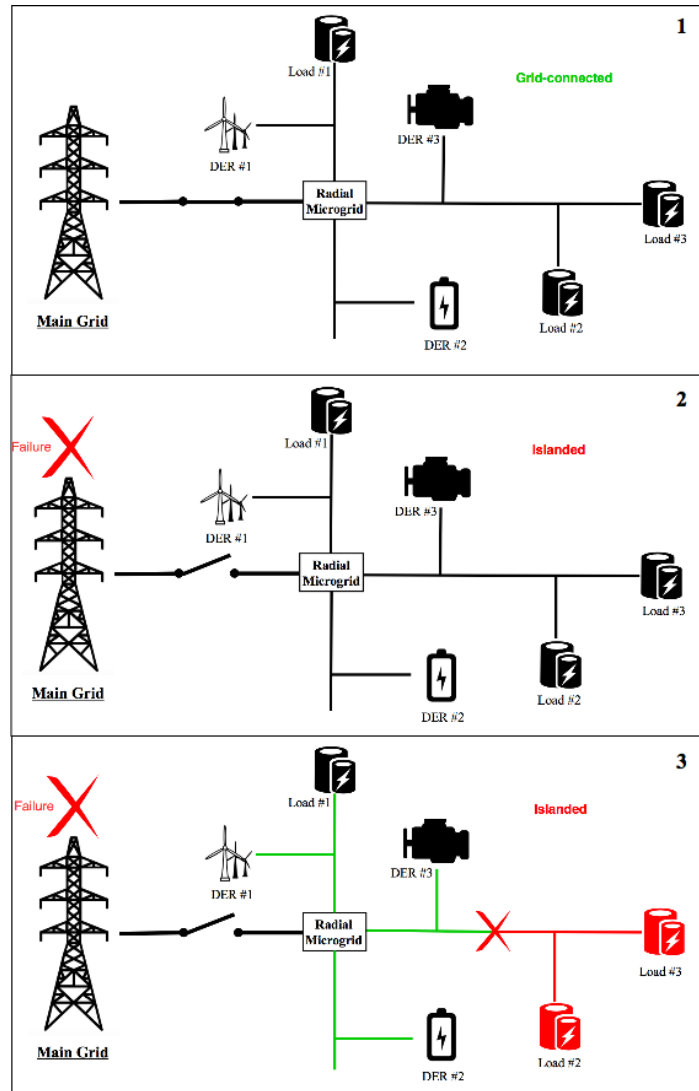


Figure 3.2: Radial-based microgrid facing failure in transmission lines.

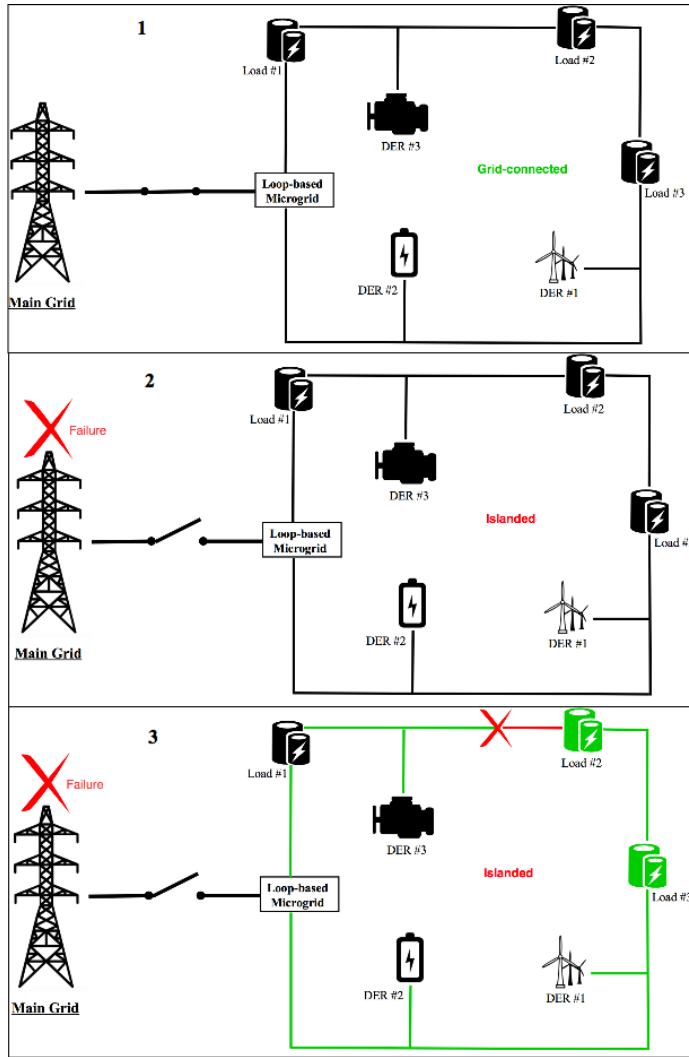


Figure 3.3: Loop-based topology microgrid facing failure in transmission lines.

Another consideration is to be highlighted involving the protection devices and their operation in our microgrid, given its bi-directional nature towards the main grid. This feature, derived from the multiple DERs implemented and the prosumer behaviour of the microgrid, result in bi-directional fault currents, that present a challenge when designing the protection schemes. According to [35], while a conventional radial network topology would struggle handling these operational threats, a loop-based topology would facilitate the protection of the microgrid against this conundrum.

In relation to the commented above, the Illinois Institute of Technology (IIT) operates a microgrid where the power distribution circuits are divided into seven loops. Each loop including several loads and DERs. If we assume that a permanent fault occurs somewhere in a loop, the associated switches would reconfigure the loop connections so that power flows could be automatically rerouted via unaffected paths. This process would ensure this operation without interrupting the power supply to loads. However, if the topology was radial and some loads were to be affected, the system would inevitably suffer an outage when any upstream component fails [24].

Meshed topology

This topology has been previously introduced in Section 2.2, where the following formal definition was provided for an infrastructure with mesh topology, "An infrastructure in which the nodes are connected to as many other as previously designed, with the possibility to achieve a full interconnection. These links are to be direct, dynamic and there shall not exist any hierarchy in-between them". In the following paragraphs its advantages and drawbacks for the functioning and resilience of a microgrid will be taken into consideration.

According to [36], the implementation of a heavily meshed microgrid would result in enhanced reliability of the system, which would improve its behaviour not only during post-fault contingencies, but also during undergoing repairs of the system. This paper also proposes a protection schema to measure and compare differential current measurements in order to detect and isolate faulted points in the network.

Diverting from the power delivery perspective, the enforcement of a mesh network in the microgrid can also provide great results in the communication field. Using this idea, [37] provides a method to deliver information by distributing it and using all the nodes of the network. This concept seeks for a reduction of traffic in bottlenecks while keeping the performance of the network within reasonable levels. If we take an specific mission of the system, for instance "Providing real-time information about

the distributed energy resources while undergoing a critical event”, the purpose of this network would be to ensure uninterrupted communication. To that mean, mesh networks rely on their multiple and redundant connections to establish multiple paths between nodes, foreseeing any possible disruption and offering a rerouting through any different group of nodes.

Lastly, and analyzing it from the N+X perspective, X would be the number of nodes (DERs and load) of the microgrid. This approach, although appealing from a resilience perspective, would not be optimal when considering the complexity of the system and its economic cost. Thus, and considering that its implementation would cut off the size of the microgrid to a few hundred kilo watts [38], we conclude that it is not well suited for microgrids.

Following the analysis of these two suitable topologies, we determine that a loop-based microgrid presents a better relation between feasibility and enhancement in the resilience of the system. However, the benefits of a meshed network cannot be obviated and thus, a compromise between the two is proposed: a meshed set of loop-based Smart Microgrids.

Meshed set of loop-based Smart Microgrids

Making use of the theoretical background provided by [24] with its concept of “Networked microgrids” and by [39] with the idea of “Community microgrids”, this configuration is presented as an optimal and feasible topology to enhance the power system resilience.

In general terms, this proposed concept of *Meshed set of loop-based Smart Microgrids* involves taking into consideration geographically-near microgrids when designing our own microgrid, and achieving a meshed interconnection between all of them. In order to be able to improve the resilience of the overall system, the following features should be implemented in each participant of the system:

- **Topology of the microgrid:** it is defined to be loop-based, according to the benefits and contributions to resilience that would be obtained and that have been thoroughly explained in the previous sections. Each microgrid shall acts as a single entity, with a bi-directional connection with the main grid and the capacity of working both grid-connected and in island mode.
- **Topology of the set:** a path connecting every pair of microgrids taking part of the group is to be designed, in order to achieve full interconnection. This configuration would result in a higher redundancy than the N+1 provided by the loop-based topology, which would also be heterogeneous, as the sections of the microgrids near the interconnection paths would have a higher one. Aiming for noticeable improvements in resilience, it would be optimal to place the connections near the critical loads, in order to translate this higher redundancy into an enhanced resilience and a higher survivability of the microgrid.
- **Master controller:** upon facing critical events with failures in the power system, this set of meshed microgrids are to act as an unified entity, who can provide an optimal response making use of every participant. This response includes tasks such transferring power between microgrids to supply loads, determining the extent of failures among them by pinging nodes from different locations or collaborating when restoring the system. Therefore, a master controller that is able to perform these operation shall be implemented by the distribution system operator (DSO). It relies on the state-of-art system awareness provided by Smart Grid’s technologies, that allows it to have a general picture of the system, real-time information about loads and DERs and the ability to physically influence microgrids by using distributed automation.

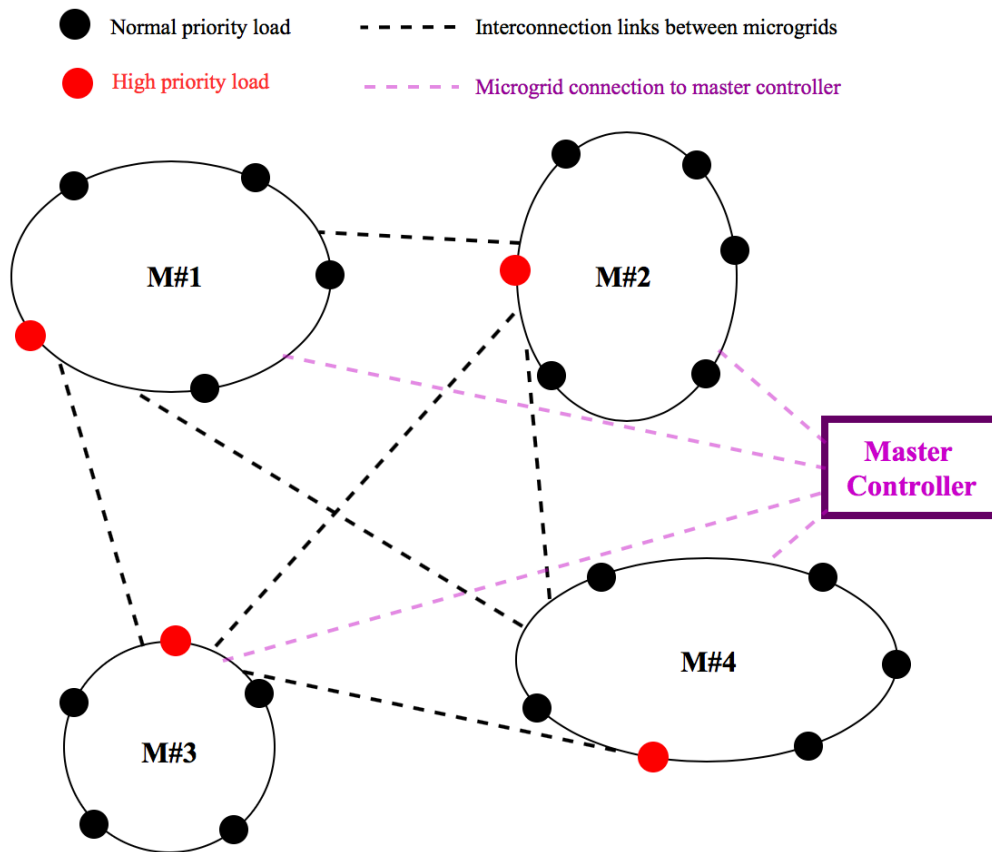


Figure 3.4: Conceptual draft of a meshed set of loop-based Smart microgrids (M#n).

This idea takes advantage of the diverse nature of the distributed energy resources implemented in different microgrids, as their response to the same critical events differ. For instance, if the region where this system has been implemented is undergoing a weather event that involves torrential rains and high-speed winds, photovoltaic generators could be receiving extremely low insolation and wind turbines may stop working when the cut-out wind speed is reached. However, other DERs such as diesel generators or hydroelectric generation units would still be functioning properly, and therefore those microgrids containing them could help the rest of the microgrids supply their loads.

Another benefit of having this *cluster* of microgrids working as an unit is their geographic dispersion. When facing a natural disaster, its effects will be different depending on where the microgrid is located, and thus, the microgrids that remain fully operational will assist the damaged ones. For example, an earthquake followed by a tsunami would have severe effects on the microgrids near the coast, but would not affect nearly as strongly the inland microgrids.

Finally, and along the lines of subsection 3.1.1, the restoration of the entire system would be accelerated, due to the distributed system operator performing a bottom-up restoration strategy at the same time as the top-down conventional procedure is being executed. This would be done with the meshed microgrids performing self-healing and restoring power supply to critical loads within their boundaries while the bulk generators of the power system would start re-energizing transmission network components.

3.4. Advanced metering infrastructure (AMI)

This section, which makes use of section 2.3 as theoretical background, is geared towards studying the possibilities and opportunities of implementing an advanced metering infrastructure within our system, in order to improve its resilience and response to critical events. As stated before, Smart Grid is a collection of technologies in which the metering side is performed by an advanced metering infrastructure. This AMI performs measurements, collection, storage and analysis of energy usage data. Moreover, it provides a two-way communication with the Smart Meters and is able to modify the service level of the customers, as well as perform load management [16]. In summary, AMI denotes a system that, when it is requested (e.g. upon the occurrence of system failure) or on a regular basis, is able to receive and analyze information from devices, such smart meters, using different communication media. This can be proven extremely helpful for the distribution system operator (DSO), as it can work with real-time feedback on consumer outages and the information about power quality of the system provided by the AMI's bidirectional communications infrastructure.

However, AMI cannot be catalogued as a single technology, but as an infrastructure that integrates several of them. Therefore, three noticeable resilience-related monitoring systems will be presented [40] [41], in lockstep with their influence in the system's response and the possibilities of their implementation in our use-case.

- **Meter data management systems (MDMS):** this key component of the advanced metering infrastructure is a database which works with data gathered by the AMI, performing validation and storage, editing and estimation for future scenarios. It interacts with operation and management systems by making use of a set of analytical tools that make this cooperation possible. These systems include: an outage management systems (OMS) that is able to perform distributed energy resources operation, distribution management systems (DMS) based on advanced sensing, geographic information system (GIS), etc.

When operating a meshed set of microgrids, we could achieve great improvements in resilience by providing the master controller with an MDMS working closely with an outage management system and a geographic information system. This would ideally result in facing critical events with full awareness of the system and an ad-hoc outage restoration strategy that takes into consideration the geographical singularities of the whole network.

- **Energy management systems:** their major objective is to obtain a better efficiency in the energy performance of buildings. Two main strategies are implemented, energy saving and flattening peak demand, and in order to do so, building systems are monitored, controlled and analyzed. This monitoring system is of interest to our group of microgrids, because these EMS rely on specific assets: sensors, switches and controls algorithms. This collection of equipment allows an individual monitoring of loads and rerouting of power flow via implementing automation in the switches. Centralized control of geographically distant networks, as well as control of numerous buildings on a campus have been achieved by installing an EMS [40], therefore, its features should be considered for our master controller.
- **Energy information systems (EIS):** according to section 2.3, these EIS would fall under the category of gateways, as they normally operate as a two-way communication between the EMS and the system. Nowadays, their main function is to gather data related to energy consumption and help with the load management.

When operating a geographically disperse set of microgrids as the proposed one, it is of high necessity to have system awareness when facing situations where failures spread along the system. Here is where EIS are of use, as they can offer monitoring and real time energy use data of the elements composing our system. They can also provide notifications of state, and allow the master controller to analyze how the operational modifications made during ongoing critical situations are affecting the system, helping in the policy-making.

In a nutshell, advanced metering infrastructures can enhance the system's resilience by improving its observability from the master controller standpoint. According to [1], and transferring the topic to

real-life situations, this results in an accelerated service restoration and a reduction in the number of affected customers during major storms. We can reach these goals by providing real time information of the system and the location of the outages, achieving the use of fewer truck rolls during restoration and using repair crews more efficiently. This whole approach relies on the AMI, which plays a main role in service restoration following outages.

One feature, previously named in EIS description, is the option to “ping” smart meters using the data communications network to verify outage status. When an outage in any part of the system is detected, the AMI starts pinging the neighbor nodes in order to establish the total extent of the failure. In our specific scenario, and given that all the microgrids composing our system are connected between them, these ping signals could be send from multiple locations, achieving a higher resolution when determining the fault.

Figure 3.5 presents a conceptual drawing of how would this pinging procedure work, applied on microgrid #1 of figure 3.4. A comparison will be presented between the case of a single microgrid where the pinging is applied, and the case of multiple microgrids with meshed connections between them. The latter, which is the selected approach in this thesis, presents enhancements in observability of the system.

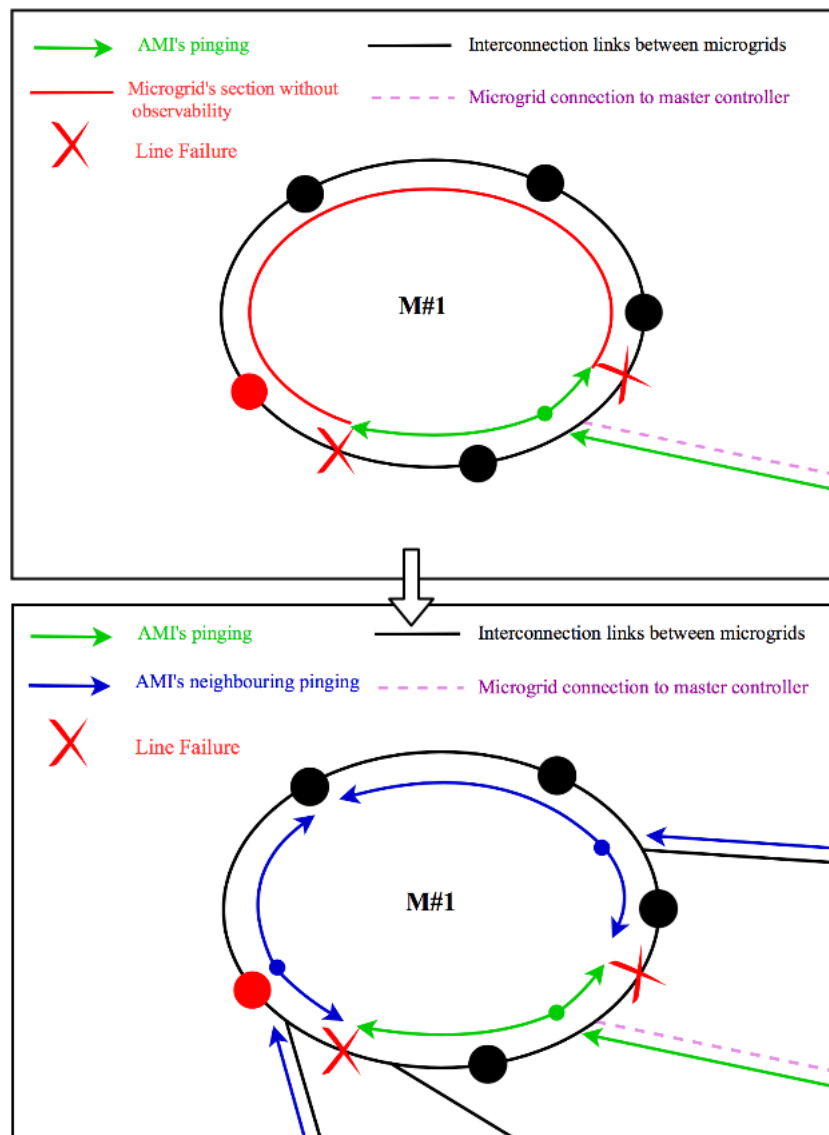


Figure 3.5: Improvement of the pinging procedure by means of the meshed cluster of microgrids.

Once the lines, loads and DERs affected are thoroughly determined, we can perform a better coordinate dispatch of repair crews to outage locations. These systems result in an optimized response to weather-related outages, as the restoration can be focused on the locations with a better ratio *time needed/number of customers affected*, achieving more efficient operations.

Another smart meter functionality that can also be make use of is the "last gasp" alarm, which is automatically sent when the power goes out. Then, a regular alarm is sent when the power comes back on. If the second alarm is not received within a pre-defined amount of time, an outage protocol is performed and neighbouring meters can be pinged to gauge the extent of the outage. When the outage has been properly determined, the restoration procedure commented above is followed. This whole process falls under the category of "self-healing" when combined with distributed automation to perform FLISR (Fault Location Isolation and Supply Restoration) and relies on an integration between the aforementioned monitoring systems:

- Data from AMI systems.
- Outage Management Systems (OMS).
- Geographic Information Systems (GIS).

3.5. Self-healing

The concept of self-healing is borrowed from the medical argot, and in this scenario implies the built-in ability of a microgrid to perform fault detection and restoration without external help. Since the self-healing protocol is activated during critical situations, its actions aim to optimally isolate the outage areas and re-distribute the distributed energy resource connections to ensure safe supply to loads [42].

The pursued double objective is to warrant the survivability of the system and to perform the first steps of system restoration, by cordoning and identifying the faults. It represents an important milestone in the study of resilience, and this section will analyse its implementation.

3.5.1. Fault location, isolation and service restoration (FLISR)

This concept, presented as a major finding by the United States government in the FLISR in 2014 [1], is ideally suited for the proposed configuration of Smart microgrids (subsection 3.3). To give an overview of its functioning, a FLISR system would rely on sensors to monitor and measure fault currents, communicating their occurrence and characteristics to the appropriate devices and to the system operator. Once this task is fulfilled, it would move on to the next step of the process, isolating the fault. To that end, both the upstream and the downstream side of it would be opened by utilizing switches. Finally, FLISR systems would change the state of the normally-open switches of neighboring networks to *closed*, restoring service to all customers.

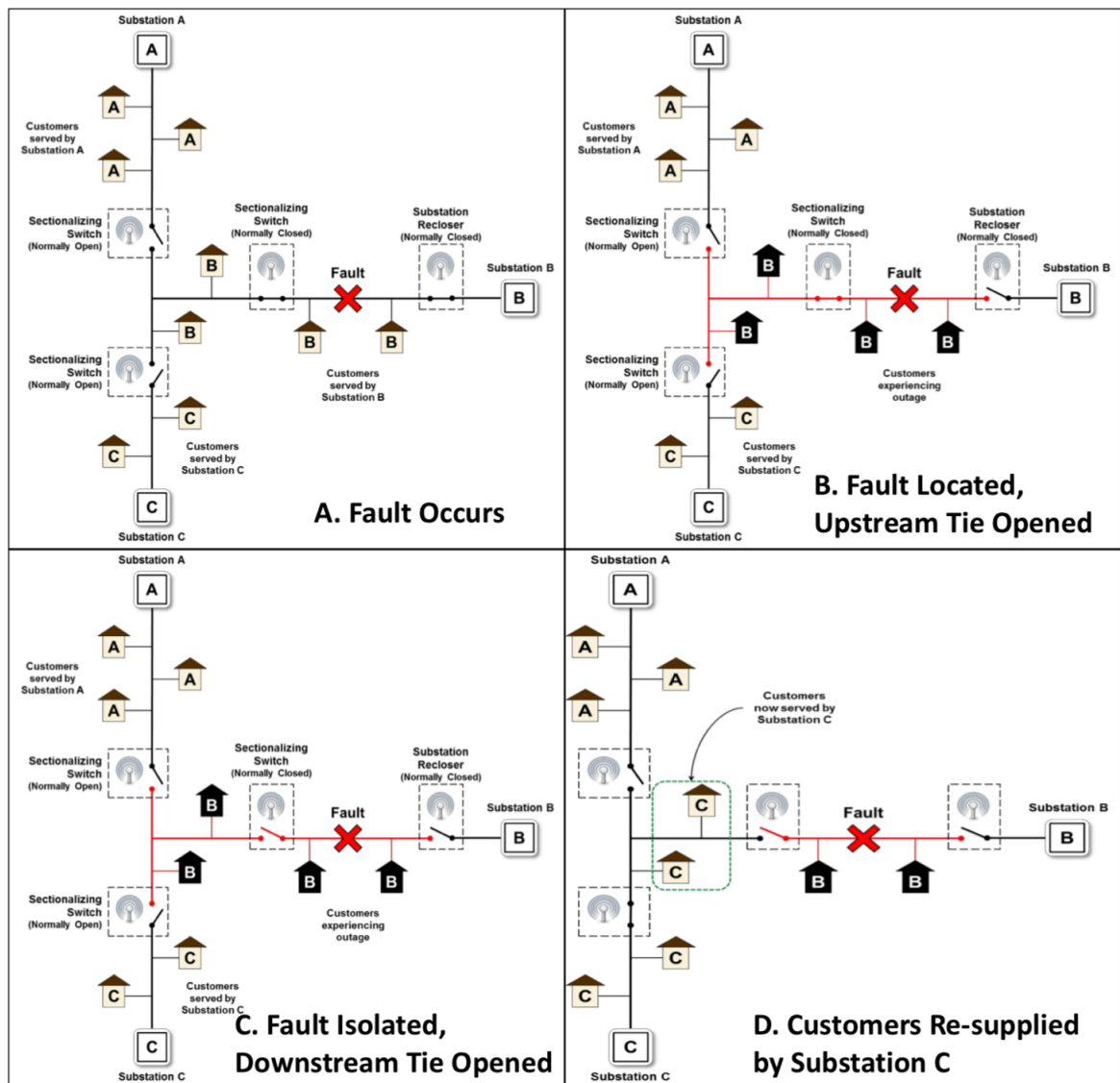


Figure 3.6: Fault location, isolation and service restoration, provided by [1] .

This outage management procedure is able to perform at high levels of efficiency due to the help of advanced metering infrastructures (Section 3.4), which helps pinpointing the fault locations. Furthermore, and in order to perform both the isolation and the system restoration parts of it, distribution automation constitutes key component.

Distribution automation

Distribution automation is a term coined by the U.S. department of energy [43] to refer to *“the appliance of advanced control and communication technologies and the integration of switches, digital controls and sensors to automate and improve electricity delivery functions that previously were either not feasible or performed by electro-mechanical or manual processes .”* DA is aimed to improve several aspects of the service provided by the actual electrical distribution grid, however, we will only focus on its **reliability and outage management** application. In order to do so, it makes use of some functions provided by Smart Grids technologies, playing an important role in the FLISR protocol. These functions include diagnosis of faults by remotely locating them, automated feeder switching, outage monitoring or providing an optimal restoration dispatch. For these resilience-related actions to take place, some advanced field devices shall be installed:

- **Smart Relays:** besides the electrical isolation that a normal relay provides, these devices make use of specific communication software and algorithms to achieve automated switching. They can also perform data-collection tasks, forwarding this information to the system operators, which can run the pertinent analysis on it. State-of-the-art sensor technologies are implemented within them, so as to even detect high-impedance faults.
- **Remote Fault Indicators:** these remote fault indicators consist on sensors, which provide information to the operator (or master controller) regarding where the fault has taken place and its extent. In order to do so, currents and voltages are continuously monitored and compared with the normal levels of operation, which allow these indicators to differentiate between faults and temporary out of the ordinary conditions (e.g. starting currents of a motor). In order to optimize the procedure of fault detection, these sensors are integrated within the advanced metering structure (AMI).
- **Automated Feeder Switches and Reclosers:** these advanced field devices constitute the core of system segmentation tasks by working side to side with Smart Relays. The automated feeder switches work in accordance with the orders sent by the master controller, performing isolation, segmentation and restoration of power to customers. They can also perform “reclosing²”, shortening the time an outage is maintained when objects fall on power lines. This feature has a great influence in the resilience of the system against major storms, whose high-speed winds usually prompt the fall of trees.

The implementation of a Fault Location, Isolation and System Restoration system that can operate in an automated way, under the requirements of a master controller run by the DSO, requires an optimal synergy between the Advanced Metering Structure and the Distribution Automation procedures and devices. Highly accurate testings and calibration should be run on the system before allowing its operation, but the reward is worthwhile. According to [1], an automated FLISR procedure could be performed in under a minute. The following section will study the benefits of implementing this system in our meshed set of Smart microgrids.

3.5.2. Implementation

When analyzing the graphical description of the FLISR functioning (figure 3.5.1) we observe that it has been conceived for radial power systems, where loads are supplied by substations, and a fault in a line leaves without power supply all downstream-customers. Thus, there is high potential in modifying this procedure, in order to apply it to our proposed meshed set of Smart microgrids.

²Instant cut of supply to a feeder that has been affected by a contingency, and posterior restoration of power when the contingency has been removed.

- Instead of working with this radial configuration, a loop-based topology has been proposed for each microgrid, with a meshed overall system, considering each microgrid as a node. These paths between nodes would be regulated by sectionalizing switches, which are normally open and can be closed when interconnection between microgrids is needed. This configuration presents higher enhancements of system resilience, as we have multiple connection and paths available for restoring power when isolating faults.
- Against the conception of supplying customers with few and centralized substation, our approach relies on distributed generation, where each DER can provide power not only to the loads within its microgrid, but also to other microgrids. This idea's benefits have been studied before, and its combination with the redundant paths available to reach every load, ensures a higher probability of supplying customers, avoiding load shedding.
- The state-of-the-art master controller implemented should coordinate the advanced metering structure and the distribution automation technologies in order to ensure both the survivability of the system during critical events, as well as an enhanced restoration after failures and outages have been managed. A full system observability and the ability to remotely influence the system are two of the main features that should conform it.

4

Microgrid model

The purpose of this chapter is to present the developed model for the simulation of a microgrid. The power system simulation software that will be used is RSCAD, version 5.003.3 (2018). The motivation behind modelling and simulating the operation of a microgrid is double-sided.

On one hand, we aim to provide an accurate model of a microgrid with a variety of distributed energy resources and several loads. The ability of working grid-connected and in island mode shall be implemented, as well as the most promising findings reached in Chapter 3 regarding the enhancement of the system's resilience. This first motivation will be thoroughly carried out within this chapter.

On the other hand, and once a robust model of a microgrid has been developed, simulations regarding switching of mode of operation as well as simulations of critical weather conditions and the failures and outages brought along with them, are to be performed. Finally, the obtained data and results will be used to prove the effectiveness of the proposed guidelines. This second motivation behind the development of a model will be conducted in the following chapters.

4.1. General overview of the system

As previously stated and corroborated by extensive scientific literature, microgrids present a symbiotic relationship with renewable energy sources due to its operational flexibility and the implementation of Smart Grid technologies. Thus, they can be a fundamental pillar for integrating this variable generation in the electric system, and our model will take this fact into consideration.

- Following the aforementioned trend, the two main renewable energy sources, solar photovoltaic and wind, will have representation within our proposed model of a microgrid. To that end, a wind turbine and a solar PV array will be modelled and included in the simulation.
- Furthermore, and in order to mitigate and smooth out the fast transients due to uncontrollable circumstances, as well as to provide support to the variable nature of the renewable energy resources, a battery energy storage system will take part of the modelled microgrid.
- Finally, and based on the real-life situations analyzed in Section 3.1.2, a diesel generator will be the fourth and last distributed energy resource implemented. This multi-purpose DER has been proved to be an excellent asset in terms of survivability and performance under critical circumstances, resulting in an improved response of the microgrids to extreme situations. Furthermore, the installation of dispatchable generation helps compensating the irregular nature of renewal energy, balancing the system by achieving an optimal load-following strategy.

In order to link our model to the real world, it will be developed in the vicinity of Delft (South Holland). Every microgrid component (DERs and loads) will be placed in a real location, taking this geographical relation into consideration when modelling the transmission lines designed for the model.

We aim to study how the deployment of microgrids could positively impact the power system resiliency against critical events. Consequently, the loads within our system will be facilities with a great impact in the daily life of Delft, which will be modelled to be included and supplied by our microgrid. The facilities chosen for our model are: a hospital, a school, the train station and a neighborhood. However, it must be noted that the numerical values of power consumption have been proposed by the designer, and are subject to change during the simulation with simple sliders.

In essence, the microgrid will be constituted by 4 DERs and 4 loads. Further details of its physical characteristics and how the modelling will be performed are to be presented in the two following subsections.

4.1.1. The microgrid

This section is focused in providing the basic features of our microgrid, in addition to the geographical location of its nodes. Given that we have designed the microgrid to integrate loads which provide essential services to the community, it is necessary to step up the size of the system to the range of megawatts (MW). This design specification impacts on the magnitude of the chosen distributed energy resources, and forces the voltage to be within a range of kV, in order to avoid major electrical losses.

Therefore, the common bus is set to be working with alternate current (AC) and an RMS¹ **voltage of 13.2 kV**. With these stated assumptions, when studying the resilience and survivability of the system, we take into consideration loads important not only for the specific microgrid but also for the city of Delft, extrapolating the result of the improvements to that extension.

Regarding Section 3.1, the microgrid is designed to be able to face failures and outages in the main grid by switching its functioning to island mode of operation. Moreover, enough generation power is installed to enable its autonomous functioning and supply of all loads even when being grid-disconnected. The potential surplus of generation could be either fed into the battery energy storage system within the microgrid itself or sent across the meshed connection with other geographically-near microgrids in the proposed set. The diesel generator was proposed and implemented due to the real-life situations analyzed in the aforementioned section, and its function is to provide enough power to perform a load-following strategy when operating in island mode, taking the role of the main grid.

The findings and conclusions reached in Sections 3.2 and 3.3 result in our microgrid designed with a **loop-based topology**. There, its benefits over the traditional radial configuration have been widely dissected, and this N+1 redundancy achieved presents an optimal compromise between economical cost and enhancement of response to eventualities. In short, this topology involves each load having two different paths to the generation, increasing the chances of survival against potential faults in the lines. The overall proposed configuration for the connection within the set of microgrids operating under the same controller (Subsection 3.3) is meshed, providing additional paths of power supply to every load an improving the overall observability, survivability and resilience of the system. However, and due to simulation constraints, the simulation of the other microgrids will be left for future lines of work.

Sections 3.4 and 3.5 shall be addressed when performing simulations later on. Along those lines, the modelled microgrid presents several functionalities:

- Possibility of performing short and long-term faults in every transmission line.
- Possibility of connecting and disconnecting DERs and loads. This allows to analyze the effects of failure in the generation, as well as the simulation of load-shedding strategies.
- Implementation of circuit-breakers controlled during run-time from the provided interface, allowing for a FLISR (Fault Location, Isolation and Service Restoration) simulation.

¹Root mean square

Graphical visualization

After giving a brief explanation of the designing decisions and the features implemented within our model, a visual representation has been developed in order to translate the concept to a real satellite image. Figure 4.1 shows both, the loop-based microgrid joining together the 4 DERs and 4 loads explained before, and its connection to the grid by means of the Wateringen substation.



Figure 4.1: Satellite image of the layout of the microgrid.

The following tables will provide information about the electrical size, location and distance between the different nodes of the microgrid. The loads will be defined to be specific facilities and will have a real location associated to them.

Distributed energy resource	Location	Coordinates
Photovoltaic System	Mekelweg 4, 2628 CD	51°59'53.0"N 4°22'27.4"E
Wind Energy System	Phoenixstraat 112, 2611 AK	52°00'50.2"N 4°21'04.6"E
Battery Energy Storage System	Middelweg 5, 2616 LV	52°01'33.4"N 4°22'23.2"E
Diesel Generator	Westblok 4, 2614 VE	52°00'27.1"N 4°19'59.7"E

Table 4.1: Specific location and coordinates of the DERs implemented in the microgrid.

As stated before, the designer's choice was to implement loads simulating the functioning of important facilities regarding the day to day life in Delft. Table 4.2 defines both the name and location of the chosen hospital, school, train station and neighborhood.

Loads	Location	Coordinates
Reinier de Graaf Hospital	Reinier de Graafweg 5, 2625 AD	51°59'51.9"N 4°20'18.2"E
Delft Station	Van Leeuwenhoeksingel 42A, 2611 AC	52°00'27.3"N 4°21'24.9"E
Kievitlaan Neighborhood	Kievitlaan, 2289 ED Rijswijk	52°01'31.1"N 4°21'07.4"E
Herman BroerenSchool	Clara van Sparwoudestraat 6, 2612 SP	52°00'51.1"N 4°22'05.8"E

Table 4.2: Loads supplied by the designed microgrid.

Once the locations of every node of the microgrid were settled, the distance between them was determined using a distance measurement tool. The values presented are the nominal ones, although it must be pointed out that these quantities would be higher in real life, as the connection line installations usually differ from the ideal scenario. They will be later used for developing an accurate modelling of the transmission lines within our simulated microgrid. Figure 4.2 and its respective table account for the distances between nodes.



Figure 4.2: Numbered sections of connection lines.

Section	Distance (km)
Substation to Diesel Generator (1)	2.06
Diesel Generator to Train Station (2)	1.59
Train Station to Wind Energy System (3)	0.79
Wind Energy System to Kievitlaan Neighborhood (4)	1.28
Kievitlaan Neighborhood to BESS (5)	1.47
BESS to Herman Broerenschool (6)	1.35
Herman Broerenschool to PV System (7)	1.86
PV System to Reinier de Graaf Hospital (8)	2.45
Reinier de Graaf Hospital to Diesel Generator (9)	1.14

Table 4.3: Distance measurements between nodes.

Rijkskwijk Wateringen Substation

In order to model a real connection to the main electrical grid, the nearest substation is to be found. For that purpose, the national transmission system operator (TSO) of the Netherlands, TenneT, is consulted. It manages and supervises the operation of the high-voltage grid (220 and 380 kV) functioning throughout the country, as well as its interconnections with the the nearby countries.

By simply visiting its web-page [44], we have access to a high-voltage grid map, which includes the substations and inter-connectors in the Netherlands and Germany. If we analyze the region where Delft is situated, the following substation is determined to be the nearest,



Figure 4.3: High-voltage grid map, provided by TenneT.

It is the **Rijkskwijk Wateringen Substation** which operates with 380 kV voltage (red lines). It forms part of the Randstad 380kV project developed by TenneT, which implements a high voltage connection between Wateringen, Bleiswijk, Vijfhuizen and Beverwijk in the Netherlands.



Figure 4.4: Satellite view of the Rijkswijk Wateringen Substation.

This substation is located in Laan van Wateringse Veld (Wateringen) and its exact coordinates are: $52^{\circ}00'57.3''N$ $4^{\circ}18'25.1''E$. The 380 kV main grid, as well as the voltage stepping down procedure to reach the 13.2 kV with which our microgrid operates, will be modelled.

4.1.2. Introduction to the modelling

The default sample-projects provided by RTDS technologies include a couple microgrid cases. These examples will be used as starting ground for the model, which will also be supported by the manuals provided within the software.

In order to achieve the modelling of a microgrid that can account for the different DERs used nowadays, four different energy resources will be modelled within the system. Each of them will be included in the system with the possibility of connection/disconnection. DER variety also has a positive impact in the system resiliency, as separate damaging events affect them in different ways. This increases the possibilities of maintaining the power supply in island mode, since some DERs might survive when others fail to continue operating. For instance, high-speed winds preceding a hurricane can stop the functioning of wind turbines by reaching the cut-out speed, but have a less harmful effect in photovoltaic systems or diesel generators.

4.2. Photovoltaic system

Solar photovoltaic energy generation is in the process of becoming one of the most important electricity production generation sources [2] and it is being widely installed worldwide. In fact, and according to data provided by the IEA ² in his Photovoltaic Power Systems Programme, the tendency of the evolution of PV installations follows an exponential curve [45].

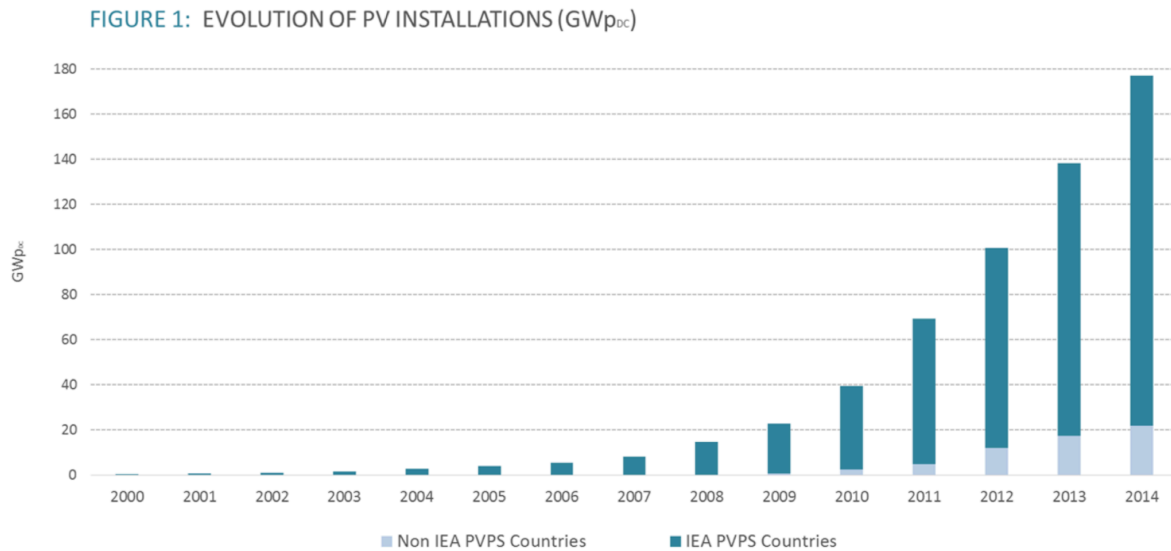


Figure 4.5: Evolution of solar PV installation, provided by IEA PVSP.

This forecasted growth of PV energy systems, along with the fact that it constitutes a great asset for distributed generation, have prompted its choosing as a DER ³ for our modelled microgrid. Now, and given that the only information provided about the photovoltaic system until this point has been its location, the reason behind that choice is to be explained in this introduction. The selected coordinates correspond to the low building of the EEMCS⁴ faculty of the TU Delft. We have chosen this location to take part of the microgrid in order to include the University in the microgrid, and on the basis that there is already an array of solar panels that can be observed on the roof of this construction.

4.2.1. PV Modelling

The basic element of a PV array is the **solar cell**, which is able to convert photons (when directly exposed to sunlight) into electric current.

In order to do so, it must be made of a semiconductor material, properly developed for this purpose. When we combine these solar cells in series and/or parallel, we conform PV modules. Then, we can combine once again these modules in series and parallel to finally form the desired PV arrays.

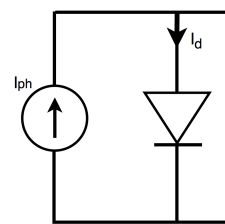


Figure 4.6: Equivalent circuit of an ideal solar cell.

In order to model the functioning of a solar cell, the chosen mathematical approach is to work with its equivalent circuit. If we were to simulate the functioning of an ideal solar cell, the equivalent circuit

²International Energy Agency

³Distributed Energy Resource

⁴Electrical Engineering, Mathematics and Computer Science

presented in figure 4.6 would be implemented.

Given that we aim to provide an accurate modelling of the PV array, we take into consideration the nonlinear current-voltage characteristics. This is achieved with the single diode, five parameter model, which includes a series and a shunt resistance. Figure 4.7 accounts for the equivalent circuit,

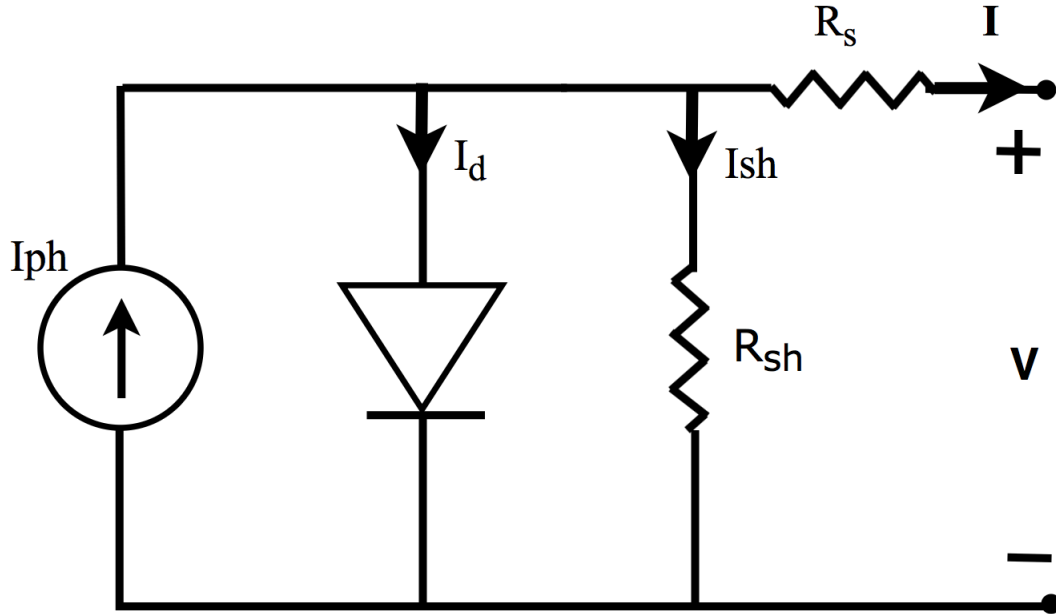


Figure 4.7: Equivalent circuit of the single diode, five parameter model.

Where,

- I_{ph} : photo-current induced by the incidence of sunlight in the solar cell.
- I_d : diode current.
- R_{sh} : shunt resistance representing the leakage current of the semiconductor material.
- I_{sh} : shunt current associated to the shunt resistance.
- R_s : series resistance result of the sum of several structural resistances.
- V : voltage provided by the solar cell.
- I : current provided by the solar cell.

Our purpose is to represent the current-voltage relationship within this equivalent model by means of the following equations,

$$I = I_{ph} - I_d - I_{sh} \quad (4.1)$$

$$I = I_{ph} - I_o \left(\exp \left(\frac{V + R_s I}{N_c a V_t} \right) - 1 \right) - \left(\frac{V + R_s I}{R_{sh}} \right) \quad (4.2)$$

$$V_t = \frac{k T}{q} \quad (4.3)$$

Where,

- I_o : diode reverse saturation current.
- a : diode ideality factor. Measures how close is the diode's behaviour to the ideal diode equation.
- N_c : accounts for the number of series connected solar cells.
- V_t : diode thermal voltage.
- K : temperature in Kelvin.
- k : Boltzmann constant ($1.38064852 \times 10^{-23}$ J/K)
- q : magnitude of an electron charge ($1.60217662 \times 10^{-19}$ C)

Then, we provide equations to calculate the photo-current, the diode reverse saturation current and its ideality factor.

$$I_{ph} = \frac{G}{G_{ref}} \cdot (I_{phref} + k_i (T - T_{ref})) \quad (4.4)$$

$$I_o = I_{oref} \left(\frac{T}{T_{ref}} \right)^3 \exp \left(\frac{E_g}{a V_t} \left(1 - \frac{T_{ref}}{T} \right) \right) \quad (4.5)$$

$$a = a_{ref} \left(\frac{T}{T_{ref}} \right) \quad (4.6)$$

Where,

- G : solar irradiance (W/m^2)
- k_i : short circuit temperature coefficient ($\%/^{\circ}C$)
- E_g : energy gap of the semiconductor material (eV)

Finally the circuit diagram is properly defined, as well as its *characteristic equation 4.1*. We can now represent the I-V curve of the solar cell, by means of substituting into equation 4.2 the following equations 4.3, 4.4, 4.5 and 4.6. This curve is composed by all the possible operation points of the solar cell, going from the short circuit ($I_{sc}, 0$) to the open circuit ($0, V_{oc}$), with a knee point in between them accounting for the maximum power point (MPP). This point, with coordinates (I_m, V_m), corresponds to the operating point where the solar cell is generating the maximum electrical power (P_{max}), and will be further taken into consideration later on. Figures 4.8 and 4.9 are two graphics taken from an actual data sheet [46], which will be used to provide real-life parameters to our model. They represent the I-V and the P-V curves of a module composed of 60 solar cells.

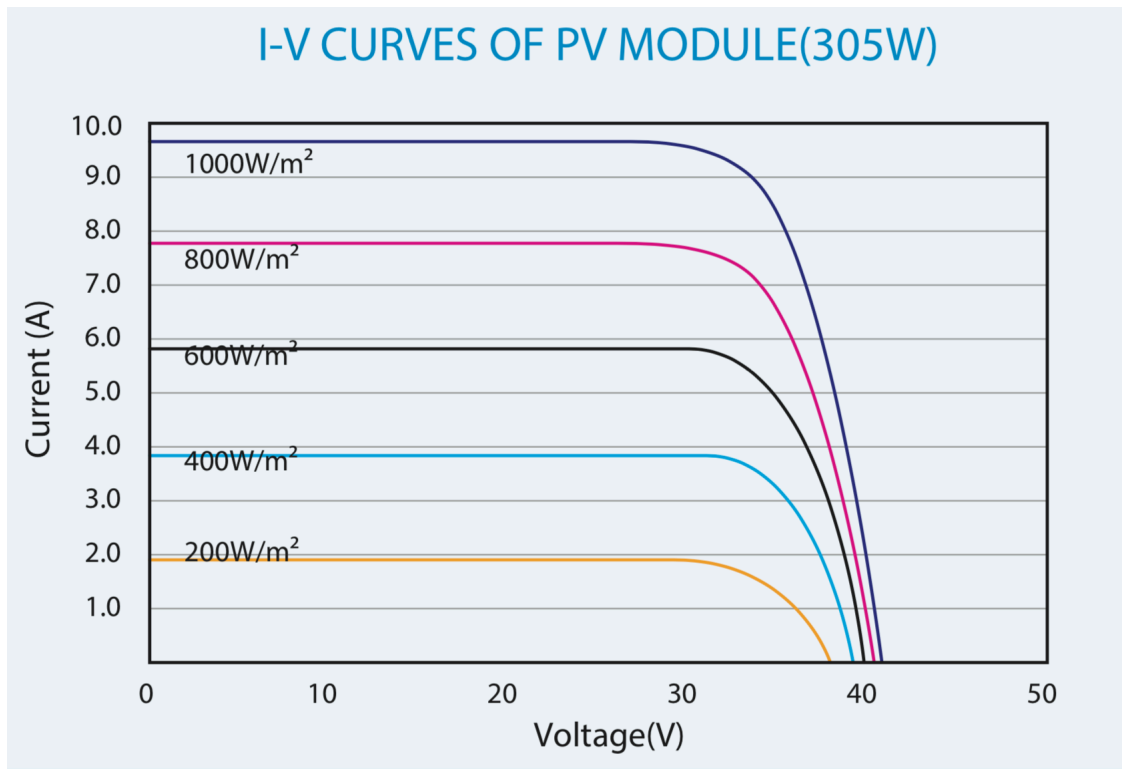


Figure 4.8: Current-Voltage curve depending on solar irradiance.

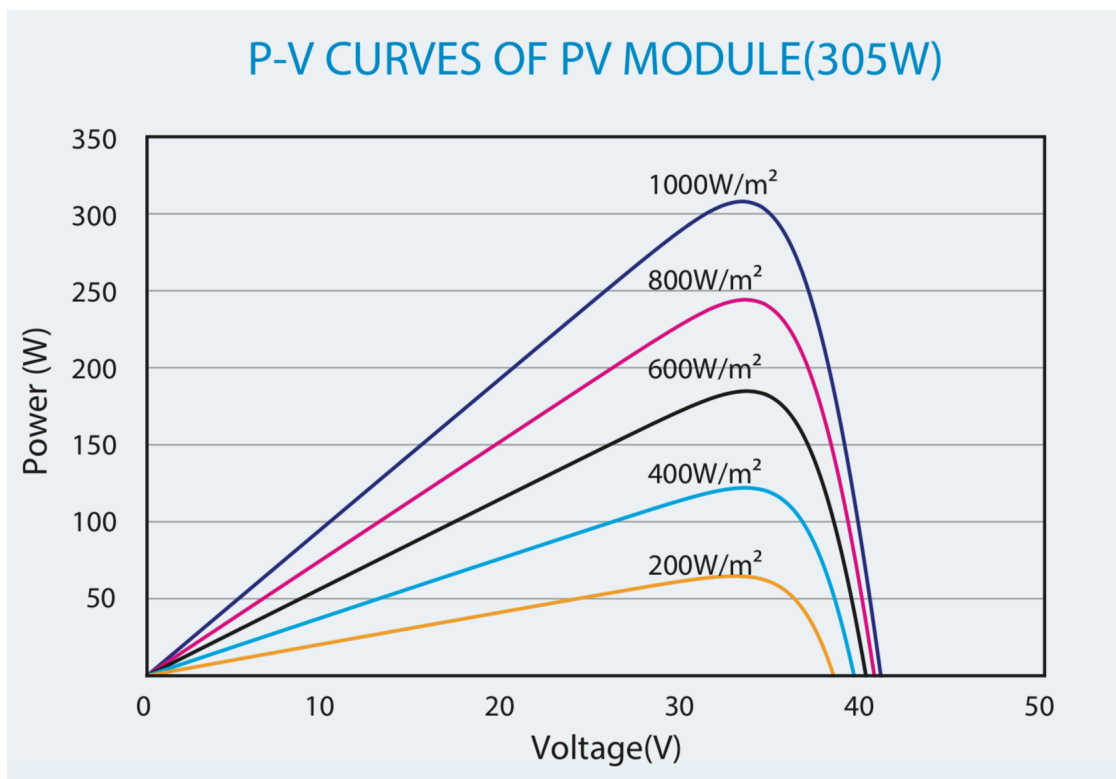


Figure 4.9: Power-Voltage curve depending on solar irradiance.

The above-presented five parameter model will be the one used for the modelling of the PV array, having the values from the data sheet as an input. However, some parameters are not available by the manufacturer, and therefore must be estimated using the STC⁵ electrical data provided. This is done by the software, allowing the user to choose whether the solar cell parameter estimation method is analytical or iterative (Newton-Raphson algorithm).

4.2.2. PV control system

The chosen control system for this grid-tied VSC⁶ is a *dq decoupled current control*. With this control strategy, we aim to regulate the real and reactive power exchange between the PV system and the grid. In a nutshell, the AC and DC voltages will be fed to the PV control system, which will then provide the firing pulses to the DC-AC converter as an output. The SPWM⁷ control technique, where a comparison between a high frequency triangle waveform and a low frequency sinusoidal reference signal is made to obtain the switching pulses, is deployed. Furthermore, other protection measures such as islanding detection, manual start&stop and voltage and current limitation will be implemented to guarantee the stability of the system under different operating conditions.

The dq decoupled current control functioning will be graphically explained through a number of control diagrams.

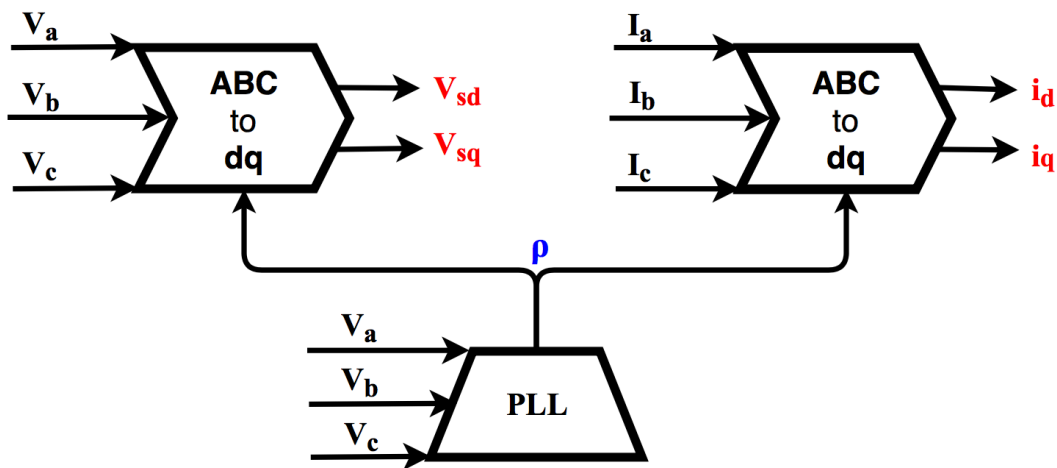


Figure 4.10: Three-phase to direct-quadrature-zero transformation of voltages and currents.

This transformation is applied on the VSC terminal voltages and currents, and the theory behind it relies on the Park's transformation matrix.

$$P = \frac{2}{3} \begin{bmatrix} \cos(\rho) & \cos(\rho - \frac{2\pi}{3}) & \cos(\rho + \frac{2\pi}{3}) \\ -\sin(\rho) & -\sin(\rho - \frac{2\pi}{3}) & -\sin(\rho + \frac{2\pi}{3}) \\ \frac{1}{2} & \frac{1}{2} & \frac{1}{2} \end{bmatrix} \quad (4.7)$$

The instantaneous transform angle ρ needed for the transformation matrix in equation 4.7 is supplied by a phase locked loop (PLL) controller, which synchronizes the converter control system to the AC microgrid voltage. This PLL must be fed with the VSC terminal voltages, as it can be seen in figure

⁵Standard Test Conditions: Irradiance 1000 W/m², Cell Temperature 25°C

⁶Voltage Source Converter

⁷Sinusoidal Pulse-Width Modulation

4.10. The scheme shown in figure 4.11 provides the core of the decoupled current control, obtaining the modulation voltages m_d and m_q .

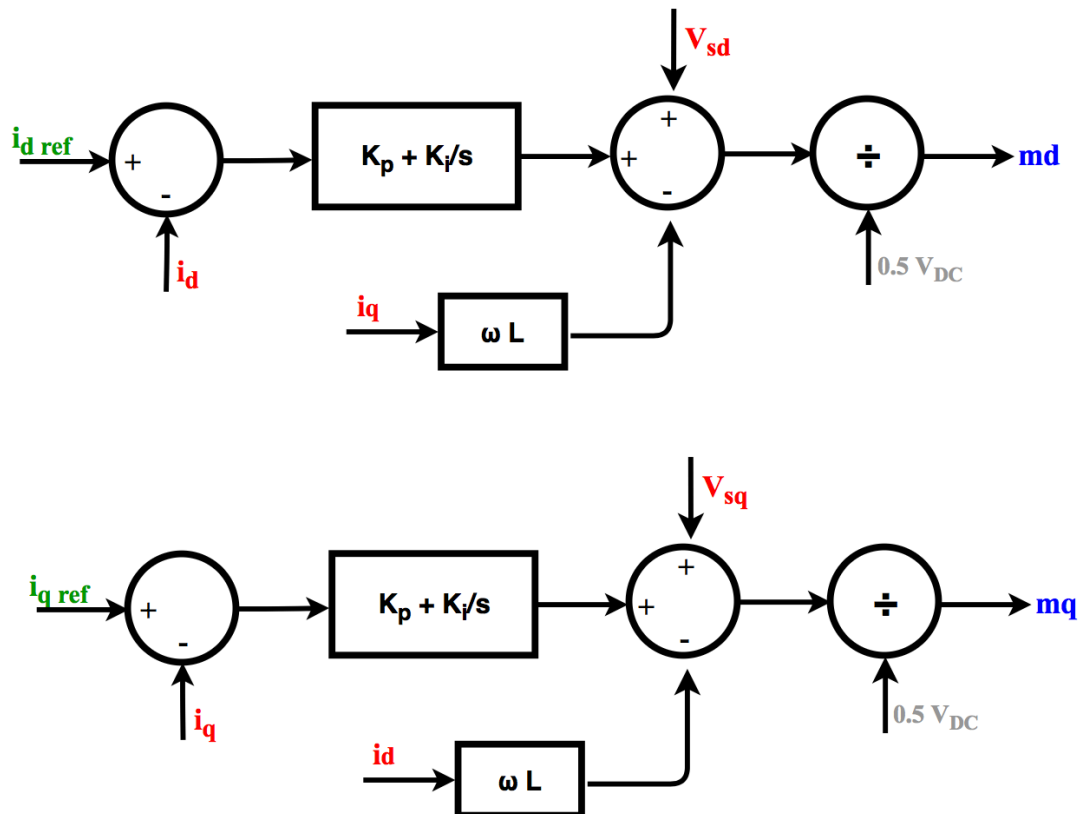


Figure 4.11: Decoupled dq current control.

The PI parameters K_p and K_i are determined by the following equation.

$$K_p = \frac{L}{\tau} \quad ; \quad K_i = \frac{R}{\tau} \quad (4.8)$$

Where L and R are the inductance and resistance of the Voltage Source Converter reactor, and τ is the time constant. This time constant is defined by the designer so that the closed loop bandwidth of the current controller is at least ten times smaller than the VSC switching frequency ($21 * 60$ Hz). With this considerations the current control is able to provide a faster response than the AC and DC voltage control loops.

Now the determination of the current control references (I_{dref} and I_{qref}) is to be deal with. The d -axis current control reference is obtained from an outer control loop used to regulate the DC bus voltage of the PV array. This bus is being regulated to a reference value obtained from the Maximum Power Point Tracking (MPPT) of the PV array voltage, as it can be seen in figure 4.12,

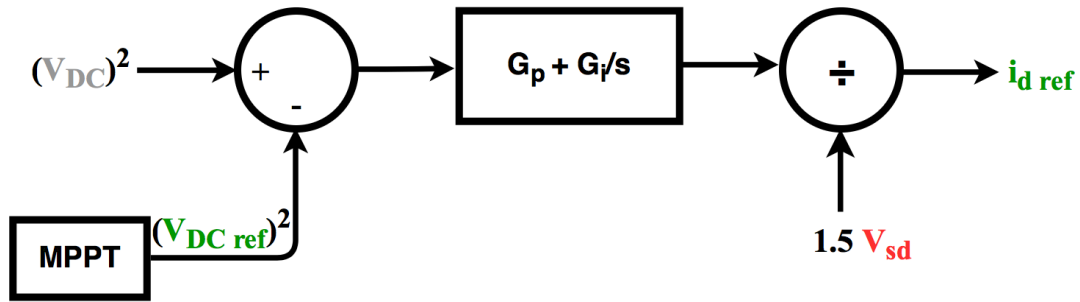


Figure 4.12: DC bus voltage control for the d-axis current reference.

Theory behind the MPPT and its attainment will be further analyzed once the control system has been properly explained. The q -axis reference for control could be set to a fixed value. That is why a typical strategy is to set it to zero, in order to stay close to unity power factor regulation. In our case, we will strive for providing AC voltage regulation, obtaining i_{qref} from an outer loop to provide grid-voltage support functions during grid transients or faults.

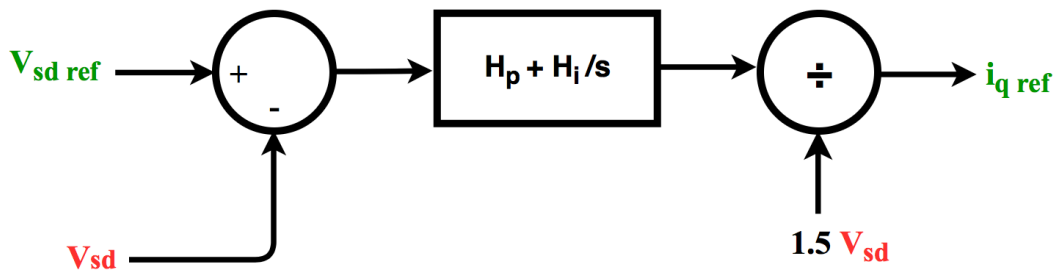


Figure 4.13: AC bus voltage control for q-axis current reference.

Where the reference for the AC voltage is obtained from equation 4.9.

$$V_{sd_{ref}} = \frac{\sqrt{2}}{\sqrt{3}} V_{rms} \quad (4.9)$$

The final step of the control involves the calculation of the VSC firing pulses, which will be the output of the whole PV control logic. To that end, both outputs of control diagrams 4.12 and 4.13 must be fed into a block performing the inverse Park's transformation (dq to ABC). Then, this three-phase output is to be the input of a block performing Sinusoidal Pulse-Width Modulation in order to obtain the VSC firing pulses, that will be fed into the DC-AC converter, completing the control loop.

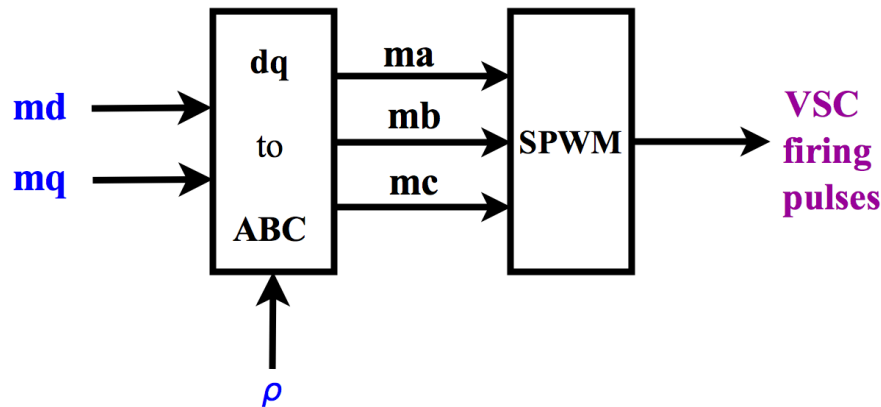


Figure 4.14: SPWM for VSC firing pulses.

Maximum Power Point Tracking (MPPT)

This subsection aims to provide general information about MPPT strategies, as well as to clarify the approach implemented in our control system.

The MPPT technique is related to the aforementioned I-V curve, which accounts for the output obtained from the solar cell. This output depends on several factors (solar irradiance, temperature of the solar cell, efficiency, etc), and for every given operating conditions there is a point where the product of the Voltage (V) and the Current (I) provides the highest power (P) output. This can be properly observed in figure 4.9, where every value of irradiance is plotted with a different curve, and every one of them presents a peak point (knee of the curve). Our system will provide maximum power in these knee points, and for every one of them there is a particular load resistance associated. Thus, an MPPT device should sample the output of the solar cell and vary the impedance seen by the PV array, in order to move the operating point towards the desired one.

Since the implemented PV array is a DC device, it makes use of a DC-AC converter to be connected to the microgrid, which can be used to perform variations on the impedance seen by the panel. In order to do so, modifications on the duty-ratio must be made. Therefore, and combining this procedure with continuous sampling of voltage and currents in order to have real-time information of the operating conditions, a dynamic tracking of the maximum power point can be achieved.

In our model two options will be provided so as to perform this estimation and feed the controller with the voltage corresponding to the MPP:

- **Direct method:** implements the widely accepted *Incremental Conductance method* algorithm due to its compromise between efficiency and computational burden. It is based in the *Hill Climbing method* (Perturbation and Observation Model), and implement small modifications to make it more robust.
- **Estimation methods:** these methods make use of the PV array's parameters to provide a direct estimation of the MPP voltage. When designing the PV control, two method are available for implementation: the *Lamber function approximation* and the *fractional open circuit voltage approximation*.

From the designer perspective there are advantages and disadvantages for the selection of both strategies. While the estimation methods present a faster point tracking with almost no oscillations in the voltage (compared to the incremental conductance method), the direct method has a more efficient implementation, as the operational complexity is lower. Both options will be implemented, leaving the decision to the user, which will be provided a switch that selects one or another.

4.3. Battery energy storage system (BESS)

Our microgrid implements four distributed energy resources, and two of them are converter-connected sources that make use of renewable energies (solar and wind). However, one of the main concerns regarding the implementation of renewable generation is that they are non-dispatchable sources of energy. Their particular intermittent nature involves that they cannot be turned on and off so that the different power needs are fulfilled.

In order to provide certain support to these two renewable DERs, a battery energy storage system (BESS) will be modelled and implemented within the electrical boundaries of the microgrid. It will serve a double function, as it can be charged when the PV system and the Wind Turbine are producing a surplus of power, and it can be discharged when the microgrid is in need of power supply, due to bad weather conditions.

Other situations in which the BESS can prove useful are the fast transients that appear when uncontrollable conditions arise, such as a violent change in the wind speed. This would result in the power output of the wind generator abruptly increasing, and if the connected AC grid is not strong enough, unwanted changes would appear in it (e.g. increase in the system frequency). The battery system can help mitigating and smoothing out the transients in these circumstances. Nevertheless, the implementation of this system obeys mainly the load leveling strategy presented above, as the simulations will be performed from a resilience perspective.

4.3.1. BESS modelling

Since the installation of batteries has the possibility of offering great benefits in the undergoing energy transition, this field is going through an extensive research. Several models and control strategies are continuously studied and proposed in the scientific community. In our model, a pre-defined block already present in the RSCAD Draft module's library will be made use of. It is based on a model which accounts for the I-V performance of a polymer Li-ion battery, taking into consideration all its dynamic characteristics [47].

The election of this type of battery attends to multiple reasons, including their high energy density, combined with a characteristic light weight. When developing the model, aiming to adjust it to reality, data from a commercial model of Li-ion polymer battery [48] has been extracted. The main parameter, which is directly taken from the data-sheet and fed into this model is the capacity of a single cell, which is 0.85 Amp-hour (Ah). Also, nominal voltage and charging voltage are specified, with values of 3.7 and 4.2 V respectively. In order to define a BESS that operates in the power range of the microgrid, several cells will be set both in series and parallel. This power output is affected by a number of key parameters, which hold direct repercussion in it:

- SOC: state of charge.
- Open circuit voltage, without load.
- Self-discharge rate
- Battery age
- Temperature dependence
- Battery charge and discharge cycles

Min/Rincon-Mora model

The model of the Li-ion battery is based on [47], which makes use of a curve-fitting method to extract the parameters. Before presenting the model, and given that the modelling is focused on the Voltage-Current characteristics of the battery (electrical behaviour), its reach must be made clear. From the aforementioned parameters, two aspects are left out of this analysis:

- Battery lifetime modelling: considering aspects such the long-term self-discharging.

- Thermal characteristics: such the thermal dependency of the circuit parameters.

With these considerations in mind, we now present the equivalent electrical circuit of the battery,

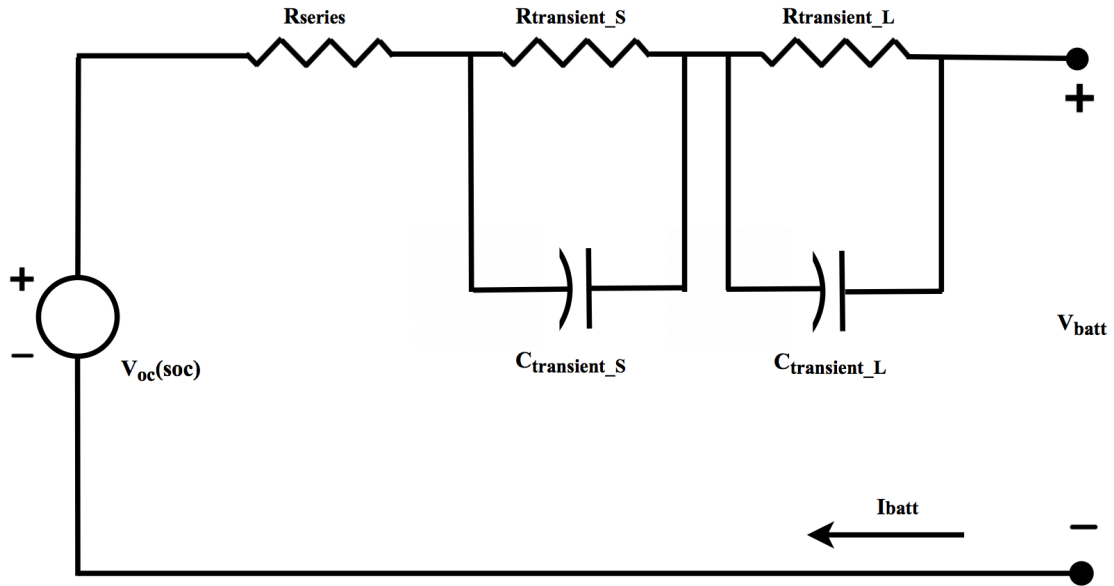


Figure 4.15: Electrical equivalent circuit of the Min/Rincon-Mora model.

Where the resistance $R_{transient_S}$ and capacitance $C_{transient_S}$ model the short-term transient of the battery, and $R_{transient_L}$ and $C_{transient_L}$ do the same for the long-term transient. The values of the RC time constants are chosen within the paper, keeping a compromise between accuracy and complexity of the model. Every parameter utilized in the equivalent circuit is non-linear and can be calculated as function of the state of charge (SOC), by using the equations presented hereafter.

$$V_{OC}(SOC) = -1.031 \cdot e^{-35 \cdot SOC} + 3.685 + 0.2156 \cdot SOC - 0.1178 \cdot SOC^2 + 0.3201 \cdot SOC^3 \quad (4.10)$$

$$R_{series}(SOC) = 0.1562 \cdot e^{-24.37 \cdot SOC} + 0.07446 \quad (4.11)$$

$$R_{transient_S}(SOC) = 0.3208 \cdot e^{-29.14 \cdot SOC} + 0.04669 \quad (4.12)$$

$$C_{transient_S}(SOC) = -752.9 \cdot e^{-13.51 \cdot SOC} + 703.6 \quad (4.13)$$

$$R_{transient_L}(SOC) = 6.603 \cdot e^{-155.2 \cdot SOC} + 0.04984 \quad (4.14)$$

$$C_{transient_L}(SOC) = -6056 \cdot e^{-27.12 \cdot SOC} + 4475 \quad (4.15)$$

The parameter State Of Charge (SOC) accounts for the quotient between the actual capacity of a battery and its nominal value. Several techniques are presented in technical literature for its estimation, and the one chosen by this model is the *Coulomb Counting Method*. The reason behind this choice is its convenience and accuracy when estimating the SOC of Lithium-Ion batteries [49]. The implementing formula is,

$$SOC(t) = SOC(t-1) + \frac{I_{cell}(t)}{Nominalcellcapacity} \Delta t \quad (4.16)$$

Given that the objective of the model is to represent the V-I characteristics, and the parameters have already been defined, the charge and discharge operation of the battery must be properly introduced. To that end, equations for the voltage V_{batt} and the current I_{batt} account for its behaviour, presenting two different cases: charge and discharge mode.

$$I_{battcharge}(t) = \frac{V_{oc}(SOC)(t) - V_{batt}(t)}{R_s + (R_{transient_S} \parallel Z_{c_{transient_S}}) + (R_{transient_L} \parallel Z_{c_{transient_L}})} \quad (4.17)$$

$$V_{battcharge}(t) = V_{source}(t) \quad (4.18)$$

$$I_{battdischarge}(t) = \frac{V_{oc}(SOC)(t)}{R_s + (R_{transient_S} \parallel Z_{c_{transient_S}}) + (R_{transient_L} \parallel Z_{c_{transient_L}}) + Z_{load}} \quad (4.19)$$

$$V_{battdischarge}(t) = V_{source}(t) \quad (4.20)$$

Finally, and once the model implemented has been accurately defined and explained, we move on to the next modelling consideration, the control.

4.3.2. BESS control

The control of the Battery Energy Storage System presents great similarities to the PV control system detailed in section 4.2.2. It is indeed a *dq decoupled current control*, which has been added the differentiation between grid-connected and islanded mode. Therefore, its explanation will not be as thorough as the one provided for the PV control system. We will focus on the differentiation between these two cases:

- **Grid-connected:** the obtainment of the references for i_d and i_q is made in the outer loop, given that is the same control technique presented in the PV case. The strategy for doing so can be faced from three different perspectives:
 1. By providing real and reactive references using P-Q sliders, that can be set by the user from the RunTime window.
 2. By performing P and Q control by means of PI controllers.
 3. By performing Voltage Control applied to the q-axis reference.

These three options will be implemented within the model, and the election of the obtainment of references shall be left for the user. From the RunTime module, and by making use of a dial, one of these three strategies can be elected.

Once this part is dealt with, the dq current control which makes use of the aforementioned references and performs the calculation of the modulation voltages is deployed by the inner loop. The schema implemented for that task is the same as the one presented in the PV control, and its implementation will be reflected in the next chapter.

- **Island mode:** when the microgrid is working in island mode, the obtention of the reference in the outer loop is performed by a direct voltage control which uses a PI controller. This results

in two values of modulation voltages different from the ones obtained in the grid-connected scenario, establishing a differentiation in the control system,

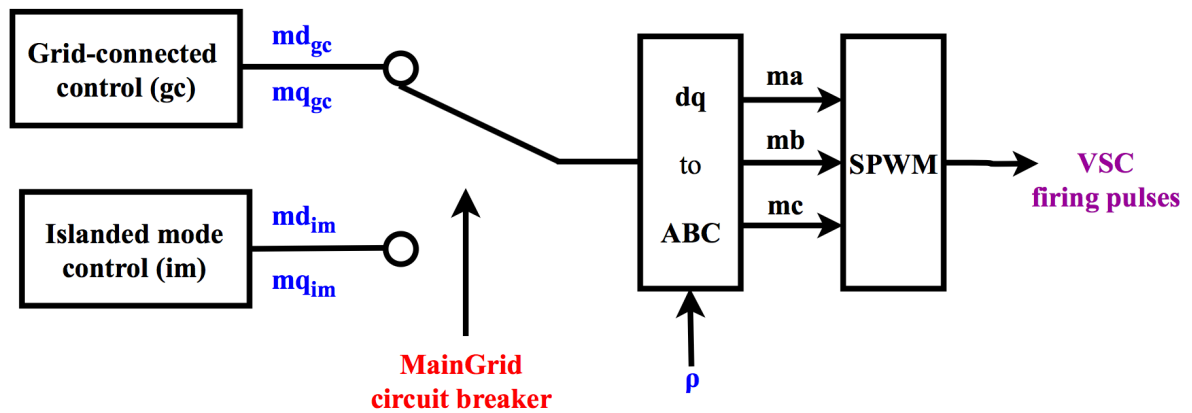


Figure 4.16: Grid-connected and islanded-mode control differentiation.

The control involving the VSC system is therefore completely explained, and the charging and discharging operation of the BESS shall be addressed next.

The power flow offered by the BESS can go in two directions, depending on whether the battery is charging or discharging. This can be controlled by varying the power values required from the system, which is made with the sliders controlling both the real and the reactive power.

- When choosing a **positive** value for the real power reference (P), we are performing a charging operation (power flow from AC to DC).
- When choosing a **negative** power order, we indicate that the system must deploy a discharging operation (power flow from DC to AC).

4.4. Wind energy system

The choice of modelling a wind energy system within our microgrid obeys two main reasons. Since one of the most important payoffs of the rise in distributed generation is the entailed penetration of renewable energies, and given that a PV system has already been modelled, the next logical step is to also implement a wind energy system. These two renewable distributed energy resources present a great rapport, as the wind turbines keeps providing power during the night, making up for the lack of photovoltaic generation.

Nowadays' energy panorama presents a widespread variety in renewable generation, and the implementation of a wind energy system helps obtaining a closer representation of it. Furthermore, and analyzing it from a resilience perspective, the fact that different distributed energy resources are included helps facing particular critical situations. For example:

- Floodings: when facing this situation, DERs situated at ground level such batteries or the diesel generator (which will be modelled in the next section) may suffer problems resulting in the cut of power supply. Nonetheless, a PV system installed on different rooftops or a prepared-enough wind turbine could keep supplying the loads through this critical situation.
- High-speed winds: may result in the wind turbines reaching the cut-out speed, and stopping its functioning. However, in this situation the PV array and the diesel generator would present fewer problems to maintain the power supply.

Finally, the non-dispatchable character of the a wind energy system and the PV system might appear as problematic when the microgrid is forced to work in islanded mode of operation. To keep the loads supplied during this situation, the previously modelled BESS and a diesel generator will provide assistance.

4.4.1. Wind energy system modelling

The wind energy generation system is to be modelled as a **Doubly Fed Induction Generator (DFIG)**. This choice, which is currently implemented in a great number of wind energy harvesting utilities, presents a basic principle derived from the problems faced by a synchronous generator. When implementing a synchronous generator, any variation in the wind's speed would make the blades accelerate/slow down. However, the aforementioned generator is fixated to the power grid's speed and cannot face these variations. The forces which arise in these situations are potentially harmful for the device, and in order to face these issues, the DFIG offers an alternative configuration.

Opposite to the concept of having a DC-field winding and an armature winding which serves as the output for the electricity, the double fed induction generation works with two 3-phase windings. The stationary one presents a direct connection with the output of the wind energy system, and the supplied power follows the desired grid frequency. The rotating one outputs power at a frequency that can differ from the grid's one. This power serves as an input for a back-to-back converter, which adjusts the phase and frequency to compensate the variations in the speed of the turbine. A DFIG presents offers several advantages over other configurations, which will be presented hereafter:

- While traditional wind turbines work with fix speed induction generators, DFIG-based wind turbines can offer the extraction of optimum wind energy in a wide range of wind speeds.
- The use of power electronics in the rotor circuit provide 4-quadrant active and reactive capabilities, allowing the induction generator to both import and export reactive power. This DER will then be able to provide reactive power support during critical situation to the microgrid, enhancing the power system stability.
- Compared to a system making use of a fully fed synchronous generator wired to a full-rated converter, the chosen configuration of the wind turbine decreases the power losses and converter costs [50]. This is derived from the fact that only a percentage of the total power (usually between 20 and 30%) is fed to the microgrid through the converter.

Once the theory behind a DFIG has been overviewed, as well as the opportunities that it offers to our modelled microgrid, a graphical representation is shown in figure 4.17. This circuitry will be duplicated in the Draft module and presented in the next chapter.

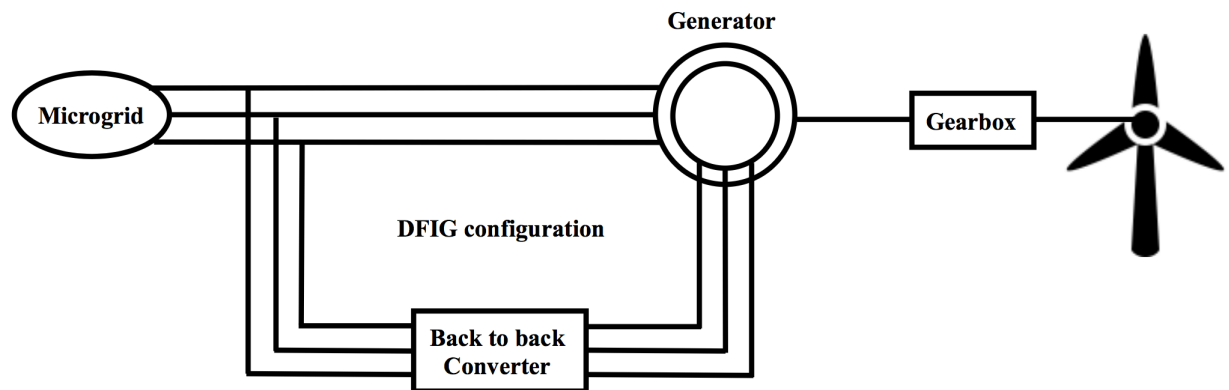


Figure 4.17: Configuration of a Double Fed Induction Generator.

Crowbar circuit

The necessity of implementing a crowbar circuit comes from the specific characteristics of the double-fed generator rotor, which usually presents between 2 or 3 times the amount of turns implemented in the stator (2.6377 in our case). The reason behind this design decision is to achieve lower rotor currents which result in a lower cost of the converter.

However, the other side of the coin involves higher rotor voltages, which when operating outside the operational range ($\pm 30\%$ synchronous speed) are above the rated rotor voltage, making the control impossible. Thus, a *crowbar circuit* must be implemented, in order to offer protection to the diodes and IGBTs of the converter. This circuitry is of vital importance during grid disturbances, which can present dangerous voltage transients, and performs a short-circuit of the rotor windings upon facing these situation. The short-circuit is applied by means of a protective shunt resistor between the back to back voltage source converters, in series with a switch. When the capacitor voltage goes above a predefined threshold or the rotor current rises beyond an upper limit, the switch closes and the capacitor voltage is reduced. These situations are often prompted by external faults in the AC system.

In particular, the type of crowbar circuit that would fit our model, from a resilience perspective, is the *active* crowbar circuit. This variation allows the removal of the short-circuit after applying it, typically within the range of milliseconds. We then gain the option of re-starting the converter almost immediately, improving the ride-through-faults capabilities of our distributed energy resource.

Wind Turbine and Multimass

In a nutshell, the model consists in a combination between the DFIG, the wind turbine and a multimass model. With these components, the mechanical torque would be calculated in the wind turbine, the speed in the multimass model and the final electrical torque would be provided by the DFIG.

- Wind turbine: its model is based on its steady state power characteristics, with the following equation accounting for it,

$$P_m = c_p(\lambda, \beta) \frac{\rho A}{2} v_{wind}^3 \quad (4.21)$$

Where,

- P_m : mechanical power output of the turbine (kW).

- $c_p(\lambda, \beta)$: performance coefficient of the turbine. Function of λ , the tip speed ratio, and β , the blade pitch angle.
- ρ is the density of air (kg/m^3)
- A : area swept out by the turbine blades (m^2).
- v : velocity of the wind (m/s)

Further information about the calculation of both the performance coefficient of the turbine and the density of the air can be found in the aforementioned manual.

- **Multimass**: simply computes the speed of its masses by integrating the difference between electrical and mechanical torque. In our case, two masses are modelled, the turbine itself and the DFIG. Self and mutual damping are left out of this analysis.

4.4.2. Wind energy system control

The modelling of the control is based on a "Wind-turbine driven doubly-fed induction generator" sample project offered in the RSCAD software, and therefore, the explanation provided will not be as profound as the ones before. The attached manuals to this project [10] can be consulted for better understanding.

VSC controls

We can differentiate two, the grid VSC control and the rotor VSC control. The main objective of the first one is to maintain at a constant level the capacitor voltage, while the rotor voltage source converter works by injecting/extracting current.

- **Grid VSC control**: it is current-regulated by transforming the three-phase currents to two-phase ones and then applying them to a rotating reference frame, extracting the AC fundamental components. These resulting currents have been already dealt with in the previous control strategies, and are called direct and quadrature currents (dq). The first one is used to regulate the capacitor voltage, and the quadrature component is used to adjust the terminal voltage.

The final output of the d and q current regulators is the voltage vector applied to create the requested currents. The first action performed on this vector is to convert it from the dq reference frame to its equivalent magnitude and angle. Then, it is converted to the stationary AC reference frame, which results in a modulation reference for each phase.

- **Rotor VSC control**: the principle behind this control is rather similar to the one applied in the grid VSC control. The rotor currents are converted with a rotating reference frame to quasi dc quantities, and then controlled with PI controls. However, in this case the rotating reference is computed as the slip angle⁸. This technique of decoupling d and q rotor currents allows us to control the torque and the rotor excitation current independently. The quadrature axis rotor current reference is derived from the optimal power reference calculation.

Optimal Power Reference Calculation

The optimal power reference calculation is used to provide the reactive rotor current reference, as the torque extracted from the DFIG can be expressed in equation 4.22,

$$T_e = -\frac{L_m i_{ms}}{2} i_{qr} pu \quad (4.22)$$

From the equation above we can see that by controlling i_{qr} we can control the electrical torque, where i_{ms} is relatively constant. Then, the optimal power that we can extract from a wind turbine is a

⁸Difference between the position of the stator flux vector and the physical rotor direct axis, which is generally changing

function of turbine shaft speed raised to the third power,

$$P_{opt} = K_{opt}\omega_r^3 \quad (4.23)$$

The expression for optimal electrical torque is almost the same as equation 4.23, except it is a function of speed squared. Finally, and to perform the obtainment of optimal power out of the wind turbine, optimal torque is calculated and then used to find the reactive rotor current reference by rearranging equation 4.22,

$$i_{qr}^* = \frac{-2 T_e^*}{L_m t_{ms}} pu \quad (4.24)$$

One last remark to make is that the rotational speed of the wind turbine is lower than the one of the DFIG, and therefore must be matched using a gearbox (as seen in figure 4.17). One per unit speed in the turbine may not be the same as one per unit speed in the DFIG, as it happens in our model, where when the turbine is turning at one per unit speed, the DFIG is doing so at 1.2 per unit.

Wind Turbine

The Wind Turbine control performs a different set of actions based on the speed of the turbine, which has been given a threshold of 1 pu.

If the speed is to rise above this value, (corresponding to a DFIG speed of 1.2 pu), the wind turbine control feathers⁹ the turbine blades. This action would also be performed if the power input to the DFIG drops below 1 pu, given that these drops in power output typically occur if the back to back VSCs are blocked.

If the speed is below the threshold, the controller acts as a proportional type control.

⁹Action of increasing the pitch angle of the blades by positioning the blades parallel to the airflow

4.5. Diesel generator

Although a diesel generator does not fall under the category of renewal-energy-related DERs, it contributes to the microgrid by enhancing its flexibility and providing certain independence from meteorological factors. Furthermore, it has been showed in Chapter 3 that microgrids with natural gas-fueled sources have been tested to have a higher probability of remaining operational after hurricanes.

One of the main reasons behind the implementation of a diesel generator as the fourth DER is the support that it provides to our microgrid when disconnection from the main grid is unavoidable. Due to its dispatchable nature, it will serve as a **load following DER**, adjusting its power output as demand for power fluctuates. Thus, the amount of power that the diesel generator provides to the microgrid will depend on:

- The meteorological situation of the environment where the microgrid is situated. If the transition to islanded mode of operation occurs during a sunny day with acceptable wind speeds, the power requirements asked to the diesel generator will be minimum. However, when facing critical situations when the power provided by the PV or the wind turbine system is below average, the diesel generator will have to account for a bigger share of the total power supply within the microgrid.
- The state of the loads, measured as the amount of power required. It varies depending on usage, hour of the day and several other factors.
- The state of other microgrids contained in the meshed system. When undergoing a widespread extreme event, nearby microgrids may be suffering from outages or failure in their generation systems, and will inquire electric supply if the modelled microgrid has a surplus of power.

To meet these requirements, the diesel generator is designed within the range of MW. In an ideal scenario, it would remain turned off during grid-connected scenarios and would only be required to provide power supply when facing unusual conditions in islanded mode of operation.

Diesel Generator modelling

The explanation provided for the Diesel Generator modelling will be brief, as it is performed with a pre-defined block available in the Draft module library, the electric machine model. Specifically, and since different cases of electric machines can be modelled, the chosen one that better suits the representation of a diesel generator is the "Synchronous machine model with transformer and loads".

As the name indicates, the block implements both the synchronous machine model and a (Δ -Y) transformer, based on zero sequence parameters given by the designer. The power size of the diesel generator has been set to 3 MW, and the model considers the inertia constant (H)¹⁰ and the synchronous mechanical damping (D)¹¹ among other parameters that will be left for the RSCAD implementation chapter,

Diesel generator parameters	
Rated apparent power	3.2 MVA
Power factor	0.9375
Inertia constant (H)	3.03 MW s / MVA
Synchronous mechanical damping (D)	2 p.u./p.u.

Table 4.4: Parameters of the diesel generator model.

Apart from the bus connection terminals, this model makes use of two inputs for its functioning and has three different outputs, which will be discussed hereunder,

¹⁰H stands for the rotational energy (in MW*second) stored in the machine rotor at rated speed per MVA of machine rating.

¹¹D prompts for the frictional damping factor, as the resulting damping torque tends to resist the speed. The damping torque factor "D" is in units of per-unit torque over per-unit speed deviation from zero speed.

- Field Voltage (EF): required as an input for the model, to provide the desired real and reactive power out of the machine for the specified machine terminal voltage. It is calculated by means of an excitation system, which is based on a PID controller, and makes use of the voltage provided by a power system stabilizer (which works with the machine speed W and a reference).
- Field Current (IF): is provided by the model as an output, and can be used for monitoring purposes.
- Machine Voltage (VMPU): output that accounts for the machine voltage in per unit, which is fed into the excitation system. The VMPU output is internally calculated by taking the square root of the sum of the line-to-line voltages squared and then scaling to per unit.
- Machine speed (W): the speed of the machine is provided as an output by the synchronous machine model, which can work in locked speed or in free speed mode. This value is then fed into a speed governor, which uses a PID controller and a speed reference to obtain the mechanical torque.
- Mechanical Torque (TM): required as an input by the block, is calculated in the aforementioned speed governor and fed to the synchronous machine model.

4.6. Loads

The modelling of loads within our microgrid does not entail a high-complexity process, as they have been modelled as dynamic loads. Thus, they will require to be supplied with active and reactive power in quantities decided by the designer during the simulation. The possibilities of simulating the change in energy consumption throughout the day, as well as critical situations where a load-shedding strategy must be followed are available with this approach.

The reason behind the selection of real life facilities as loads in our system has been previously discussed, as it is meant to establish a close relation between the survivability/resilience of our microgrid and the well-being of the vicinity in which it has been deployed. The geographic coordinates of each one of the four loads can be found in table 4.2, and their satellite location is defined in figure 4.1.

- Reinier de Graaf Hospital: a hospital is a top priority facility of a city, and the electricity supply must be guaranteed with no exception. It was chosen as a challenge to the microgrid, which will have to ensure its power supply through every critical event.
- Delft Station: connecting Delft with the cities nearby, it is the core of transportation and therefore, it is of high importance for the day-to-day life of its citizens. If it were to stop functioning, although it would not be considered a catastrophe, the consequences would be negative.
- Kievitlaan Neighborhood: this load accounts for the houses situated in the neighborhood, which would suffer a black-out in the case of the microgrid not being able to supply them. This situation is not desirable, but could be prompted if load-shedding is needed to ensure the survivability of higher-importance loads during a critical event.
- Herman BroerenSchool: accounts for a school facility, which should only require electric-supply during daytime, and whose disconnection in critical situations can be faced without big consequences for the vicinity.

From the provided descriptions it can be seen that there is a hierarchy between loads, based on the importance of their continuous functioning.

Hospital > Station > Neighborhood > School

Finally, it must be brought up that the values of these loads are purely fictional and will be estimated by the designer. Furthermore, they can be easily modified by the user in the RunTime module before, or while the simulations are taking place.

4.7. Cable calculations

This section aims to define the type of cable used in the microgrid, taking into consideration its topology and the loads and distributed energy resources that conform it.

To that end, we will focus on its material, section and insulation. Then, in the following chapter, another section will deal with the RSCAD implementation of an accurate cable model.

4.7.1. Material selection

The working voltage of the designed microgrid stands at 13.2 kV, categorizing our installation as medium voltage. Nowadays, and due to its competitive prices and excellent mechanical and electrical characteristics, aluminum-based cables are used in medium and high voltage applications. Therefore, when considering copper and aluminum as possibilities for the material used in the connecting wires, aluminum is the one selected.

In order to provide a more advanced insight on the reasons behind this design choice, a comparison between copper and aluminum properties will be presented [51].

First, the following material properties are exposed so as to consider the use of both materials as conductors: density, electrical resistivity, thermal expansion and ultimate tensile strength.

Property	Measurement units	Aluminum	Copper
Density (20°C)	$g \cdot cm^{-3}$	2.70	8.94
Electrical resistivity (20°C)	$n\Omega \cdot m$	28.2	16.78
Thermal expansion (25°C)	$\mu m \cdot m^{-1} \cdot K^{-1}$	23.1	16.5
Ultimate tensile strength	MPa	200	380

Table 4.5: Material *properties*¹¹ of aluminum and copper.

Reviewing the material properties from a conductivity perspective, the following conclusions are reached:

- The electrical resistivity ratio per volume of Copper compared to aluminum is approximately 3 to 5. Thus, if we want to have equal resistivity between both materials, the aluminum volume shall be increased by 68%. This results in aluminum conductors having larger cross sections for equal current carrying capacity.
- Aluminum and Copper's density relate as 1:3, which makes Copper around three times heavier than an equal volume of Aluminum.
- Finally, and combining both previous inferences, the balance tips in favor of aluminum. This is due to the resistivity ratio per mass of copper, which compared to aluminum is 2 to 1. This means that per kg, aluminum is two times better conductor than copper.

¹¹The values of the material properties are referred to pure elements, and therefore, they might differ per alloy.

LME COPPER HISTORICAL PRICE GRAPH



Figure 4.18: Price of commercial copper, given by LME¹.

12

LME ALUMINIUM HISTORICAL PRICE GRAPH

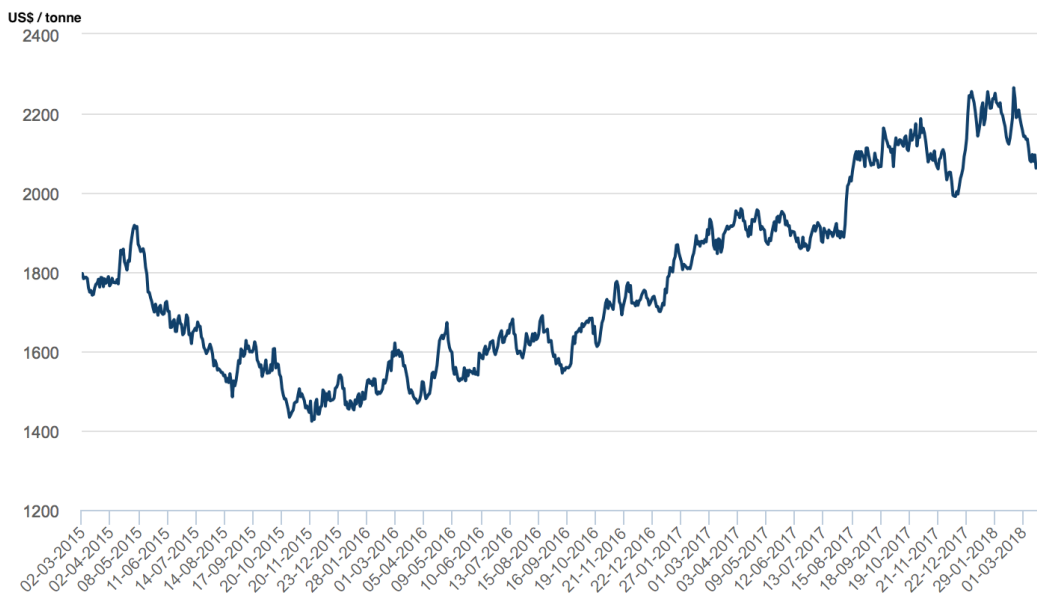


Figure 4.19: Price of commercial aluminum, given by LME.

When considering the price variations of the raw materials in the last three years, we observe a similar upward trend and a copper vs aluminum ratio of 3:1. Concretely on 1st of April, the prices are: 6683 US\$/tonne for Copper and 1996.5 US\$/tonne for Aluminum (real ratio: 3.347). Thus, combining the pricing and physical characteristics, the cost per amperage relation between Copper and Aluminum

¹²London metal exchange.

is above 6 to 1.

Finally, and involving the tensile strength in this comparison, we observe that raw copper has almost double the tensile strength of raw aluminum. However, electrical grade aluminum alloys enhance this characteristic, achieving the tensile characteristics of copper conductors.

4.7.2. Electrical calculations

The framework used for the electrical calculations is the Spanish royal decree-law 223/2008 [52], which approved the regulation regarding technical conditions and security guaranties in high voltage electric lines and its complementary technical instructions (ITC-LAT 01 to 09). This regulation applies to high voltage electrical installations, which include every installation with alternate three-phase current that operates under 100Hz and whose nominal voltage between phases is above 1kV.

Admissible current

For our particular case, the complementary technical instruction 06 will be used [53], and the area of the conductors will be determined based on its section 6, "admissible currents".

For each installation, and depending on its characteristics, configuration, operating conditions and insulation, the designer is to calculate the maximum current in permanent regime that does not exceed the assigned maximum temperature. This calculation must be done according to the UNE 21144 [54] This specific complementary instruction has been chosen because it applies to buried cables with voltage under $U_o/U =^{13}$ 18/30 kV. More specifically, for the purpose of determining the maximum admissible current, the installation is considered to use single-pole cables with dry insulation which are directly buried one meter deep in all their extension. The average thermal resistance of the ground is set to be $1.5 K \cdot m/W$, with an ambient ground temperature of 25°C and an ambient air temperature of 40°C. With these general specifications, table 4.20 provides a relation between the material of the conductor, its insulation and the minimum section necessary to work with a current that does not exceed the assigned maximum temperature,

Section (mm ²)	EPR		XLPE		HEPR	
	Cu	Al	Cu	Al	Cu	Al
25	125	96	130	100	135	105
35	145	115	155	120	160	125
50	175	135	180	140	190	145
70	215	165	225	170	235	180
95	255	200	265	205	280	215
120	290	225	300	235	320	245
150	325	255	340	260	360	275
185	370	285	380	295	405	315
240	425	335	440	345	470	365
300	480	375	490	390	530	410
400	540	430	560	445	600	470

Figure 4.20: Maximum admissible currents (A) in permanent regime.

¹³ U_o : assigned RMS (root mean square) voltage between each conductor and the cable shield, with industrial frequency, for which the cable and accessories have been designed.

U: Assigned RMS voltage between any two conductors, with industrial frequency, for which the cable and accessories have been designed.

Ethylene Propylene Rubber (EPR), Cross-linked polyethylene (XLPE) and High Ethylene Propylene Rubber (HEPR) stand for the different standard types of insulation that can be applied to the cables. For our calculations EPR insulation is chosen, as XLPE is recommended for applications with higher temperatures and HEPR is not widely used [55].

Then, the next step involves calculating the current that would be passing through the designed cable, in the worst case scenario. This would be the case of all the distributed energy resources operating at maximum power,

Distributed energy re-source	Active Power (MW)	Power Factor ($\cos \phi$)
Diesel Generator	3.00	0.9375
Battery energy storage system	0.5	1
Wind energy system	2.00	0.91
Photovoltaic system	1.74	1

Table 4.6: Active power generated by the DERs taking part of the microgrid.

As the microgrid operates with a star configuration and the system is balanced, we can calculate the current that would appear in the worst case scenario with the following equation,

$$P = 3 \cdot U_f \cdot I_f \cdot \cos \phi \quad (4.25)$$

$$7.24 \text{ MW} = 3 \cdot (13.2 \text{ kV} / \sqrt{3}) \cdot I_f \cdot 0.9492$$

$$I_f = 0.3336 \text{ kA}$$

Then, with this value of $I_f = 333.6 \text{ A}$ we enter the aluminum column under the EPR insulation in the table, obtaining a standardized section of 300 mm^2 . Given that the value was too close to the previous row, it has been decided to slightly oversize the design.

Voltage drop

Once the section has been determined based on the current that flows through the cables in the worst case scenario, this value must be verified with the voltage drop criterion. To that end, and assuming that each DER installation makes use of a voltage regulator that ensures the line to line 13.2 kV voltage of the microgrid, the longest distance between two DERs must be determined. It can be found between the Diesel Generator and the Photovoltaic system, being the total distance: **3.59 km**.

The calculations will be performed in accordance with [56], which presents the procedure of calculating the voltage drop in transmission lines under 50 km of length. These short transmission lines can be modelled with the circuit shown in figure 4.21,

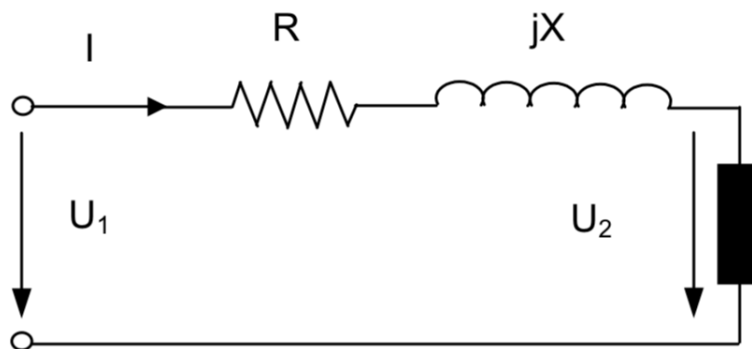


Figure 4.21: Equivalent circuit of a short transmission line.

Then, its vector diagram is provided, from which we will infer the formulas used in the voltage drop calculation.

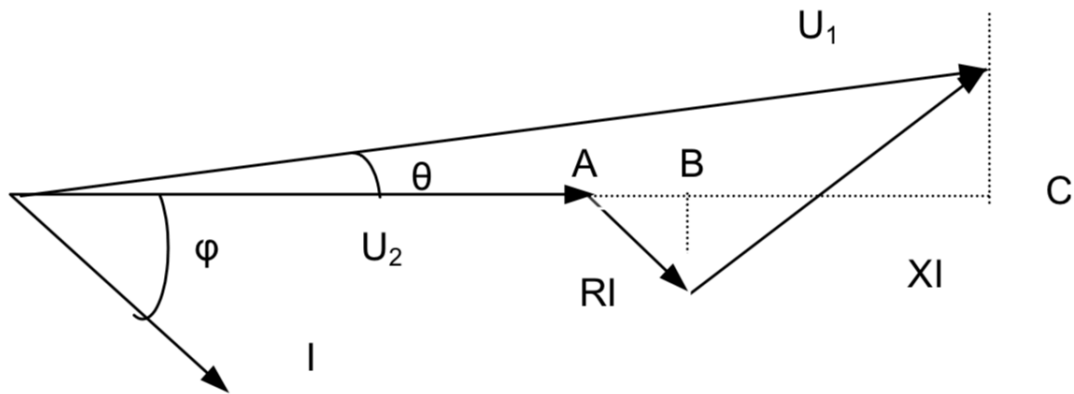


Figure 4.22: Vector diagram of the short transmission line equivalent circuit.

Giving the relatively small value of the θ angle, between the voltage at the origin and at the end of the line, we can assume with insignificant error that the U_{U1} vector matches its horizontal projection. Therefore, the voltage drop can be determined using the following equation,

$$AU = U_{U1} - U_2 \cong_u AB + BC = R \cdot I \cdot \cos\phi + X \cdot I \cdot \sin\phi \quad (4.26)$$

Giving that the power carried by the line is,

$$P = \sqrt{3} \cdot U_{U1} \cdot I \cdot \cos\phi \quad (4.27)$$

We can calculate the total voltage drop by substituting the current calculated by means of the equation 4.27 in the equation 4.26. Then, the following equation appears,

$$AU_{III} = (R + X \cdot \tan\phi) \cdot (P/U_{U1}) \quad (4.28)$$

Where,

- AU_{III} : line voltage drop in a three phase system (V).
- R: resistance of the line (Ω).
- X: reactance of the line (Ω).
- P: power carried by the line (W).
- U_{U1} : line three phase voltage (V).
- $\tan \phi$: tangent of the angle corresponding to the power factor.

Finally, and so as to obtain the value of the voltage drop, both the resistance and the reactance of the lines shall be calculated.

The value of the reactance (X) varies with the diameter and the spacing between the conductors. For determining its value, the document offers two different options: in absence of data it can be estimated to be 0.1 Ω /km, and it can also be calculated as an additional increment of the resistance. The latter option is chosen, and using the table values provided in the document we estimate the reactance of the line as,

$$X \cong 0.25 \cdot R \quad (4.29)$$

The value of the resistance (R) of the cable is calculated with a combination of equations, given in the document, that result in,

$$R = c \cdot \rho_{20} \cdot [1 + \alpha \cdot (\theta - 20)] \cdot L/S \quad (4.30)$$

Where,

- ρ_{20} : resistivity of the conductor with a temperature of 20 °C ($\Omega \cdot mm^2/m$).
- α : variation coefficient of specific resistance per conductor temperature ($^{\circ}C^{-1}$).
- c: increase in resistance in alternate current. Can be estimated to be 1.02 for link installations.
- θ : conductor temperature ($^{\circ}C$).
- L: line length (m).
- S: conductor section (mm^2).

Once we have reached this point, we have all the data necessary to obtain both R and X, needed for the final calculation of the maximum voltage drop.

Material	ρ_{20} ($\Omega \cdot mm^2/m$)	α ($^{\circ}C^{-1}$)	L (m)	S (mm^2)
Aluminum	0.029	0.00403	3590	300

Table 4.7: Data necessary for voltage drop calculation referred to aluminum cables.

The values of active power (7.24 MW) and working line-to-line voltage of the microgrid (13.2 kV) had already been determined. The conductor temperature is set to be 90°C, as specified for EPR insulations by table 5 of complementary technical instruction [53]. Thus, we proceed to calculate the values of resistance and reactance using equations 4.30 and 4.29,

$$R = 1.02 \cdot 0.029 \cdot [1 + 0.00403 \cdot (90 - 20)] \cdot 3590/300$$

$$\mathbf{R = 0.4538 \Omega}$$

$$\mathbf{X = 0.25 \cdot R = 0.1135 \Omega}$$

With this values we substitute in equation 4.28, obtaining,

$$AU_{III} = (0.4538 + 0.1135 \cdot \tan(18.34)) \cdot (7.240.000 \text{ W} / 13.200 \text{ V})$$

$$\mathbf{AU_{III} = 269.54 \text{ V}}$$

This result represents a voltage drop of 2,04%, which is acceptable as it stands below the 3% limit. This calculation validates the initial section obtained with the *admissible current* criterion and therefore, **S=300 mm^2** will be the used section in our microgrid.

5

RSCAD implementation

This chapter is focused on the implementation of the model developed in chapter 4, which will be done by making use of the RSCAD software. The microgrid's sample-projects provided by RTDS technologies [10] are used as the starting ground. Thorough and concise explanations of both the software and the implemented modelling will be provided, so that any person with an engineering background would be able to follow the implementation process.

5.1. Modelling tool

Its name is **RTDS Simulator**, a real time power system simulation tool that allows to perform distributed generation studies and power electronics simulation among other functions. It has been developed by RTDS technologies [10], and it consists in an "all-in-one" software and a custom hardware, enabling the deployment of all the phases needed to prepare and run simulation, as well as to analyze their results. It is able to operate in real time, providing continuous and accurate data within a frequency range that goes from DC to 3 kHz. Against traditional programs in the field of stability and load flow simulation, which perform studies in a limited frequency range, the RTDS simulator offers a better depth of analysis.

Custom Hardware

The working hardware of the simulator is modular and consists on a chassis, that can accommodate from 1 to 10 cores. Maximum expansion of the system that could be achieved while maintaining full connectivity is 60 chassis. The TU Delft university has made available for the Intelligent Electrical Power Grids group a chassis with eight installed cores, which will be used when running the desired simulations.

What makes the RTDS Simulator a world standard for real time power system simulation is the ability to simulate complex networks with time-steps between 25 and 50 μs and particularly, the simulation of *fast* switching power electronic devices within a frequency range of 1 to 4 μs . The latter allows to perform enhanced real time EMT ¹ simulations, by means of small time-step sub-networks. The principle behind this feature is the modification proposed and executed by RTDS technologies on the Dommel-conductance for the device, which results in the modification of the conductance matrix [57].

Furthermore, the chassis comes with standard DIN rails where I/O cards and other components can be installed. This feature presents functionalities out of the scope of the project, but could allow our simulation to be interfaced with external equipment (e.g. protective relays) in further extensions of the project.

The newest generation of this state-of-the-art simulation hardware is called NovaCor, and our equipment presents two NovaCor cores. These cores, in addition to several improved features, allow to

¹ElectroMagnetic Transient

simulate hundreds of nodes on a single core, which turns out specially helpful in our particular modelling/simulation.

All-in-one Software (RSCAD)

The aforementioned custom hardware has an ad-hoc software to be interfaced with, called RSCAD. As the RTDS Simulator works in real-time, the simulated model can be operated similarly to a real power system. Thus, the software allows parameters to be modified and faults to be applied while the simulation is running, providing the user with the possibility of watching the system's response in real time. Its *all-in-one* nature comes from the fact that it consists on seven modules designed to provide the users with all the necessary tools to prepare and perform precise and accurate simulations. These modules are named: FileManager, Draft, RunTime, TLine, Cable, MultiPlot, and CBuilder. Although the two main used tools in our modelling are Draft and RunTime, a brief explanation of all of them will be provided.

- **FileManager:** graphical interface which allows the user to organize and share simulation projects and cases. It acts as a launcher for the other modules.
- **Draft:** it is the main tool when designing the circuit, as it is used to graphically assemble the diagram of the system. It comes with libraries regarding power system, control, automation component models, and protection, which allow the designer to make use of pre-defined models. The compiling of the circuit is performed in this module, which is linked to the next one (RunTime), where the simulation runs.
- **RunTime:** running on the host computer, this module allows to load, run and control the simulation of the circuits designed and compiled in the Draft tool. It presents an interactive canvas, where the designer can place switches, buttons, sliders, plots, meters, etc.
- **TLine:** it has a double function. The user can enter data of DC and AC transmission lines for the module to convert it into a form used by the Draft module, and it can also be used to calculate parameters for traveling wave models, which will be made use of.
- **Cable:** allows to convert physical cable data into a form used in the Draft module
- **Cbuilder:** module that can be used when the user needs customized blocks for the circuit or when changes to the standard ones need to be applied.
- **MultiPlot:** allows an accurate analysis of the RTDS Simulator results, with several plotting and data export options.

5.2. General overview of the model

Following certain parallelism with Chapter 4, we start from a general plane and the following sections will be dedicated to specific DERs and loads. This current section aims to give the overview of the developed simulation model, choosing for that purpose the circuitry developed in the Draft module. Once the whole implementation, both general and particular-based, has been properly explained, the interface developed in the RunTime module will be presented.

Given that the Draft canvas has a landscape format, and in order to provide a higher resolution of the image, we have divided it in two different figures. The first one (figure 5.1) accounts for the microgrid's connection to the main grid,

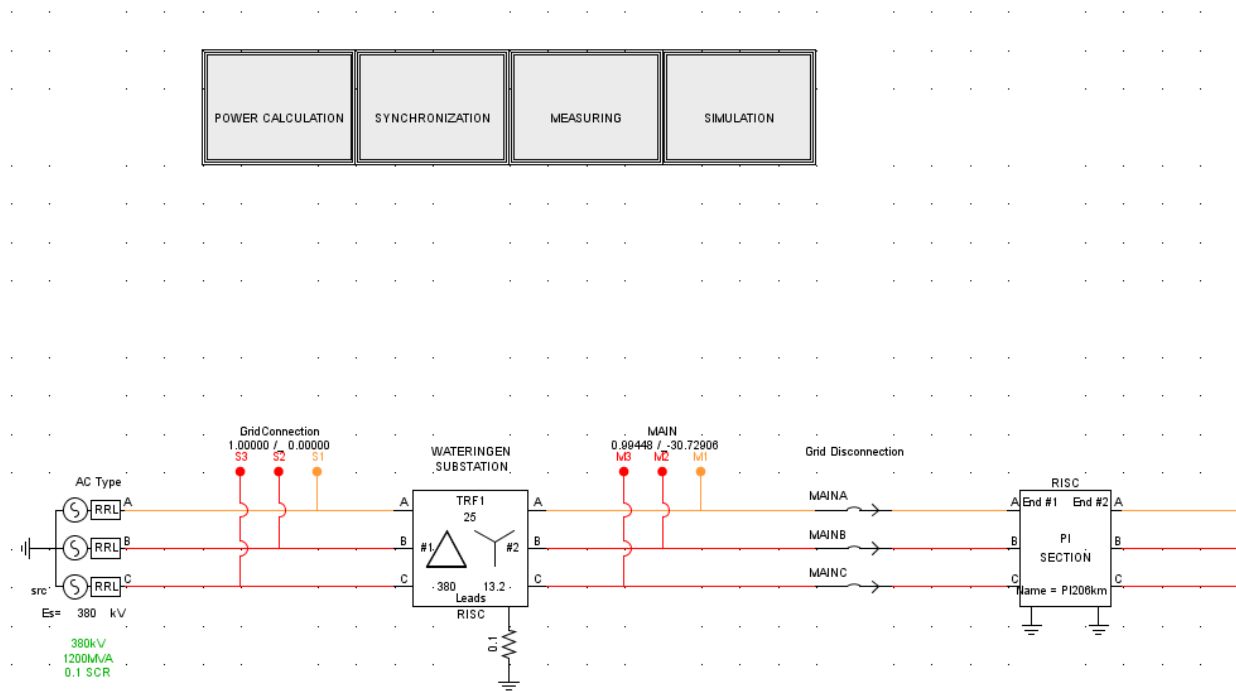


Figure 5.1: Draft circuitry of the microgrid's connection to the main grid.

In this part of the circuit diagram we can observe that the lines are represented in 3-phase format, with every line section presenting a different nomination for each phase. Furthermore, we can differentiate four elements composing this left side of the Draft canvas:

- **The main grid**, modelled as a 380kV source. This specific voltage has been chosen according to the high-voltage line to which the Rijswijk Wateringen Substation is connected (figure 4.3). The specified frequency is 60 Hz, given that RTDS technologies is a Canadian company, which provides most of the documentation and sample-projects with that frequency. Furthermore, the most advanced studies and implementations of resilience in Smart microgrids are being conducted in the United States, which works with the same frequency.
- A **three phase circuit breaker** that allows both connection and disconnection from the main grid. It can be triggered by a failure of the grid, by the command of the microgrid's control or manually from the RunTime interface.

C Phase Breaker Data		INITIAL LOADFLOW DATA			
A Phase Breaker Data		B Phase Breaker Data			
Name	Description	Value	Unit	Min	Max
Anam	A Phase Breaker Name	MAINA			
ARcls	A Phase Breaker Closed Resistance	0.1	ohm	1E-9	
Aholdi	Extinguish Arc for abs(I) at or below:	0.0	kA	0.0	10.0
Asig	Signal Name to control breaker	MAIN			
Abit	Active bit number in Asig to control breaker	1		1	21
Amon	Monitor breaker current	Yes			
IAnam	Breaker Current Signal Name	MAINIA			

Figure 5.2: Block parameters of the three-phase breaker.

As it can be seen in figure 5.2, every phase of the breaker can be properly designed by the user. Opposite to the ideal model of a breaker, where the closed resistance is set to be zero, here we can provide a value. The chosen value is 0.1 Ω . Moreover, and when command to open is given to the breaker, this block will compare the absolute value of the current flowing with the "Aholdi" item value. If this absolute value of the current is at the threshold or below, current will be interrupted. Normally, the designer provides a value 0.0 to this threshold, since interrupting current in an inductive circuit would result in a voltage spike.

The control of the breaker is made with a signal, in this case by the name of *Main*. It is interpreted as a binary signal, where the "Abit" parameter assigns a bit number of the signal to control this phase of the breaker. It can be chosen differently for every phase when desired. In this case the same bit number is controlling all three phases, which will make the breaker being closed when it is high and open in the opposite case.

Furthermore, the option to monitor the current of every phase of the breaker is enabled, providing great possibilities when simulating and analyzing the results.

- A block called **PI section**, that models the line (with length 2.06 km in this particular section) that separates the substation and the first node of the microgrid. It does so with a lumped parameters representation. We do not go into details, as it will be further explained in the section regarding the cable utilized in the microgrid. Both the calculation needed and the implementation of the results in the block are left to be explained.
- The **Rijkswijk Wateringen Substation**, modelled as a transformer that reduces the high-voltage to the 13.2 kV used in the microgrid. The transformer can be modelled with an ideal, linear or saturation model. The latter has been chosen, in order to provide a more accurate simulation of this substation. Figure 5.3 shows the transformer parameters.

FLUX OFFSET INPUT SETUP		MONITORING		FLUX & MAGN CURRENT MONITORING		
CONFIGURATION		CORE ASSIGNMENT		WINDING #1	WINDING #2	SATURATION
Name	Description	Value	Unit	Min	Max	
Trf	Transformer Name	TRF1				
YD1	Winding #1 Connection	Delta				
YD2	Winding #2 Connection	Y				
Lead	Delta lags or leads Y	Leads				
type	Transformer Model Type	Saturation				
tapCh	Tap Changer (type cannot be Linear)	No				
edge	Tap Trigger on	Rising Edge				
inps	Tap Changer Inputs	RunTime				
Tmva	Transformer rating (3 Phase)	25	MVA	0.0001		
f	Base Frequency	60.0	Hz	1.0	300.0	
xl	Leakage inductance of Tx	0.08	p.u.	0.001		
NLL	No load losses	0.002	p.u.	0.00	1.0	
NLLtp	No load loss branch type	Winding				

Figure 5.3: Configuration parameters of the transformer.

The saturation has been chosen to be in the first winding, with a magnetizing current of 1%. This winding has a delta configuration, while the second has a Y configuration, shared with the microgrid.

FLUX OFFSET INPUT SETUP		MONITORING		FLUX & MAGN CURRENT MONITORING		
CONFIGURATION		CORE ASSIGNMENT		WINDING #1	WINDING #2	SATURATION
Name	Description	Value	Unit	Min	Max	
Sat	Saturation Placed on Winding	#1				
Xair	Air core reactance	0.2	p.u.	1E-3	10.0	
Tdc	Leaky Integrator Time Constant	100.0	sec	1E-3		
Xknee	Knee voltage	1.25	p.u.	0		
Lw	Loop width	30	%	0	100	

Figure 5.4: Configuration parameters of the transformer.

The second figure 5.5, representing the right part of the Draft canvas is displayed hereafter. It accounts for the configuration of the circuitry of the microgrid, where the resilience-related improvements defined in section 4.1.1 have been implemented.

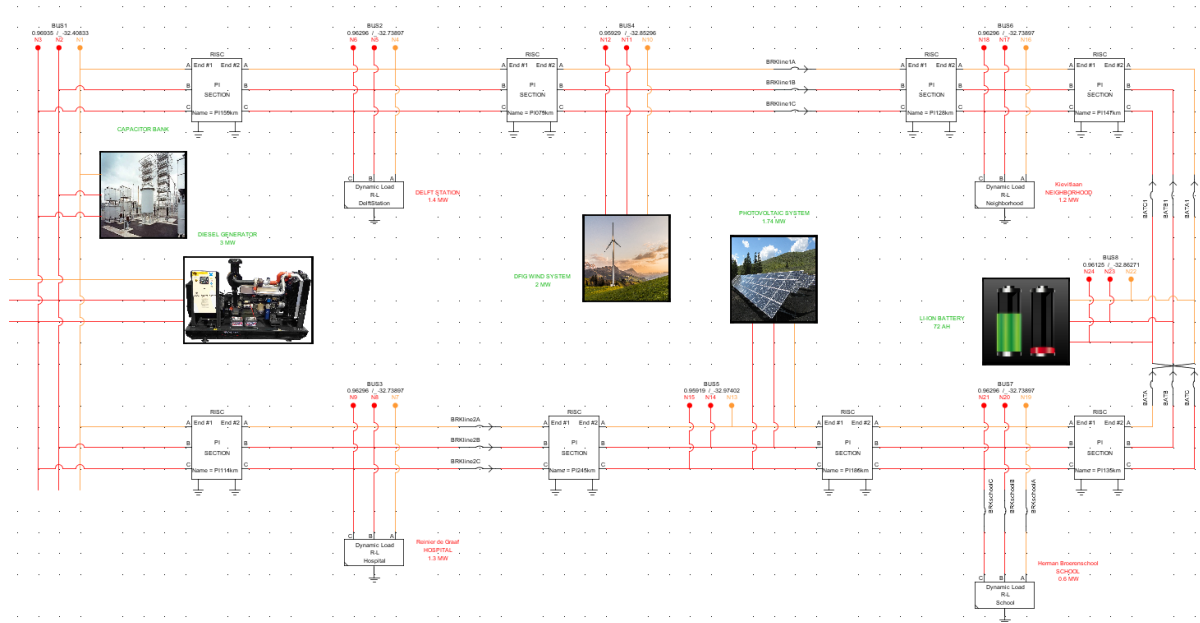


Figure 5.5: Draft circuitry of the complete microgrid.

We can observe a clear loop-based topology applied to the microgrid, where the four distributed energy resources previously defined and mathematically modelled are included as square blocks. The circuitry behind these blocks, which implements the mathematical approach developed in chapter 4 will be thoroughly explained in the following subsections.

The loads are here represented as Dynamic Loads, given that the power consumption of the facilities may be changing due to customer schedules, daily activity or exceptional situations. They start with a standard value provided by the designer, and will be subject to modifications from the RunTime interface.

Finally, a block already presented in figure 5.1 can be seen in all the connection between loads and DERs, the PI SECTION. As previously stated, it accounts for the behaviour of the transmission lines, and its implementation and the parameter calculation will be later explained.

5.3. Photovoltaic system

The general RSCAD implementation of the photovoltaic system can be seen in figure 5.5, where it is represented as a square block with a photo showing a photovoltaic panel. The Draft software tool allows to group circuitry and components under these type of "block" constructions, showing a simpler overview of the system. In order to explain how the implementation of the model has been deployed, we proceed layer by layer, starting from the most general one.

5.3.1. Solar cell parameters

This first subsection is going to serve as a link between the model and a real-life solar cell. To that end, a data-sheet from one of the biggest PV manufacturers, TrinaSolar, has been chosen [46]. The parameters used in the deployed model will be taken from this data sheet, in an attempt to provide an accurate and up-to-date PV system modelling.

The chosen PV module works with module configurations of 60 cells, providing power in the range of 275-315 W. Its electrical data, under STC², is presented in figure 5.6,

ELECTRICAL DATA (STC)

Peak Power Watts- P_{MAX} (Wp)*	275	280	285	290	295	300	305	310	315
Power Output Tolerance- P_{MAX} (W)	0 ~ +5								
Maximum Power Voltage- V_{MPP} (V)	31.4	31.7	31.8	32.2	32.5	32.6	32.9	33.1	33.3
Maximum Power Current- I_{MPP} (A)	8.76	8.84	8.97	9.01	9.08	9.19	9.28	9.37	9.46
Open Circuit Voltage- V_{OC} (V)	38.4	38.4	38.5	38.9	39.6	39.8	40.0	40.2	40.5
Short Circuit Current- I_{SC} (A)	9.24	9.42	9.51	9.66	9.68	9.77	9.85	9.94	10.0
Module Efficiency η_m (%)	16.8	17.1	17.4	17.7	18.0	18.3	18.6	18.9	19.2

STC: Irradiance 1000W/m², Cell Temperature 25°C, Air Mass AM1.5.
*Measuring tolerance: $\pm 3\%$.

Figure 5.6: Data-sheet of the electrical characteristics under STC.

The 300W Peak Power Watts model has been chosen, presenting the following particular data (table 5.2),

Electrical data (STC)	
Power Output Tolerance	~ + 5 W
Maximum Power Voltage (V_{MPP})	32.6 V
Maximum Power Current (I_{MPP})	9.19 A
Open Circuit Voltage (V_{OC})	39.8 V
Short Circuit Current (I_{SC})	9.77 A
Module Efficiency	18.3%

Table 5.1: Electrical data of the chosen 300W version.

These values will be later introduced in the model, along with the temperature-coefficients that are needed for the equations presented in section 4.2.1. The manufacturer provides the data for these values,

²Standard Test Conditions

TEMPERATURE RATINGS

NOCT (Nominal Operating Cell Temperature)	44°C ($\pm 2^\circ\text{C}$)
Temperature Coefficient of P_{MAX}	- 0.39%/°C
Temperature Coefficient of V_{OC}	- 0.29%/°C
Temperature Coefficient of I_{SC}	0.05%/°C

Figure 5.7: Temperature ratings for the PV 300W module.

Once the model is fed with the electric data provided in the data-sheet, we are able to make an estimation of the maximum power that we could obtain from the system when operating under Standard Test Conditions. To that end, these simple equations must be used in order to calculate the voltage and current that the PV array outputs,

$$V_{DC} = N_s \cdot V_{MPP} \quad (5.1)$$

$$I_{DC} = N_p \cdot I_{MPP} \quad (5.2)$$

Where,

- N_s accounts for the number of modules in series.
- N_p accounts for the number of modules in parallel.

We intend to design a PV system which under these Standard Test Conditions is able to provide 2 MW. To that end, and knowing beforehand V_{MPP} and I_{MPP} (table 5.2), we determine the installation to comprise 62 modules in series and 94 in parallel.

$$V_{DC} = N_s \cdot V_{MPP} = 62 \cdot 32.6 \text{ V} = 2.021 \text{ kV}$$

$$I_{DC} = N_p \cdot I_{MPP} = 94 \cdot 9.19 \text{ A} = 0.864 \text{ kA}$$

Then, we calculate the power injected to the microgrid under these circumstances by means of ,

$$P_{\text{solar}} = V_{DC} \cdot I_{DC} = 2.021 \text{ kV} \cdot 0.864 \text{ kA} = \mathbf{1.745 \text{ MW}}$$

The next logical step is to characterize the mechanical parameters of the PV module. These values are not fed into the modelling, but can help envisioning the real system. Furthermore, the response of the product under critical environmental condition is slightly exposed. The mechanical data table 5.8 provided by [46] is,

MECHANICAL DATA

Solar Cells	Monocrystalline 156.75 × 156.75 mm (6 inches)
Cell Orientation	60 cells (6 × 10)
Module Dimensions	1650 × 992 × 35 mm (65.0 × 39.1 × 1.38 inches)
Weight	18.6 kg (41.0 lb)
Glass	3.2 mm (0.13 inches), High Transmission, AR Coated Tempered Glass
Backsheet	White [DD05A.08(II)]; Black [DD05A.05(II)]
Frame	Black Anodized Aluminium Alloy [DD05A.08(II), DD05A.05(II)]
J-Box	IP 67 or IP 68 rated
Cables	Photovoltaic Technology Cable 4.0mm ² (0.006 inches ²), 1000 mm (39.4 inches)
Connector	MC4
Fire Type	Type 1 or Type 2

Figure 5.8: Mechanical data of the 300W PV module.

Data such the dimensions of the solar cells, the dimensions of the module or the total weight gives an idea of the physical characteristics of the system, while data regarding the cable dimensions accounts for the electrical connections. Then, a brief resilience-related summary of mechanical characteristics is given. It consists of the wind load, snow load and resistance against hail stones.

Certified to withstand	
Wind Load (Pa)	2400 Pa
Snow Load (Pa)	5400 Pa
35 mm hail stones	At 97 km/h

Table 5.2: Withstanding of challenging environmental conditions.

5.3.2. Grid-connected PV system Draft overview

Getting back to the RSCAD implementation, the first layer of the PV array implementation can be accessed by entering the aforementioned block (figure 5.5). Inside this construction we can find the schematic diagram of a grid-connected PV system, which makes use of a DC-AC converter. Another block containing all the circuitry concerning the PV control can be found in this layer and will be later thoroughly explained.

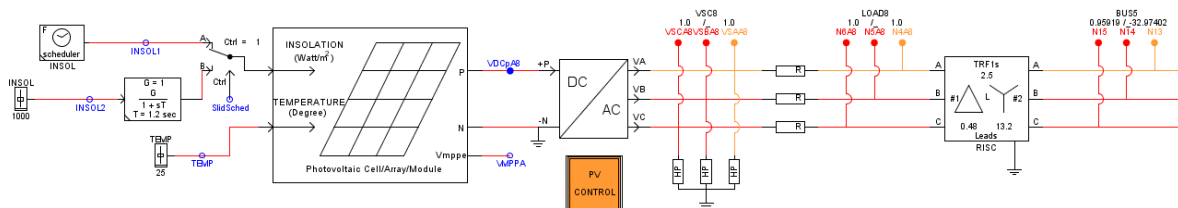


Figure 5.9: Grid-connected PV system Draft overview.

Starting the analysis of figure 5.9 from left to right, we can differentiate a series of specific components.

PV array model

It consists of a pre-defined model arranged and offered by RTDS technologies within the libraries implemented in the Draft Module. From the figure at the beginning of the subsection we can already see that it presents two inputs and two outputs.

- *Inputs*: the two inputs are the solar irradiance (W/m^2) and the temperature of the solar cells of the PV array, measured in °C. They can be set to a predefined value or modified dynamically during the simulation, using sliders or "schedulers". A scheduler is a simple block, which gives the opportunity of reading data from a file and outputting these values on command or every fraction of time (second, minute or hour).
- *Outputs*: there are two, the voltage and current produced by the PV array. They will be dependent on the characteristics and number of the chosen solar cells, as well as on the inputs.

This pre-defined block implements the mathematical modelling of the solar cell provided in section 4.2.1, and allows the designer to feed it with data from the real product data-sheet presented in the previous section. The following figures will account for the choices made towards an accurate representation, as well as for the physical values applied to it.

SIGNAL MONITORING		SIGNAL NAMES		CORE ASSIGNMENT			
CONFIGURATION		MODULE DATA AND CONFIGURATION		ARRAY CONFIGURATION			
Name	Description	Value	Unit	Min	Max		
Name	Component name	Array1A					
Model_Type	Select solar cell model	Single Diode Five Parameter ...		0	1		
calcPara	Select calculation of solar cell parameters	Analytical Method		0	1		
EMPP	Enable estimation of maximum power point	Yes		0	1		
MPPT	Select MPP estimation technique	Lambert function approximat...		0	1		
EnbShd	Enable shading effect	No		0	1		
Mon	Enable monitoring of PV Parameters	Yes		0	1		

Figure 5.10: Configuration window of the PV array model block.

It can be observed that the solar cell implemented model is the "Single Diode, Five Parameters", as previously stated in section 4.2.1. There, it was also outlined that the solar cell parameter estimation method could be iterative or analytical, being the latter the chosen one. This particular method uses the five equations to estimate the unknown values.

$$R_{sh} = R_{sho} \quad (5.3)$$

$$a_{ref} = \frac{V_{mref} + I_{mref}R_{so} - V_{ocref}}{V_t \left[\ln \left(I_{scref} - \frac{V_{mref}}{R_{sho}} - I_{mref} \right) - \ln \left(I_{scref} - \frac{V_{ocref}}{R_{sho}} \right) - \left(\frac{I_{mref}}{I_{scref} - \frac{V_{ocref}}{R_{sho}}} \right) \right]} \quad (5.4)$$

$$I_{oref} = \frac{I_{scref} - \frac{V_{oref}}{R_{sh}}}{\exp \left(\frac{V_{oref}}{N_c a_{ref} V_t} \right)} \quad (5.5)$$

$$R_s = R_{so} - \left(\frac{\frac{a_{ref} V_t}{I_{oref}}}{\exp\left(\frac{V_{oref}}{N_c a_{ref} V_t}\right)} \right) \quad (5.6)$$

$$I_{phref} = I_{scref} \left(1 + \frac{R_s}{R_{sh}} \right) + I_{oref} \left(\exp\left(\frac{I_{scref} R_s}{a_{ref} V_t}\right) - 1 \right) \quad (5.7)$$

This parameter estimation is performed automatically by the block utilizing the values introduced by the designer.

Furthermore, and continuing with the explanation of figure 5.10, the Maximum Power Point Tracking technique is enabled, and the model will be providing its voltage (V_{MPP}). Calculation of this voltage is made by an estimation method: the *Lambert function approximation*. Its implementation is conducted through the following equation 5.3.2,

$$V_{mp} = V_{im} - \left(I_{im} - \frac{V_{im}}{R_{sh}} \right) R_s \quad (5.8)$$

Where,

$$V_{im} = N_s N_{cs} a V_t \left(\text{lambertW} \left(\frac{I_{ph} \exp(1)}{I_o} \right) - 1 \right) \quad (5.9)$$

$$I_{im} = \frac{V_{im} I_o}{N_s N_{cs} a V_t} \exp\left(\frac{V_{im}}{N_s N_{cs} a V_t}\right) \quad (5.10)$$

As we shall later explain, this estimation technique is not the only possibility of implementing the Maximum Power Point Tracking. A direct method is also offered in the PV control section, leaving the choice to the user.

The last two parameters implemented within the "Configuration section" of the PV array block are the shading effect and the monitoring of the PV parameters. The first one can be dealt with in the simulation by including bypass diodes and/or blocking diodes in the PV array model. However, in order to achieve a compromise between accuracy and computational burden, it will be left out of the scope of the project. The monitoring of the parameters is activated and made use of when performing simulations.

The next two figures (5.11 and 5.12) that finish the implementation of the PV array model block are self-explanatory and account for the "Module data and configuration", and the "Array configuration".

SIGNAL MONITORING		SIGNAL NAMES	CORE ASSIGNMENT		
CONFIGURATION		MODULE DATA AND CONFIGURATION		ARRAY CONFIGURATION	
Name	Description	Value	Unit	Min	Max
Nc	Number of series connected cells per string per module	60		1	
Ncp	Number of parallel strings of cells (Note: Total cells per module= nsc*...)	1		1	
Vocref	Open circuit voltage (Voc @ STC Tref, INSref)	39.8	Volts	0.	100
Iscref	Short circuit current (Isc @ STC Tref, INSref)	9.77	Amps	0.	100
Vmp...	Voltage at Pmax (@ STC Tref, INSref)	32.6	Volts	0.	50
Impref	Current at Pmax (@ STC Tref, INSref)	9.19	Amps	0.	10
Eg	Energy gap: select semiconductor material of solar cell	Monocrvstall...		0	13
Jtmp	Short circuit current temperature coefficient	0.05	%/degC		
Kv	Open circuit voltage temperature coefficient	-0.29	%/degC		
Tref	Reference temperature at standard test conditions (typically @STC Tr...)	25	degC	0.	1e3
INSref	Reference solar intensity (typically @ STC INSref = 1000 Watts/m^2)	1000	Watts/m...	0.	1e4
Rso	Open circuit series resistance (Slope of -dV/dI = Rso at Vocref)	0.5	ohms	0.0	1e3
Rsho	Short circuit shunt resistance (Slope of -dV/dI = Rsho at Iscref)	100	ohms	0.0	1e3

Figure 5.11: Module data and configuration window of the PV array model block.

In this window, all the real parameters deducted from the data-sheet in subsection 5.3.1 are implemented: series connected cells of the module, voltages and current values, temperature coefficients and standard test conditions. The open circuit series resistance and the short circuit shunt resistance were not in the data-sheet and thus have been defined by the designer. Semiconductor material of the solar cell can be chosen from multiple options, and an energy gap value will be used in consequence. In our case, the data-sheet model works with Monocrystalline solar cells.

SIGNAL MONITORING		SIGNAL NAMES	CORE ASSIGNMENT		
CONFIGURATION		MODULE DATA AND CONFIGURATION		ARRAY CONFIGURATION	
Name	Description	Value	Unit	Min	Max
Ns	Number of modules in series	62		1	
Np	Number of modules in parallel	94		1	

Figure 5.12: Array configuration window of the PV array model block.

This last window is merely the definition of the array configuration previously determined. This is: 62 modules in series and 94 in parallel.

DC-AC converter

The PV array is interfaced to the microgrid using a DC-AC converter, which represents the center of the PV control. We obtain the control inputs from the AC and DC buses to which it is connected, and the firing pulses that constitute the output of the control system are the inputs of this Voltage Source Converter.

In order to model it, the option of using a small-step model appears as a plausible option. The concept of **small time step bridge box** is a novelty deployed by RTDS technologies [10] within this software, which allows to solve the VSC circuit as a sub-network that can be interfaced to the main network solution. When doing this, the main network is solved with a time step in the range of 50-75 μ s, while the VSC circuit is solved within a time-step of 1.4-2.5 μ s. What we achieve with this

technique is an accurate representation of the IGBT³ and GTO⁴ devices of the voltage source converter.

However, this detailed modelling of power electronic converters requires dedicated parallel processors on the RTDS simulator to solve the aforementioned small time step bridge box. Given that the amount of nodes and switching devices is limited, **average value models** can be used to reduce the hardware requirements. These AVMs provide a simplified simulation to represent the converter dynamics. Considering that the scope of the project involves the simulation of a complete microgrid, a compromise between accuracy and hardware requirements is to be found in order to be able to do so with a rational number of racks. Therefore, an average value model is chosen to represent the DC-AC converter.

High-pass filter and transformer

This high-pass filter, implemented in the AC side of the connection to the microgrid, is used to make the converter switching harmonics injected to the grid smaller. To that end, the following formulae is used to calculate its parameters,

$$X_{filt} = \frac{V_{bus}(L - L_{rms}) \cdot V_{bus}(L - L_{rms})}{MVA(filter)} \quad (5.11)$$

$$C_{filt} = \frac{1}{X_{filt}(2 \cdot \pi \cdot f_{grid})} \quad (5.12)$$

$$L_{filt} = \frac{1}{C_{filt} \cdot (2 \cdot \pi \cdot f_{resonance}) \cdot (2 \cdot \pi \cdot f_{resonance})} \quad (5.13)$$

$$R_{filt} = (2 \cdot \pi \cdot f_{resonance}) \cdot L_{filt} \quad (5.14)$$

Given that the AC voltage must be stepped up to the microgrid's voltage (13.2 kV), a transformer is needed to perform the last connection. Its parameters are defined in the configuration window, as it can be observed in figure 5.13,

³Insulated Gate Bipolar Transistor

⁴Gate Turn-Off Thyristor

If_rtds_sharc_sld_TRF3P2W					
WINDING #1	WINDING #2	MONITORING	SIGNAL NAMES		
CONFIGURATION			CORE ASSIGNMENT		
Name	Description	Value	Unit	Min	Max
Trf	Transformer Name	TRF1s			
YD1	Winding #1 Connection	Delta			
YD2	Winding #2 Connection	Y			
Lead	Delta lags or leads Y	Leads			
type	Transformer Model Type	Linear			
tapCh	Tap Changer (type cannot be Linear)	No			
edge	Tap Trigger on	Risina Edae			
inps	Tap Changer Inputs	RunTime			
Tmva	Transformer rating (3 Phase)	2.5	MVA	0.0001	
f	Base Frequency	60.0	Hz	1.0	300.0
xl	Leakage inductance of Tx	0.15	p.u.	0.001	
NLL	No load losses	0.001	p.u.	0.00	1.0
NLLtp	No load loss branch type	Windina			

Figure 5.13: Configuration window of the transformer modelled in the PV system.

The first winding works with a delta configuration, while the second one does it with the microgrid's configuration (Y). This transformer has been modelled in a simpler way (linear model) than the one simulating the Wateringen substation (section 5.2), given the difference in importance to our model. The parameters can be seen from the figure above, and both windings present a magnetizing current of 1%.

5.3.3. PV control system

The control system has been thoroughly explained in Section 4.2.2 by a combination of theoretical principles and the use of diagrams. Given that the circuitry of the model is developed in the Draft module, we shall expect an implementation with certain resemblance to the diagrams presented before.

In a nutshell, the PV array model works microgrid-tied by means of a Voltage Source Converter, which is controlled using a *dq decoupled current control*. We obtain a regulation of real and reactive power exchanged between the PV system and the grid, by working with the AC and DC voltages as inputs and obtaining the firing pulses for the converter as the output. The entire process has been previously explained with five different figures, that will now be modelled through the Draft circuitry.

General view of the control blocks

Inside the PV control block of figure 5.9 we can find the next layer of the control implementation, which is displayed hereafter. We have divided it in four different sections, numbered from 1 to 4, in order to facilitate its explanation and the concordance with dq decoupled current control.

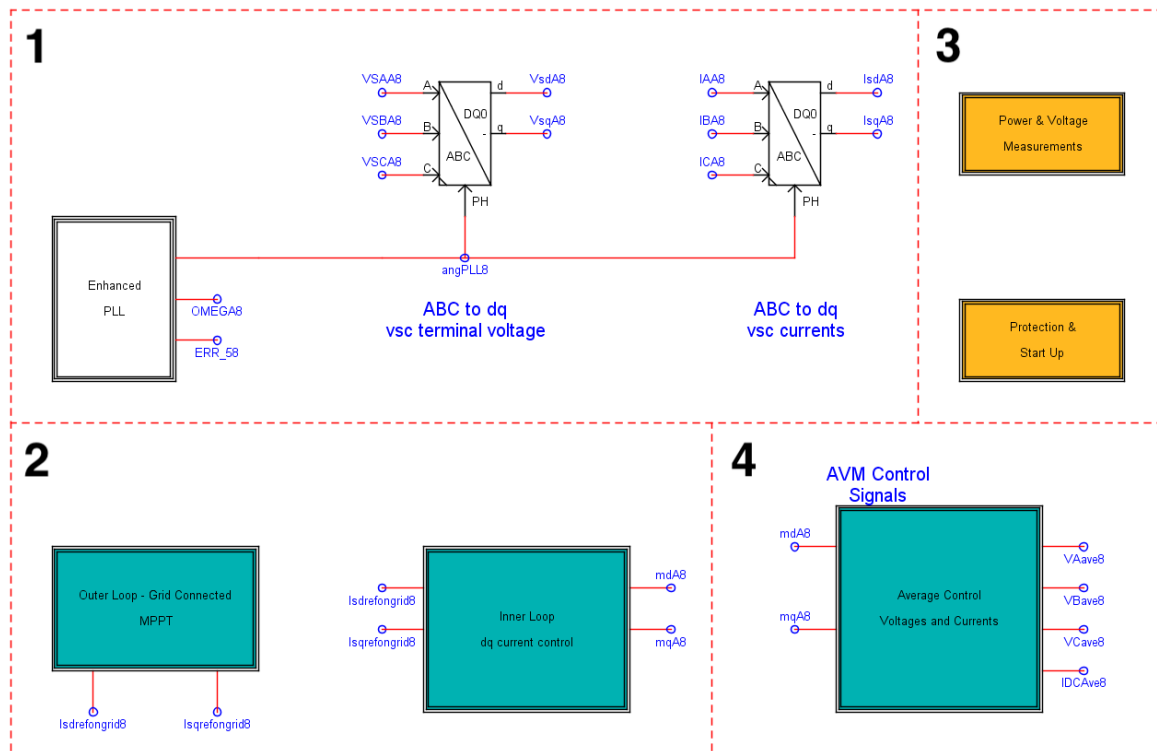


Figure 5.14: General view of the PV control schema.

The first section can already be expounded, as its construction is fairly clear. It consists on the implementation of the three-phase to direct-quadrature-zero transformation of voltages and currents presented in figure 4.10. This is done through a block that performs the Park’s transformation matrix (eq. 4.7) in order to transform the 3-phase rotating vectors of voltages and currents into stationary dq vectors. Those signals are given the names: V_{sd8} , V_{sq8} , I_{sd8} and V_{sq8} , and can be used from any block of the Draft module.

However, the Park’s transformation needs the instantaneous transform angle ρ , which must be supplied by a phase locked loop (PLL) controller. The objective is to synchronize the converter control system to the AC microgrid voltage. The implemented schema, while being quite long and complex, does not add any important standpoint to the control and shall be left for the Appendices.

Outer and Inner Loops (2)

The second section of the control schema accounts for the outer and the inner loops of the control, presented and explained in figures 4.11, 4.12 and 4.13. It includes the calculation of both i_d and i_q references, as well as the PI controllers and the obtention of the modulation voltages m_d and m_q .

In the figure above we can observe that the outer loop is in charge of providing those references, based on the voltage V_{MPP} obtained from maximum power point tracking strategies. Then, these references are served as an input to the inner loop, which obtains the modulation voltages by implementing a dq current control technique. The two following figures (5.15 and 5.16) will show the circuitry behind the blocks involving both loops,

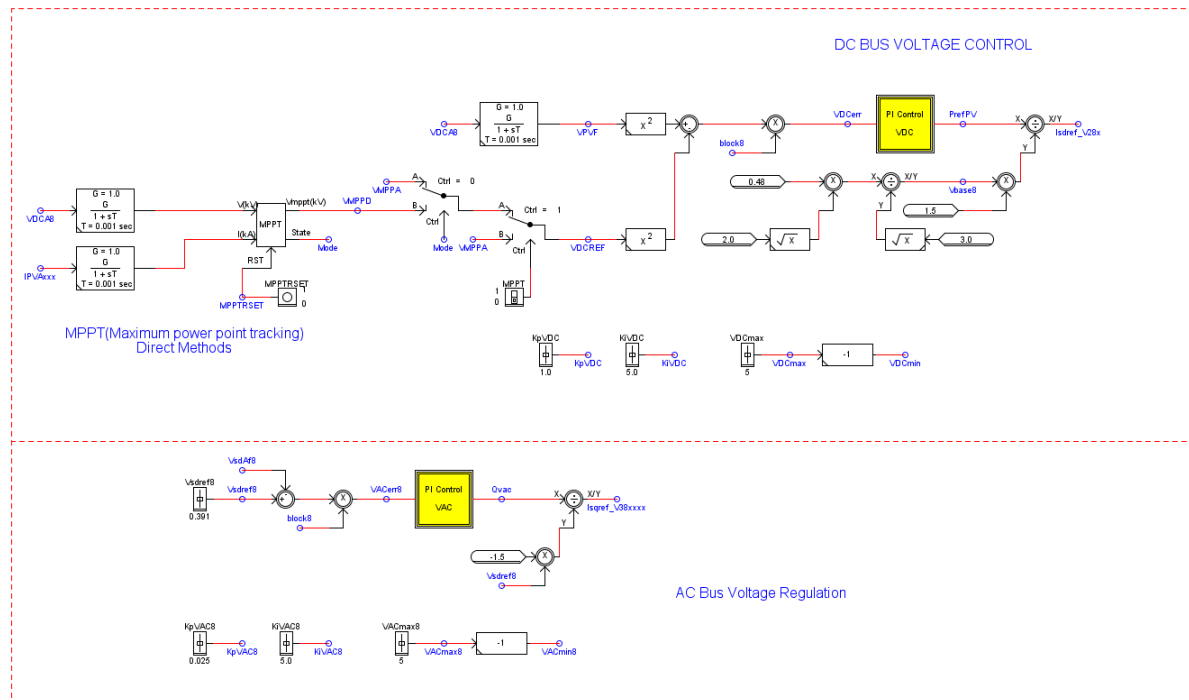


Figure 5.15: Outer loop calculation of i_{dref} and i_{qref} .

The top section of the diagram is the Draft representation of the control strategy presented in figure 4.12, where the d-axis current reference is obtained with the objective of regulating the DC bus voltage of the PV array. The exact control diagram has been replicated here, with a variation regarding the Maximum Point Tracking Method. For this control scheme, two different methods of calculating the voltage of the MPP are provided, a direct method (implemented with the block "MPPT") and an estimation method, represented in the draft by the "VMPPA" node. The first one consists in the Incremental Conductance method algorithm, and the latter is a node provided by the PV array model, which performs a Lambert function approximation to estimate it. The user is given the option of choosing the preferred one with a switch, which will have its proper representation in the RunTime module.

Figure 5.16 is the representation of the figure 4.13 control strategy, regarding the q-axis. Instead of choosing the option of setting its reference to zero and staying close to unity power factor regulation, we implement a control schema that provides AC voltage regulation.

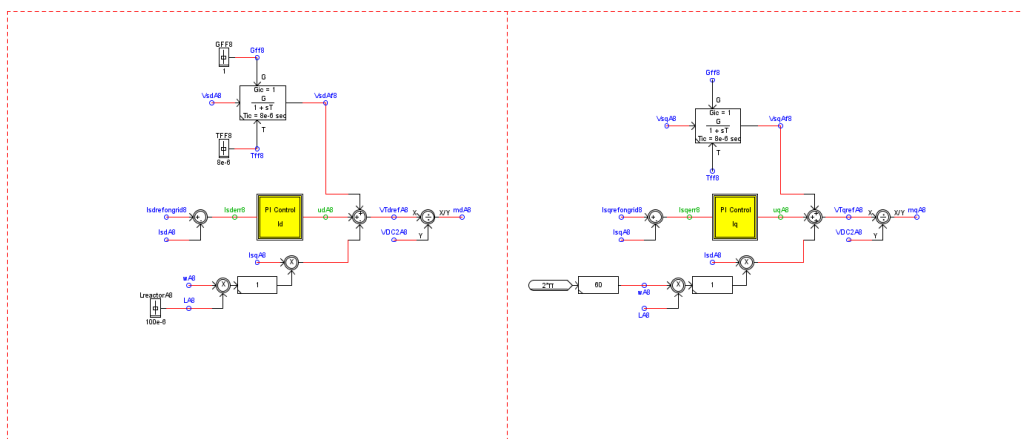


Figure 5.16: Inner loop dq current control.

This figure 5.16 accounts for the inner loop circuitry, which utilizes the references calculated in the outer loop and provides the dq decoupled current control presented in figure 4.11. The modulation voltages m_d and m_q obtained here, with the node names of "mdA8" and "mqA8", are the output of the block.

Regarding the PI control blocks, and so that the amount of figures used in the explanation of the control implementation remains within acceptable limits, they will be left for the Appendix A, where they can be consulted by the reader.

Measurements & Protection & Start-Up

The measurement block, although being useful for the display and calculation of power values in the simulations, falls short of importance when explaining the PV control.

Nevertheless, the protection and start-up block circuitry is displayed hereafter, as it implements three different ways of disconnection from the microgrid:

- When voltage limits (0.5 to 1.5 kV) are reached.
- When frequency limits (55 to 65 Hz) are reached.
- Upon desire of the user, by means of a switch.

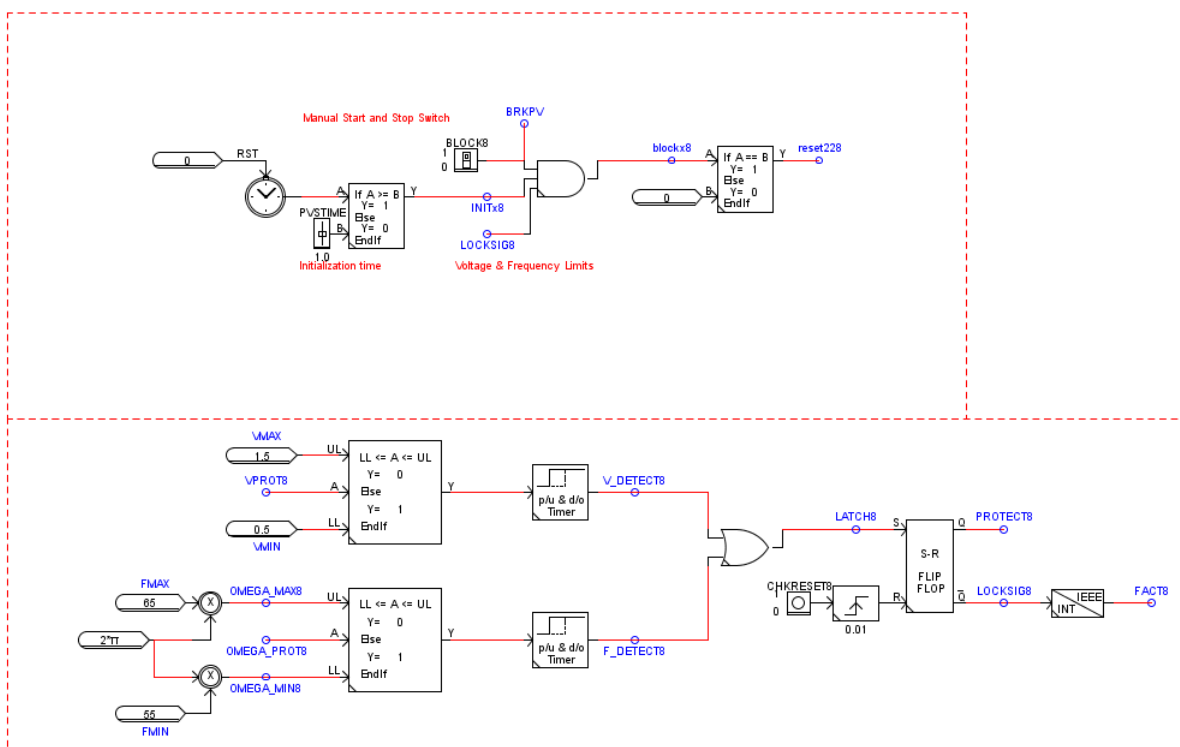


Figure 5.17: Protection logic applied to the PV system.

The voltage and frequency range is continuously checked with a simple selector, which outputs a zero when the values are within the limits and outputs a one when there are not.

Average Control Voltage and Currents

This block represents the last phase of the PV control, and does so by implementing the circuitry needed to conduct the diagram of figure 4.14. In order to do so the modulation voltages m_d and m_q are fed into the block, and by means of applying the inverse Park's transformation we obtain the three-phase

voltages. Then, these values are converted to average AC voltages and fed to the DC-AC converter to perform Sinusoidal Pulse Width Modulation. This finalizes the control strategy, obtaining the desired regulation of real and reactive power exchange between the PV system and the grid.

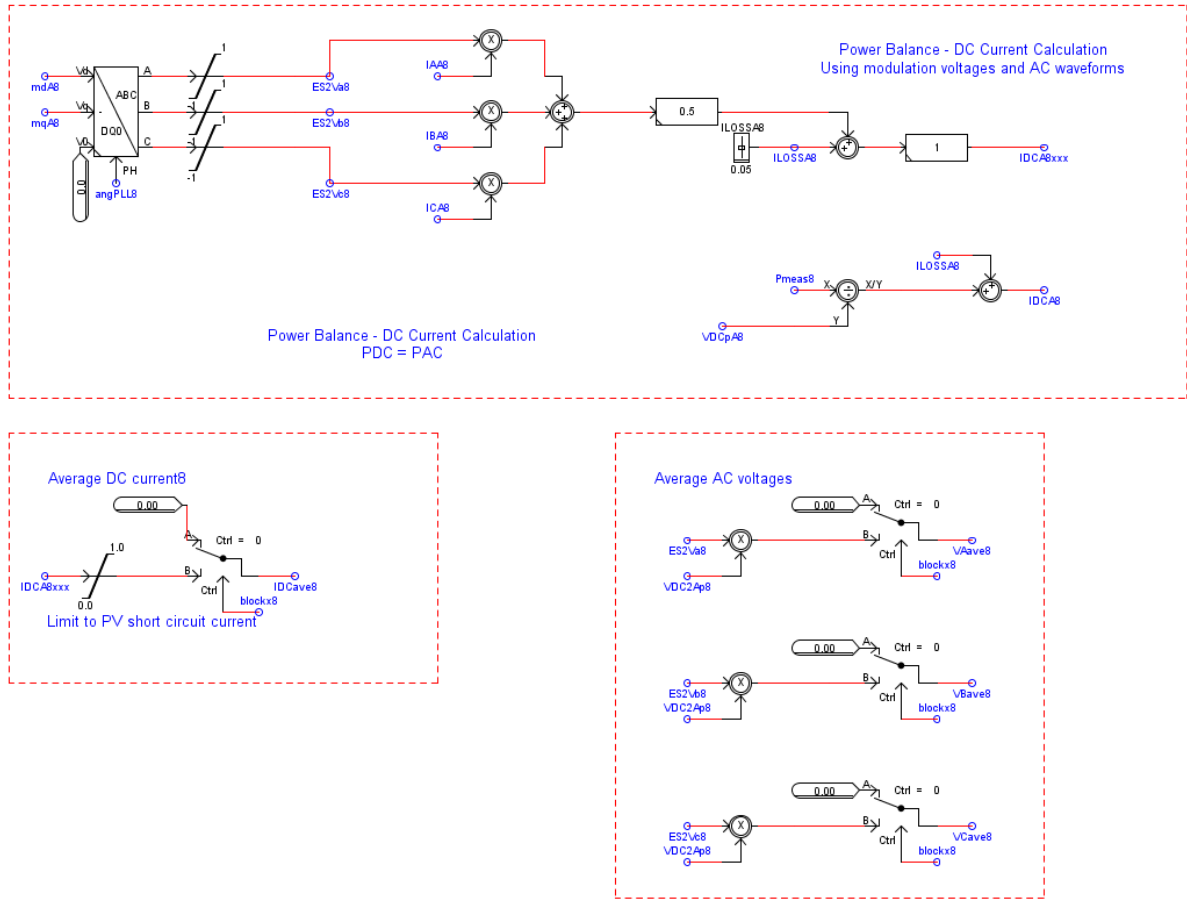


Figure 5.18: Average Control of Voltages and Currents.

5.4. Battery energy storage system (BESS)

The control of the voltage source converter of the battery energy storage system is based on a decoupled dq control, similarly to the photovoltaic system. Therefore, the amount of detail provided in the previous section will not be met here. Instead, the explanation of the implemented control will have a representative character, with a focus on the parts that differ from the PV control system. One of these slight differences is an additional voltage balancing control for the DC bus voltages.

Furthermore, the charging and discharging operation of the BESS is controlled by changing the power order reference, which can be done with a slider. A positive power order indicates a charging operation (power flow from AC to DC), and a negative power order indicates a discharging operation (power flow from DC to AC).

5.4.1. Battery parameters

Following the same structure of the previous section, and with the objective of providing an accurate modelling of the battery energy storage system in mind, the real parameters⁵ from the selected data-sheet are to be presented.

Main battery parameters [48]	
Capacity	880 mAh
Nominal voltage	3.7 V (average)
AC Impedance Resistance	$\leq 45 \text{ m}\Omega$
Discharge cut-off voltage	3.00 V
Charge voltage	4.2 V
Operating charge temperature	0 ~+ 45°C
Operating discharge temperature	-20 ~+ 45°C

Table 5.3: Main parameters of the chosen lithium-ion battery.

Once a proper definition of the main parameters has been provided, we can specify the voltage and capacity of the battery system implemented. This is done by applying two simple formulas to the number of battery cells in series and parallel.

$$V_{batt}(t) = N_s \cdot V_{cell}(t) \quad (5.15)$$

$$Capacity = N_p \cdot AH \quad (5.16)$$

Where,

- N_s : number of battery cells in series.
- N_p : number of battery cells in parallel.
- V_{cell} : nominal voltage of one cell.
- AH: capacity of one cell.

The implemented system comprises 250 cells in parallel and 250 cells in series and therefore, its working voltage is $V_{batt} = 925 \text{ V}$ and its total capacity is $Capacity = 220 \text{ Ah}$.

⁵The AC impedance resistance is measured in an alternating current method (1kHz LCR meter) after standard charge at $25 \pm 2^\circ\text{C}$.

5.4.2. BESS Draft overview

This subsection presents the first layer of the BESS control system, which can be accessed from the general overview (figure 5.5) by entering the battery block. The circuitry provided for this model presents numerous similarities to the one made use of in the PV system draft overview. The reason behind this fact, is that in both cases a DC distributed energy resource has been modelled, with its connection to the AC microgrid following the same control strategy.

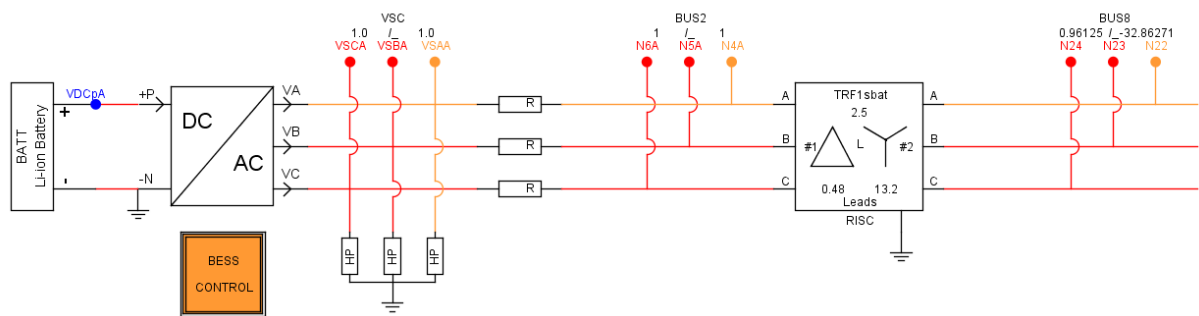


Figure 5.19: Grid-connected BESS system Draft overview.

Given that the elements that are part of this circuitry have been explained in section 5.3.2, we will only focus on the Li-ion battery block. This model, which has a fairly simple design interface, presents two different windows where the parameters must be chosen/introduced in order to achieve an accurate representation of the electrical behaviour of our modelled battery.

PARAMETERS: Min/Rincon-Mora type		MONITORING			
CONFIGURATION		CORE ASSIGNMENT			
Name	Description	Value	Unit	Min	Max
Name	Component name	BATT			
Ns	Number of cells in series in a stack	250	EA	1	1000000
Np	Number of stacks in parallel	250	EA	1	1000000
Cf	Capacity fading factor	0.0	percent	0.0	99.0
cntyp	Battery type	Min/Rincon-Mora		0	1

Figure 5.20: Configuration window of the Li-ion battery block.

This configuration window gives us the option of selecting the number of cells in series in a stack, and the number of stacks in parallel. The values introduced are in accordance with the calculations already performed. Furthermore, the electrical equivalent circuit of the Min/Rincon-Mora model has been selected to be the one used to perform the simulation, as previously explained in section 4.3.1. Finally, the fading factor has been left out of the model in order to reduce its complexity.

PARAMETERS: Min/Lincon-Mora type		MONITORING			
CONFIGURATION		CORE ASSIGNMENT			
Name	Description	Value	Unit	Min	Max
AH	Capacity of a single cell	0.88	AH	0.01	1000000
SOC	Initial state of charge in a single cell	85	percent	5	100

Figure 5.21: Parameters window of the Li-ion battery block.

This second window of the block is where the designer must introduce the two main parameters: capacity of a single cell and the initial state of charge. The first parameter is taken directly from the data-sheet [48]. The latter, which is selected by the designer, is of high importance when calculating every parameter of the equivalent circuit (equations 4.10, 4.11, 4.12, 4.13, 4.14 and 4.15).

5.4.3. BESS control system

The content of the BESS control block will be displayed hereafter, with the focus set on the differences between it and the previously explained PV control system. The general view of the control blocks presents the structure of figure 5.22,

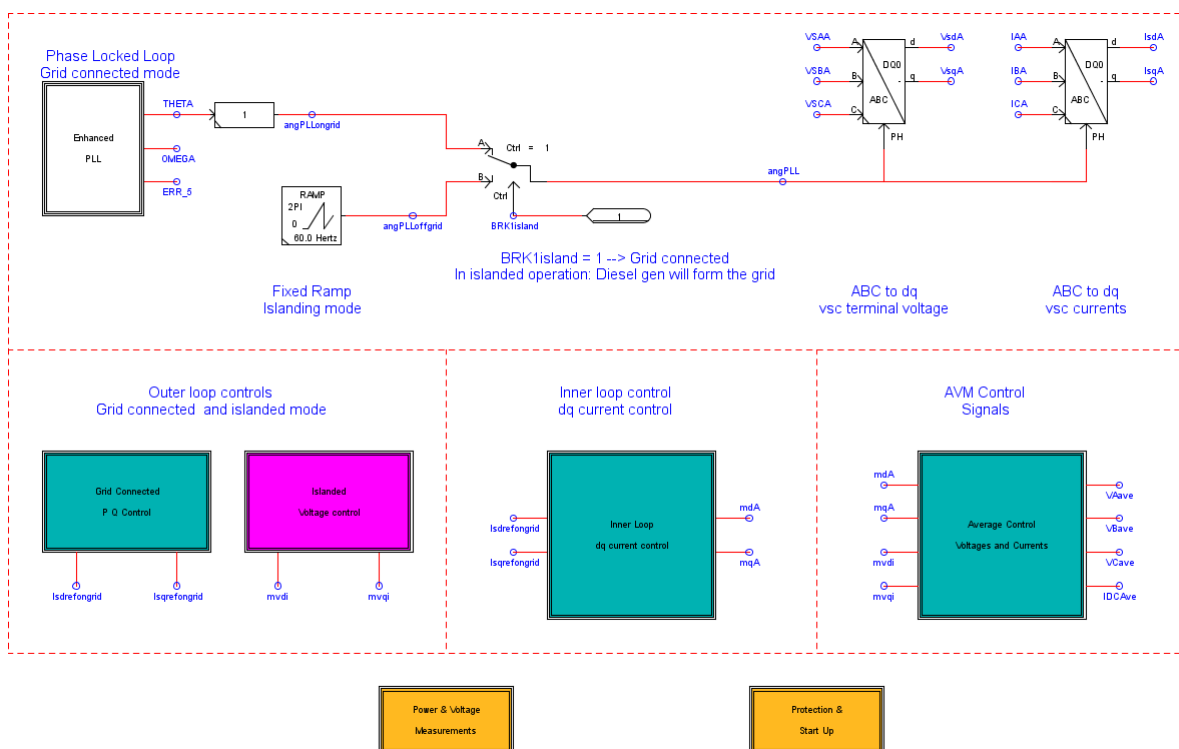


Figure 5.22: General view of the BESS control schema.

Following the same decoupled dq control as the PV system, we present the content of the blocks performing the outer loop (grid connected) and inner loop.

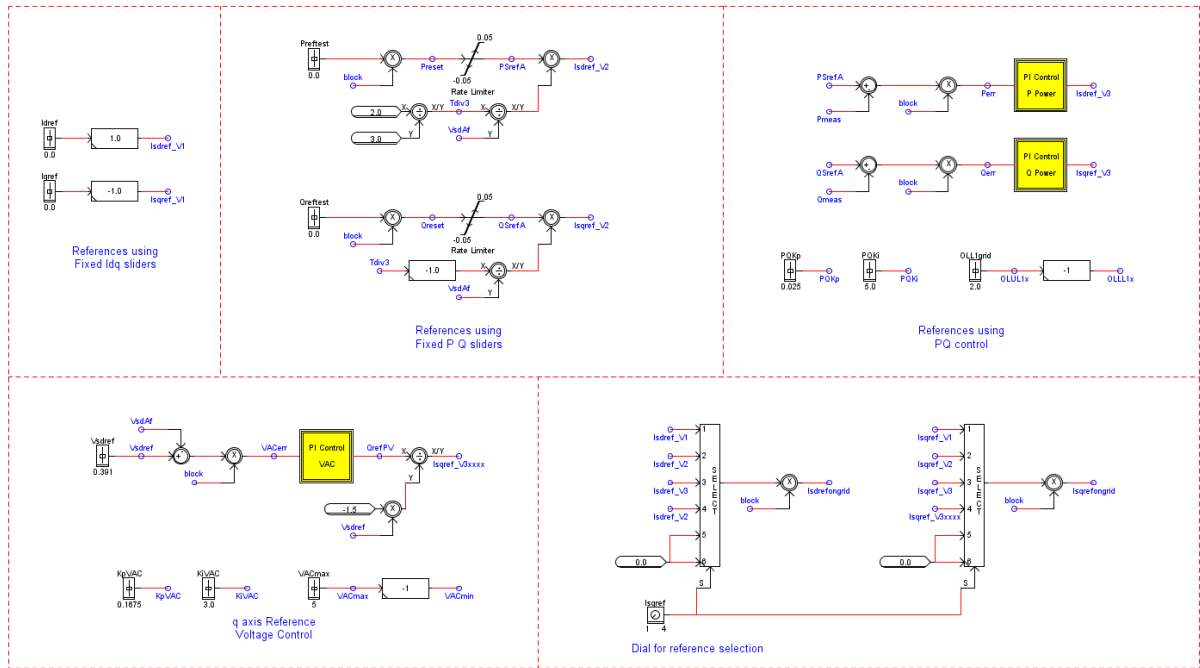


Figure 5.23: Outer loop calculation of i_{dref} and i_{qref} in the grid-connected scenario.

The calculation of the references for i_d and i_q can be done following different techniques: providing its direct value, calculating it from pre-set active and reactive powers, making use of PQ control or utilizing the q-axis to provide voltage control. All these options are offered in this outer loop implementation, leaving the choice to the user by means of a dial. Again, the PI controls are not explicitly presented in this section, as they have been left for Appendix B. Figure 5.24 accounts for the Inner Loop control block.

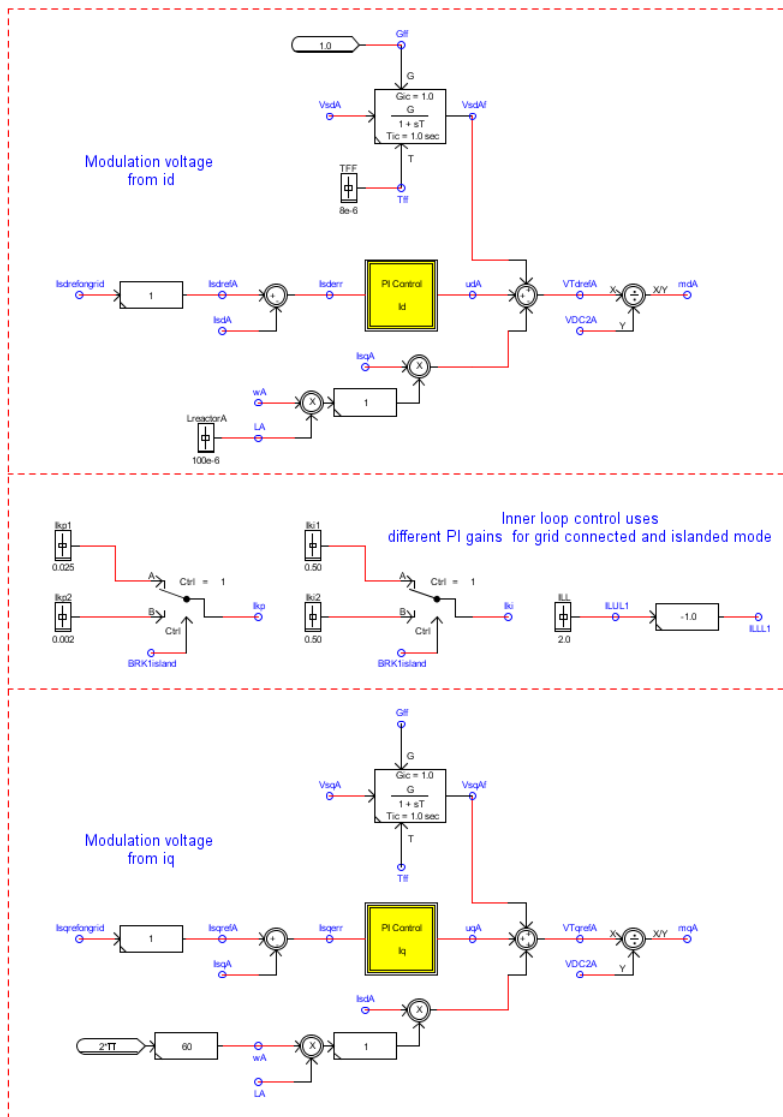


Figure 5.24: Inner loop calculation of the modulation voltages.

This block performs the dq current control, and it is fed the references obtained in the previous one as an input. The final outputs obtained are the modulation voltages m_d and m_q . Furthermore, we can observe that there are different PI gains applied to the grid-connected and the islanded mode, establishing the duality implemented in figure 4.16.

This duality can also be seen in the overview of the BESS control draft, where the calculation of the instantaneous angle is different depending on the operation mode of the microgrid. This angle, which is necessary to perform the three-phase to direct-quadrature-zero transformation of voltages and currents, is obtained from a different source in grid-connected and in islanded mode of operation. Figure 5.25 accounts for the content of the block performing the islanded mode outer loop control.

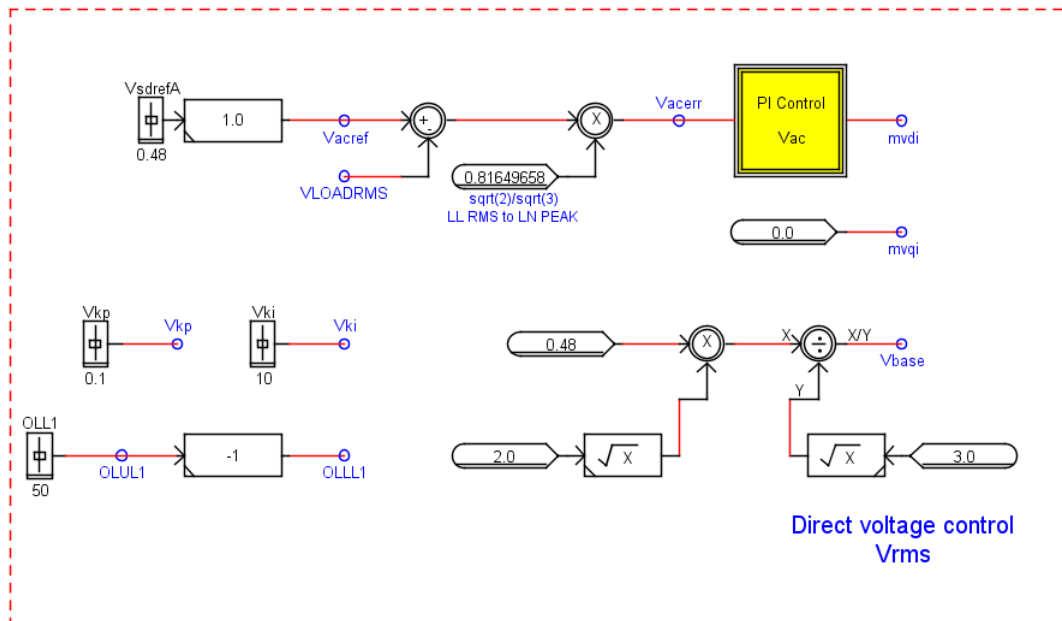


Figure 5.25: Outer loop for islanded mode of operation voltage control.

This fairly simple schema gives a zero value to the modulation voltage "mq", and performs the calculation of "md" following a voltage balancing control technique. The content of the PI control is also left for Appendix B.

Finally, the obtainment of average control voltages and currents that are fed into the DC-AC converter module block modelled in figure 5.19 is presented in the following block. Differently from the PV control system, this block has two pairs of modulation voltages fed as an input instead of one. The circuitry behind it, completing the control loop, is shown hereafter,

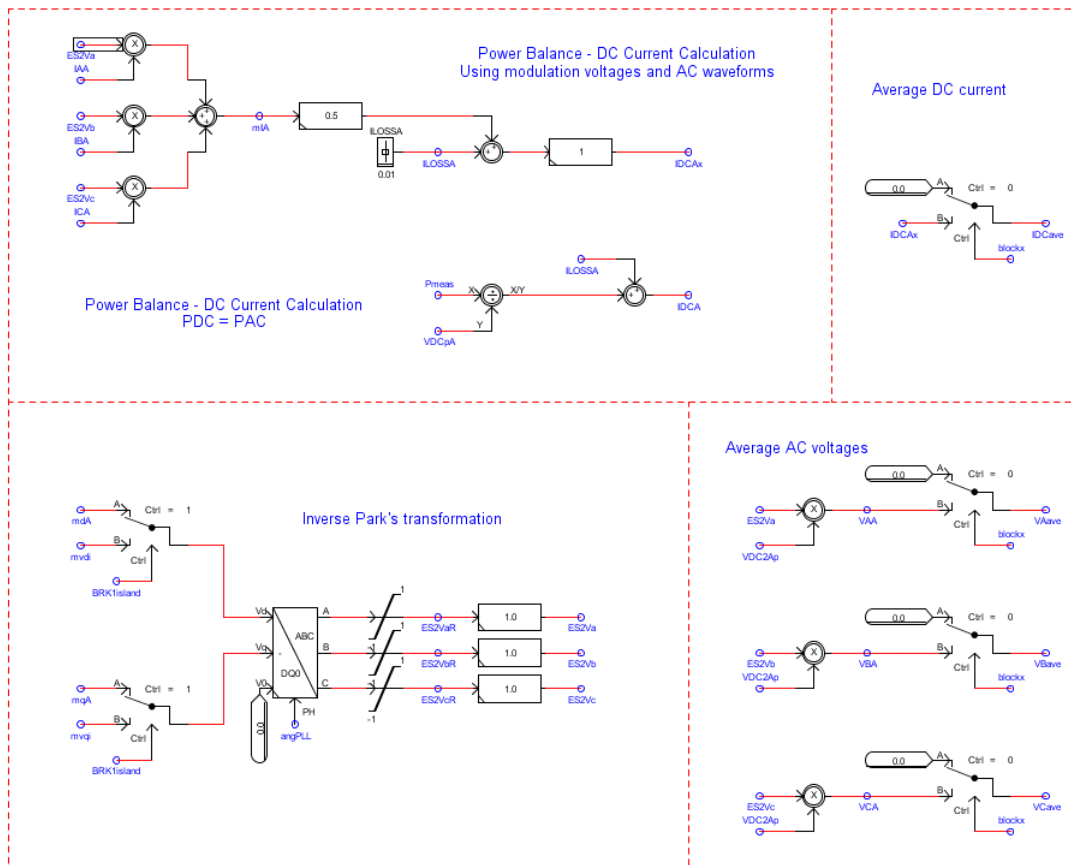


Figure 5.26: Obtainment of control signals needed for the VSC.

The Power and Voltage measurements block lacks of enough importance to be presented in this section, as the values monitored are meant to be used in the RunTime module. The Protection and Start Up is similar to the one implemented in the PV control, and therefore it is self-explanatory. In a nutshell, it also implements a manual switch to start and/or stop the functioning of the BESS, as well as limits in the frequency and voltage values of the system.

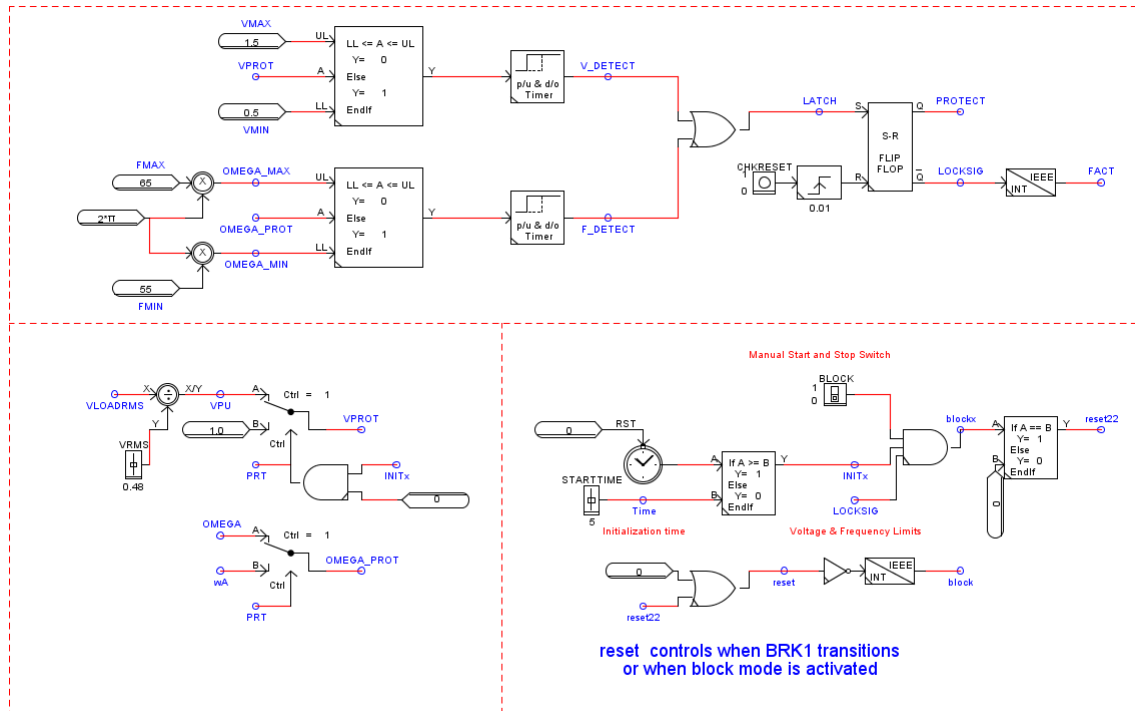


Figure 5.27: Protection&Start Up block implemented in the BESS control.

5.5. Wind energy system

The RSCAD implementation of the wind energy system will follow a different schema than the two previous DER implementations. First, a visualization of the main circuitry implementing the DFIG is to be done, which will be followed by the definition of the wind turbine and the multmass. Further explanation of the complete model can be found in the manual provided by RTDS technologies, which has been previously brought up.

5.5.1. Wind energy system Draft overview

This subsection presents the first layer of the Wind energy system, accessed from the general overview of the microgrid's model, whose schema is shown in figure 5.5. The circuitry designed for this model implements the DFIG configuration previously explained and portrayed in figure 4.17.

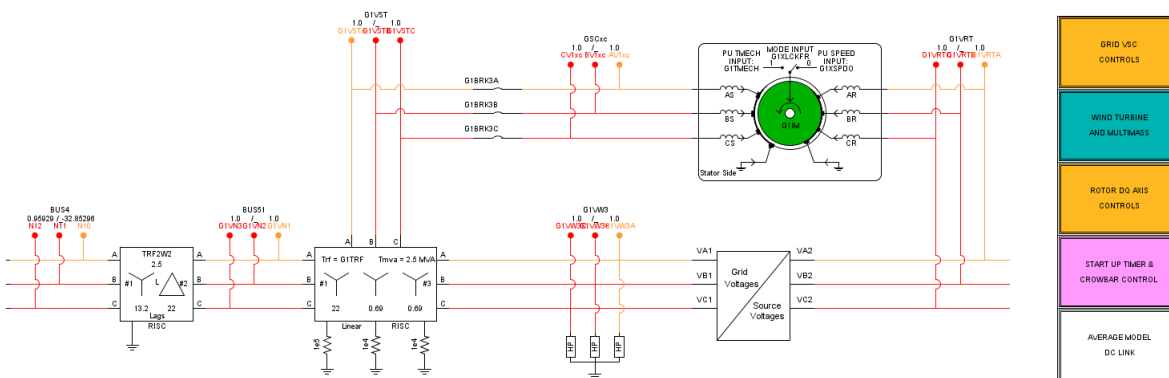


Figure 5.28: Microgrid-connected wind energy system Draft overview.

The circuitry follows the same construction explained in the previous chapter, and most of the elements present in this system overview have already been used. The Induction Machine pre-defined block is the novelty of this Draft overview, and the selection of its parameters will be explained hereafter. It is used for modelling the DFIG, given that it allows to model an induction machine with three stator windings with angular space of 120° electrical and a rotor with three windings located in an angular displacement of 120° electrical. The theory behind this model presents three assumptions:

- Machine windings are assumed to produce a sinusoidal magnetomotive force, therefore space harmonics are ignored.
- Saturation is modelled by adjusting the magnetizing inductance as a function of the total magnetizing current peak value. This is due to the fact that the rotor is cylindrical and round.
- Saturation in the leakage paths is ignored.

The basic induction machine configuration parameters provided by the designer are shown in figure 5.29,

Name		Description	Value	Unit	Min	Max
Name	Component name:		G1IM			
tysat	Specification of Magnetizing Curve		Linear ▼		0	2
rf2cn	External rotor connection is:		Active ▼		0	2
nprt	Number of sets of rotor windings:		One ▼		0	2
rf2in	Enable added internal rotor resistance:		No ▼		0	1
radd1	-- If Yes, initial added internal R:		0.0	p.u.	0.0	30.0
spcsp	-- for Not Active rotor, specify initial:		Slip ▼		0	1
zroc	Override: Force all initial currents to 0:		No ▼		0	1
sw2nd	Enable access to both ends of stator winding?		No ▼		0	1
sngnd	Ground Stator Neutral?		Yes ▼		0	1
rw2nd	Enable access to both ends of rotor winding?		No ▼		0	1
rngnd	Ground Rotor Neutral?		Yes ▼		0	1
Sbrk	Enable Stator Winding Breaker ?		No ▼		0	1
enscl	Enable dynamic scaling of machine MVA:		No ▼		0	1

Figure 5.29: Induction Machine configuration window.

The selected induction machine is rated **2 MW** and 0.69 kV RMS line to line on the stator, with the following electrical parameters (all values referred to the stator).

Electrical parameters	
Stator resistance (Rs)	0.001 Ω
Rotor resistance (Rr)	0.0013 Ω
Stator reactance (Xs)	0.022 Ω + 0.941Ω
Magnetizing reactance (Xo)	0.941 Ω
Rotor reactance (Xr)	0.024 Ω + 0.941 Ω
Rotor/Stator Turns Ratio	2.6377 Ω
Stator connection	wye (Y)
Rotor connection	wye (Y)

Table 5.4: Electrical parameters of the induction machine model.

Supposing a power factor of 0.9, the apparent power of the motor is 2.2 MVA. With this value, and due to the RSCAD induction machine model requirement of per unit values, we calculate the stator base impedance,

$$Z_{bs} = (0.69^2)/2.2 = 0.21641$$

Then, and once all parameters have been defined, the model can be successfully fed with the designated values, as it is done in the "Motor Electrical Parameters" window.

Name		Description	Value	Unit	Min	Max
vbsll	Rated Stator Voltage (L-L RMS)	0.69	kV	0.01		
trato	Turns Ratio, Rotor over Stator	2.6377		0.01		
pbase	Rated MVA	2.2	MVA	0.0001		
hrtz	Rated Frequency	60	Hertz	5.0	150.0	
ra	Stator Resistance	0.00462	p.u.	0.002		
xa	Stator Leakage Reactance	0.102	p.u.	0.01		
xmd0	Unsaturated Magnetizing Reactance	4.348	p.u.	0.75		
rfd	First Cage Rotor Resistance	0.0060	p.u.	0.003		
xfd	First Cage Rotor Leakage Reactance	0.08596	p.u.	0.003		
rkd	Second Cage Rotor Resistance	0.2	p.u.	0.003	1.0e6	
xkd	Second Cage Rotor Leakage Reactance	0.07	p.u.	0.0	1.0e6	
xkf	Rotor Mutual Leakage Reactance	0.0	p.u.	0.0	1.0e6	

Figure 5.30: Induction Machine’s motor electrical parameters window.

Mechanical parameters must also be fed to this model, whereof the most important one is the inertia constant (H). In the multimass model, the inertia constant of the turbine is set to 1.0 and the one for the DFIG is set to 0.5. The sum of these two values matches the value for H requested in this section of the model (1.5).

5.5.2. Wind turbine and multimass

This section is focused in the circuitry where the multimass model and the wind turbine are implemented.

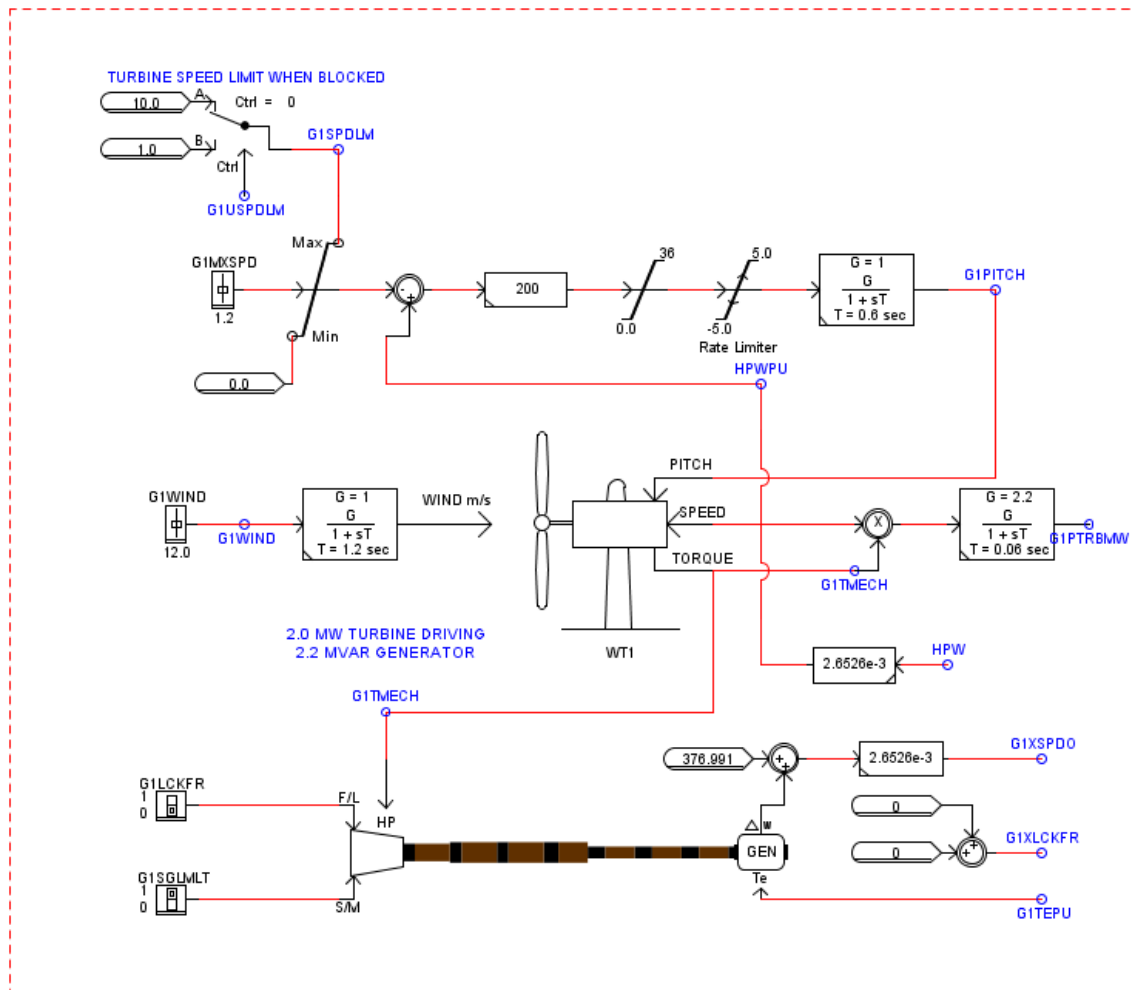


Figure 5.31: Circuitry deployed to implement the Wind Turbine and Multimass model.

From the schema of figure 5.31 we can outline three different signals: the slider-defined "G1WIND", "G1TMECH" and "G1XSPDO". The first one accounts for the wind velocity, and can be modified by the user in the Runtime module with direct repercussions in the wind energy system's power output. The second and third one stand for the mechanical torque and the speed, calculated by the wind turbine and the multimass model respectively.

The wind turbine model has been properly defined in section 4.4.1, and that model has been used to calculate the values fed to the pre-define model that accounts for its behaviour. The 2.2 MVA rated generator power, the rated speed (12 m/s) or the cut-in wind speed (6 m/s) are among the selected parameters. The performance coefficient of the turbine and the air's density are also defined within this block.

CONFIGURATION		TURBINE DATA		COEFFICIENT TYPE 2		AIR DENSITY	
Name	Description	Value	Unit	Min	Max		
GR	Rated Generator Power	2.2	MVA	0.1	1000.0		
TR	Rated Turbine Power	2.0	MW	0.1	1000.0		
WR	PU Gen Speed @ Rated Turbine Speed	1.2	pu	0.1	10.0		
WSR	Rated Wind Speed	12.0	m/s	1.0	100		
WSCI	Cut-in Wind Speed	6.0	m/s	1.0	100.0		
PCT	Power Coefficient Type	TWO		0	0		
PlotPC	Plot Power Coefficient for Multiplot	YES		0	0		
PlotPO	Plot Power vs Windspeed for Multiplot	YES		0	0		

CONFIGURATION		TURBINE DATA		COEFFICIENT TYPE 2		AIR DENSITY	
Name	Description	Value	Unit	Min	Max		
n1	$C_p(\text{lmda}, \text{Beta}) = (n1 - n2 * \text{Beta}) *$	0.47		0.0	1.0		
n2	$\sin(1.57 * (\text{lmda} - 3y) / (n3 - n4 * \text{Beta}))$	0.0167		0.0	1.0		
n3	$-(\text{lmda} - 3y) * n5 * \text{Beta} + n6 / (1 + \text{lmda})$	7.5		0.0	10.0		
n4		0.15		0.0	1.0		
n5	$y = 1 - \exp(-\text{lmda} / 3)$	0.00184		0.0	1.0		
n6		0.01		0.0	1.0		

CONFIGURATION		TURBINE DATA		COEFFICIENT TYPE 2		AIR DENSITY	
Name	Description	Value	Unit	Min	Max		
Tmp	Temperature of Air	0.0	deg. C.	-40.0	40.0		
Alt	Altitude Above Sea Level	0.0	meters	0.0	1e4		

Figure 5.32: Wind Turbine model implementation.

5.6. Diesel generator

The fourth and last DER designed within our microgrid is the diesel generator, and its RSCAD implementation is straight-forward compared to the previous models. This section's structure will be divided in two. First, the overview of the Draft block will be presented, including a description of the parameters choice in the synchronous machine block. Then, the circuitry behind the other three blocks will be provided.

5.6.1. Diesel generator Draft overview

By clicking on the diesel generator block we enter the second layer of the Draft project, which contains the general schema of its implementation. The components that conform it have been already accounted for in section 4.5.

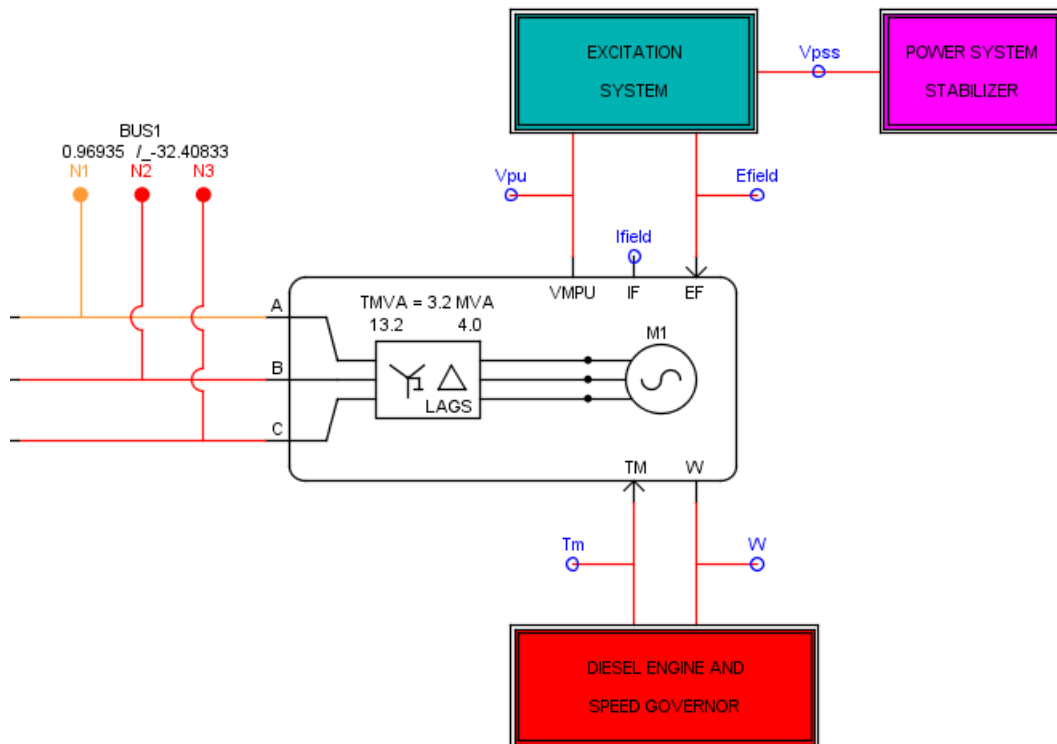


Figure 5.33: Microgrid-connected diesel generator Draft overview.

The block around which the schema is based is the "Synchronous machine model with transformer and loads", and the other three blocks are the ones in charge of making use of the outputs provided by it and obtaining the inputs needed for its correct functioning. The electric machine model can be designed to a level of detail that escapes the scope of the project, and therefore, we will focus on the general model configuration, the mechanical data and the transformer parameters.

MACHINE ZERO SEQUENCE IMPEDANCES			TRANSFORMER PARAMETERS		
MACHINE ELECT DATA:			GENERATOR FORMAT		
MECHANICAL DATA AND CONFIGURATION			MACHINE INITIAL LOAD FLOW DATA		
GENERAL MODEL CONFIGURATION			CORE ASSIGNMENT		
Name	Description	Value	Unit	Min	Max
Name	Machine name:	M1			
cnfg	Format of Machine electrical data input:	Generator			
cfgr	Number of Q-axis rotor windings:	Two			
trfa	Is D-axis transfer admittance known ?	No			
mmva	Rated MVA of the Machine:	3.2	MVA	0.0001	
Vbsll	Rated RMS Line-to-Line Voltage:	4	kV		
HTZ	Base Angular Frequency:	60.0	Hertz		
satur	Specification of Mach Saturation Curve	Linear			
MM	Get Delta Speed Order (r/s) from CC ?	No			
spdin	Initial Speed in the first time steps is:	Rated			
tecc	Send Elect Torque in PU, TE to CC ?	No			
vtcc	Send Mach Bus V in PU, VMPU to CC ?	Yes			
trfmr	Include Optional Y-D Transformer ?	Yes			
ldmh1	Include Optional Machine Load No. 1 ?	No			
ldmh2	Include Optional Machine Load No. 2 ?	No			
Sbrk	Enable Stator Side Breaker ?	No		0	1

MACHINE ZERO SEQUENCE IMPEDANCES			TRANSFORMER PARAMETERS		
MACHINE ELECT DATA:			GENERATOR FORMAT		
MECHANICAL DATA AND CONFIGURATION			MACHINE INITIAL LOAD FLOW DATA		
GENERAL MODEL CONFIGURATION			CORE ASSIGNMENT		
Name	Description	Value	Unit	Min	Max
H	Inertia Constant	3.03	MWs/MVA		
D	Synchronous Mechanical Damping	2	pu/pu		
MSW	Location of Lock/Free Mode Switch:	RunTime			
spdm	-- Initial Mode of Lock/Free Switch	Lock			
inh	CC input for External H: EX_H	No			
ind	CC in for Extern Damp: EX_D EX_W	No			
upexw	- If (ind=Yes), upper limit on EX_W =	1.15	pu		
loexw	- If (ind=Yes), lower limit on EX_W =	0.85	pu		

OUTPUT OPTIONS			SIGNAL MONITORING IN RT AND CC: MAC		
MACHINE ZERO SEQUENCE IMPEDANCES			TRANSFORMER PARAMETERS		
MACHINE ELECT DATA:			GENERATOR FORMAT		
MECHANICAL DATA AND CONFIGURATION			MACHINE INITIAL LOAD FLOW DATA		
GENERAL MODEL CONFIGURATION			CORE ASSIGNMENT		
Name	Description	Value	Unit	Min	Max
vtpri	Transformer Primary L-L RMS kV	13.2	kV	0.001	
vtsec	Transformer Secondary L-L RMS kV	4.0	kV	0.001	
dlagp	Delta Leads or Lags Primary 30 Deg.	Laas			
TMVA	Transformer MVA rating	3.2	MVA	0.001	
trpos	Positive Sequence Resistance:	0.0	pu	0.0	
txpos	Positive Sequence Reactance:	0.1	pu	0.0001	
itzro	Is there a TRF zero sequence path ?	Yes			
trzro	-- Zero Sequence Resistance:	0.0	pu	0.0	
bzro	-- Zero Sequence Reactance:	0.1	pu	0.0001	
tloss	Shunt Conductance at TRF Primary:	0.0001	pu	0.0	2.0

Figure 5.34: Electric machine model's definition of parameters.

From the first window of figure 5.34 , general model configuration, we can see that the electric machine is set to work as a generator, with a rated voltage of 3.2 MVA and with the inclusion of a transformer within the model. The parameters of this transformer are exposed in the next window, where the step-up of the voltage from 4kV to the microgrid's voltage (13.2 kV) is determined. Furthermore, the secondary winding of the transformer (Δ) is set to lag, and the transformer power rating matches the 3.2 MVA. The third and last explained heading, mechanical data and configuration, accounts for the inertia constant and synchronous mechanical damping provided in table 4.4.

5.6.2. Diesel generator control

The machine can be operated in lock (speed) mode or in free (torque) mode. In the first case the mechanical equations of the model are ignored, and the speed of the machine is decided by the control input. However, in the latter case the mechanical torque on the shaft is an input from a control signal and the speed of the machine is decided by solving the swing equations.

The control of the diesel generator relies on three different blocks, which are interconnected to the electric machine block. In short, the machine model passes field current and terminal voltage to the excitation system, and this excitation system in turn provides the excitation voltage to the synchronous machine model. Furthermore, when the machine is in free mode, speed (ω) is sent to the governor model and mechanical torque (T_m) is received from it.

- **Power System Stabilizer (PSS):** this supplementary excitation controller is meant to soften electro-mechanical oscillations. As it can be observed in the following figure representing its circuitry, the user has the option of connecting / disconnecting it from the excitation system by means of a switch. Figure 5.35 represents the Draft view obtained when entering the Power System Stabilizer block in figure 5.33.

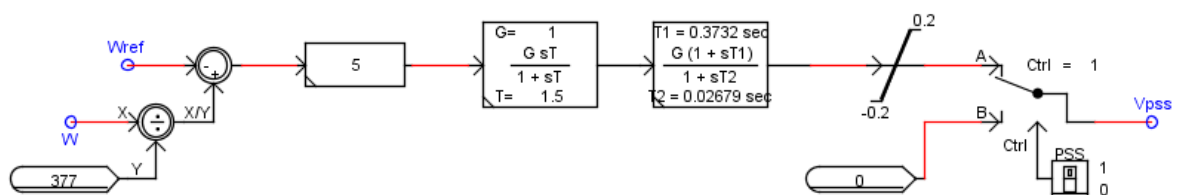


Figure 5.35: Circuitry implemented in the PSS block.

- **Excitation System:** based on a PID controller, receives the terminal voltage (in per unit) from the electrical machine model and outputs the excitation voltage in return. The implemented circuitry contained in the Excitation System block is presented hereafter.

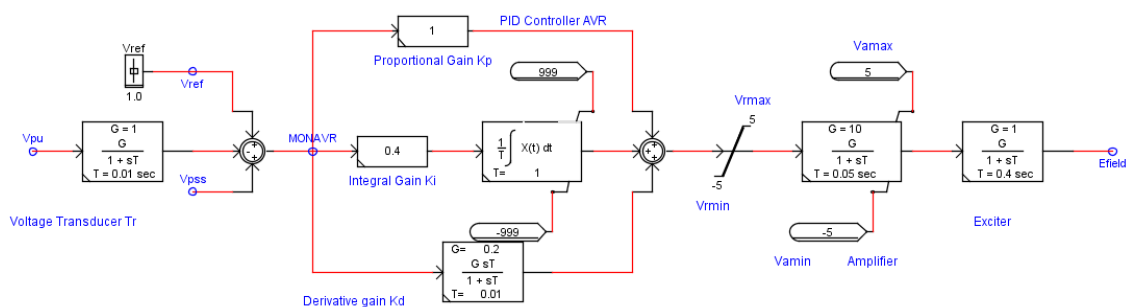


Figure 5.36: Circuitry implemented in the Excitation System block.

- **Speed Governor:** the governor implemented in the Diesel Generator control works with the speed (ω) provided by the electric machine model and a reference. With these inputs, and a PID controller working in series with a model of the diesel engine dynamics, it is able to provide the mechanical torque needed by the machine model. It also presents the option of selecting between an isochronous and a droop speed control.

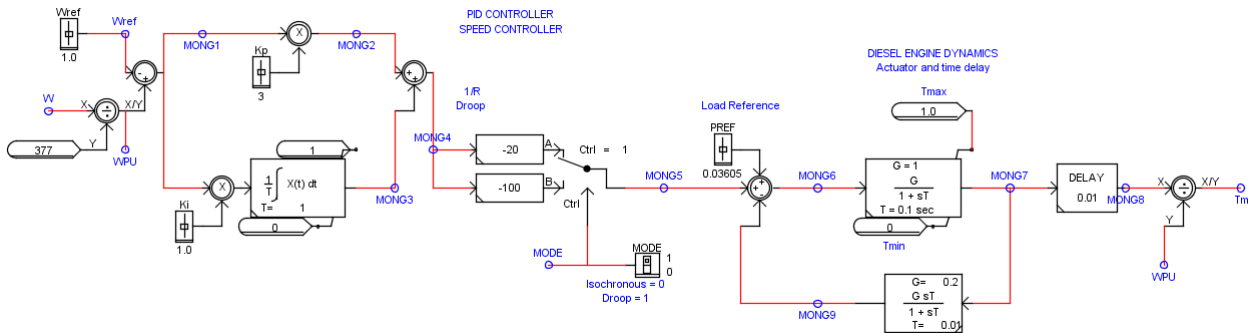


Figure 5.37: Circuitry implemented in the Speed Governor block.

5.7. Loads

As stated in the previous chapter, the four loads that take part of our microgrid are modelled as dynamic loads. To that end, a pre-defined "Dynamic Load" block, which can be found in the libraries within the Draft module of the RSCAD software, will be used.

The implementation is rather straightforward, given that the dynamic block accounts for the load behaviour, and the only thing left for the designer is to choose its parameters. The load connection (Y) must be in accordance with the working connection of the microgrid, and the same is enforceable to the selected voltage (13.2 kV), which will be allow to drop only to 0.5 pu. The option of selecting both the active and reactive power by means of sliders is chosen, and it will be made use of in the next chapter. We will work with the assumption of constant frequency, allowing a maximum deviation of 2 Hz.

MONITORING		MONITORED SIGNAL NAMES			
PARAMETERS		P AND Q SETTINGS		CORE ASSIGNMENT	
Name	Description	Value	Unit	Min	Max
Name	Component Name	DelftStation		0	0
type	Type of Load	RL		0	0
bal	Balanced Load	YES		0	0
btype	R & X in parallel ?	R-X		0	2
YD	Load connectoin type	Y		0	1
cc	P & Q Controlled by	Slider		0	3
gnd	Include Neutral Connection Point?	No		0	1
Vmeas	Bus Voltage Measurement	Internal		0	1
Vbus	Rated Line to Line Bus Voltage	13.2	kV(RMS)	0.1	2000
Vmin	Minimum Bus Voltage(L-L)	0.5	p.u.	0.5	1.0
constF	Assume Constant Freq	Yes		0	1
freq	Base Frequency	60	Hz	1	200
FreqDevMax	Maximum frequency deviation from rated value	2.0	Hz	0.0	
T	Time Constant for setting R, X values	0.01	sec	0.001	100.
Tm	Time Constant for measuring Vbus	0.003	sec	0.001	100.0

Figure 5.38: Parameters window of the dynamic load model.

The "P and Q settings" window will not be shown here, but allows to provide an initial value for reactive and active powers of the load, as well as a range characterized by maximum and minimum P and Q values.

5.8. Implementation of lines

The RTDS software (RSCAD) [10] presents two different models in its library in order to represent lines: travelling wave transmission line and PI section models. Typically, it is recommended to use *travelling wave transmission line models* to represent transmission lines [57], since:

- They are a distributed parameter representation of transmission lines and much more accurate for modelling long lines than the lumped parameter representation used in the PI section models.
- PI sections tend to use more simulator hardware because of the need to cascade several PI sections to represent the line and because of the need to model the network nodes between the individual sections.
- Travelling wave line models provide the opportunity of separating the power system into mathematically isolated subsystem which can run in different RTDS racks if required. This presents the opportunity of modelling different microgrids, which can be interconnected while running their simulation in separate racks.

Nevertheless, when the line we want to model is too short, PI sections are to be used. This concept of "short" is dependent on the time step used for the simulation. In our case we are working with 75 microseconds time-step, so the minimum line length that is possible to represent with a travelling wave transmission line models is,

$$\text{Time step} \times \text{speed of light} = 75 \times 10^{-6} \text{ s} * 299.792.458 \text{ m/s} = 22,484 \text{ km}$$

Thus, and giving that the longest connecting line between two nodes in the smart microgrid has a length of **2.45 km**, PI sections will be used. The PI section block requires seven different parameters for its characterization: line frequency, positive sequence series resistance, inductive reactance and shunt capacitance of the line, and the same three values for the zero sequence.

In order to calculate them we make use of the TLine program, a member of the RSCAD family of tools that is used to lay out and define the geometry and parameters of N-conductor travelling wave transmission lines.

However, our line cannot be defined using the standard procedure, because of its aforementioned length. In this specific case, we have to create a Tline file with the parameters of our line and compile it. Then, the program will automatically generate a series of files, among which we can find a .tlo file. Thanks to an RTDS technologies employee kind contribution, we are able to read this file and obtain the values of travel time (τ), characteristic impedance (Z_c) and series resistance (R_s) of our modelled connecting line.

The description of the “tlines” file that generated from the Convert Module:

For a typical section of data in “tlines” as shown below:

```
T1.3
3 0 %3d %3d 60.00 80.00 1.000000 0.0 0.0 /
%3d %3d 0.122746 1000.287788 19.837500 19.837500 5.773503e-01 8.164967e-01 0.000000e+00 / -----(1)
%3d %3d 0.087676 400.115115 1.322500 1.322500 5.773503e-01 -4.082483e-01 7.071068e-01 / -----(2)
%3d %3d 0.087676 400.115115 1.322500 1.322500 5.773503e-01 -4.082483e-01 -7.071068e-01 / -----(3)
```

Color Zone	description
Color	T-Line Name
Color	Number of Conductors
Color	Base Frequency
Color	Base Frequency
Color	(Not Used information)
Color	Travel time τ (msec) = \sqrt{LC} ; L in Henry, C in Farads
Color	Characteristic Impedance $Z_c(\Omega) = \sqrt{\frac{L}{C}}$
Color	Series Resistance R (Ω/m); corresponding to the base frequency
Color	Series Resistance R (Ω/m); corresponding to the base frequency
Color	Transformation Matrix (modal domain \rightarrow phase domain)

Row (1) --- For Zero Sequence

Row (2) --- For Positive Sequence

Row (3) --- For Negative Sequence

%3d --- Data Format

Figure 5.39: Description of the tlines provided in the .tlo file.

Once we have them, and using the following equations, we are able to obtain the lumped parameters necessary to characterize our PI section model.

$$\tau = \sqrt{LC} \tag{5.17}$$

$$Z_c(\Omega) = \sqrt{\frac{L}{C}} \tag{5.18}$$

$$Rs(\Omega) = R * l \tag{5.19}$$

Therefore, we open Tline and create a .tli file introducing the values calculated in section 4.7.2. Giving that the defined section was 300 mm², its radius in cm would be 0.97721, and from the value of resistivity used in the equation 4.30, we infer that the DC resistance per sub conductor in Ω/km is 0.09666. Thus, we introduce these values in the *Conductor Data* section and compile the file.

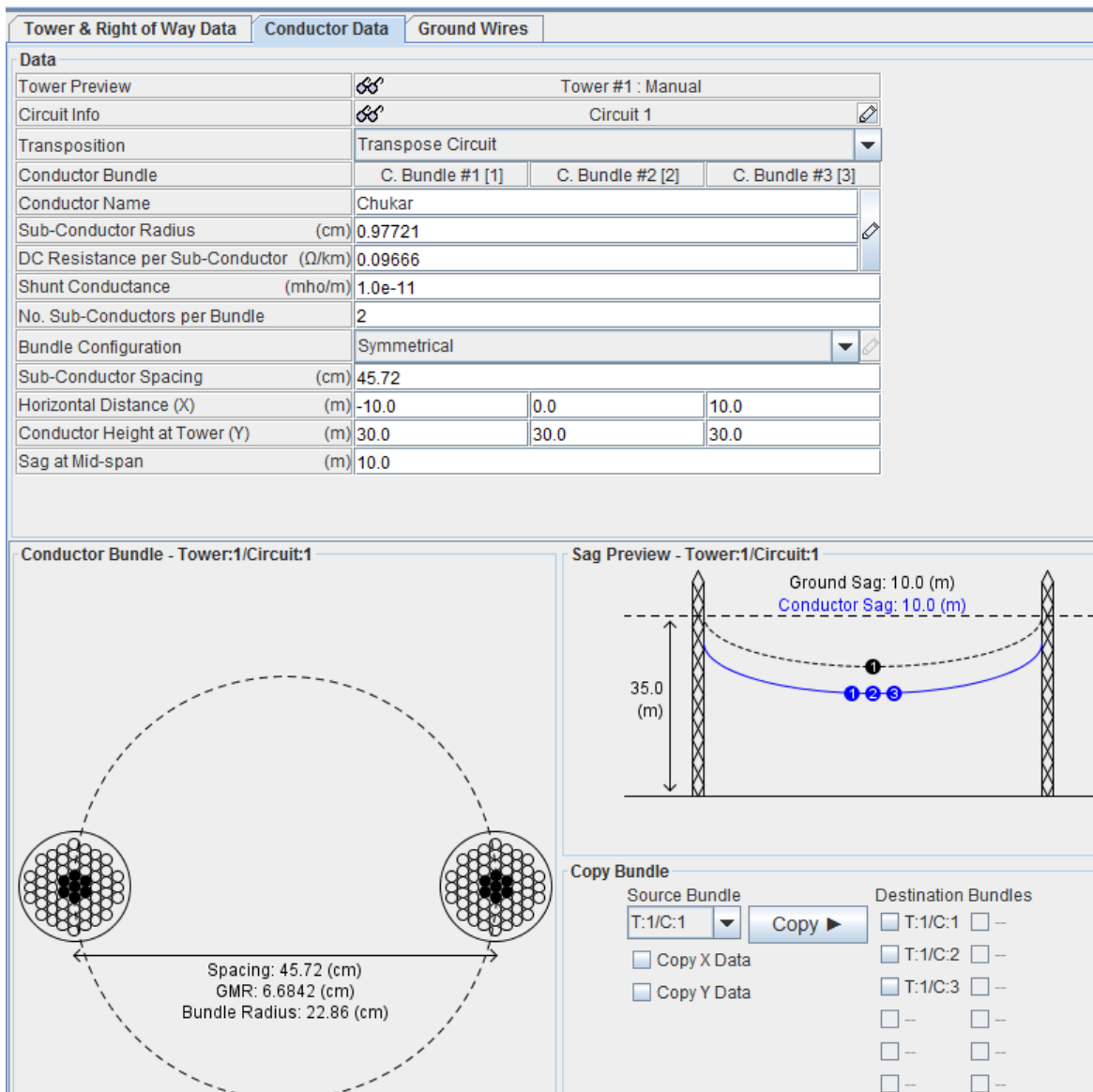


Figure 5.40: Conductor data section in the Tline tool.

Once the compilation is done and the .tlo file has been generated, we proceed to obtain the values for the travel time, characteristic impedance and series resistance using the guidance of figure 5.39.

	Travel time (s)	Characteristic Impedance (Ω)	Series Resistance (Ω/m)
Zero Sequence	0.1193 e-04	724.39	0.31812e-03
Positive Sequence	0.8331 e-05	316.31	0.49240e-04

Table 5.5: Values obtained from the .tlo file.

Substituting the values of travel time, characteristic impedance and series resistance in equations 5.17 5.18 5.19 we obtain the values of inductance (L), capacitance (C) and resistance (Rs). The resistance value will be directly used, but for the inductive reactance and shunt capacity of the line we need to use,

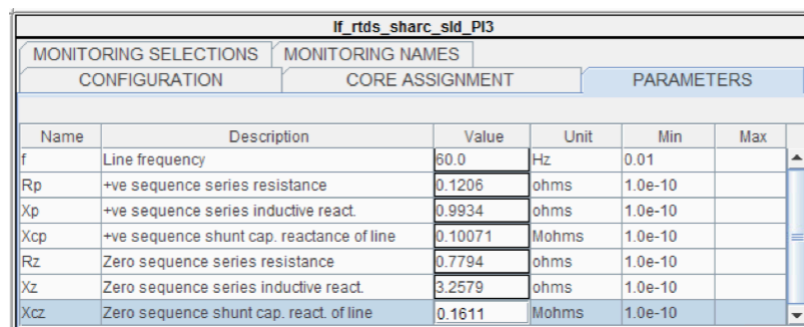
$$X_l = 2 \pi f L \tag{5.20}$$

$$X_c = \frac{1}{2 \pi f C} \quad (5.21)$$

The final implemented values for this particular PI section are shown in the following table. This process will be run in the calculation of each line section.

	Series resistance(Ω)	Inductive reactance (Ω)	Shunt capacitance (Ω)
Zero Sequence	0.7794	3.2579	1.6110e5
Positive Sequence	0.1206	0.9934	1.0071e5

Table 5.6: Final PI section values.



Name	Description	Value	Unit	Min	Max
f	Line frequency	60.0	Hz	0.01	
Rp	+ve sequence series resistance	0.1206	ohms	1.0e-10	
Xp	+ve sequence series inductive react.	0.9934	ohms	1.0e-10	
Xcp	+ve sequence shunt cap. reactance of line	0.10071	Mohms	1.0e-10	
Rz	Zero sequence series resistance	0.7794	ohms	1.0e-10	
Xz	Zero sequence series inductive react.	3.2579	ohms	1.0e-10	
Xcz	Zero sequence shunt cap. react. of line	0.1611	Mohms	1.0e-10	

Figure 5.41: PI section parameters in the Draft block.

6

Microgrid simulations

This culmination chapter consists of simulations performed with the microgrid model developed and implemented in the RTDS simulator along chapters 4 and 5. This model, in turn, has been designed by following the guidelines extracted from the resilience study performed in chapter 3. Therefore, the simulations performed within this chapter will be meant to validate both the model and the implemented enhancements in resiliency.

6.1. Graphical User Interface

The RunTime module is responsible for providing a graphical user interface, as it allows to load, run and control the simulation of the circuitry designed and compiled in the Draft tool. In particular, we provide an interactive canvas, which must perform the following double-function:

- **Representation** of the state of the microgrid, to every extent. Information about connection lines, load-supply, actual states of distributed energy resources and performance of the system must be granted to the user in a graphical and simple manner. To that end, a similar train of thought as the one used in the Draft implementation has been followed. While fundamental data and parameters of the microgrid are in plain sight, the user also has the opportunity of getting access to specific DER parameters or performance graphics by clicking on different blocks.
- **Interaction** with the model. The user is given the option of modifying design parameters to adjust the control of DERs, as well as the ability to change the power consumption of the loads. Furthermore, connection-disconnection of loads and DERs is available, alongside with the possibility of varying some meteorological factors, such wind speed and solar irradiance.

The RunTime canvas, with the graphical user interface described above is presented hereafter by means of figure 6.1,

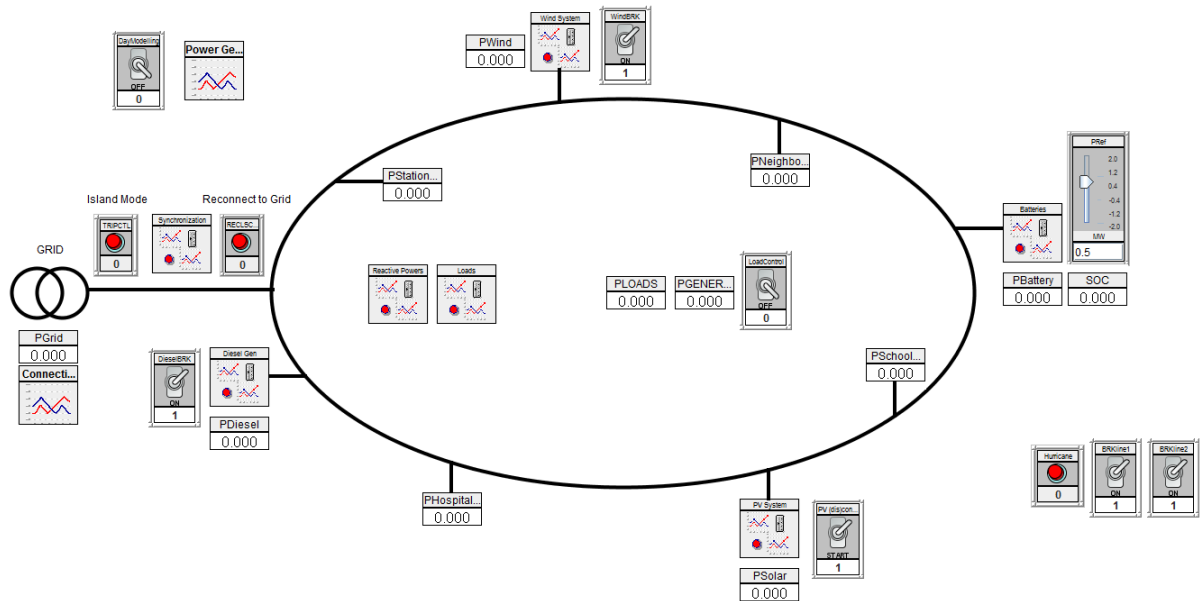


Figure 6.1: Graphical User Interface designed in the RunTime tool.

This section aims to guide the reader through the implemented representation of the microgrid, providing insight on how the model is to be dealt with. To that end, various components of the RunTime representation will be explained.

Topology

The modelled topology is loop-based, and thus the representation of the microgrid has been conceptualized to an ellipse. The order of DERs and loads follows the spatial relationship set in figure 4.1.

The RunTime tool offers the opportunity of assigning the color of drawing lines to certain variables of the Draft circuitry. This option has been made use of, and normal operation of the connecting electric lines is represented with black. However, upon disconnection from the main grid, or when a load/DER fails to continue functioning, the corresponding lines are to turn red.

DERs

The four designed DERs of the microgrid (PV system, Wind Turbine, BESS and Diesel Generator) are represented in the canvas, each of them providing a meter to measure the real power (P) production. Furthermore, a switch is implemented next to every DER, allowing its disconnection upon user's desire. This option can be used to simulate maintenance tasks or failure of generation during critical events.

In addition to this straightforward representation, every distributed energy resource comes with a block where the user can get a better idea of its functioning and perform parameter modifications.

- **PV System block:** presents the opportunity of modifying the solar cell temperature and solar irradiance fed into the developed model by means of sliders. Further information is offered regarding the voltage and current (DC) provided by the photovoltaic array, with the possibility of calculating the DC source power.
- **BESS:** the outside view of the battery energy storage system not only has a meter showing the amount of power generated/consumed by the DER, but also a meter showing the state of charge (SOC) and a slider allowing the user to select the amount of real power that is required from/by the BESS.

Its specific block gives a better understanding of the system, providing meters with the current and voltage (DC) produced by the Li-Ion battery. We can also find a switch, which allows the user to manually start/stop the system. The option of referencing the reactive power (Q) and a meter showing the efficiency of the system are included. Finally, a sub-block is also implemented, where every parameter of the BESS control (section 5.4.3) can be modified using sliders. Furthermore, the different procedures applied in the calculation of the i_d and i_q references in figure 5.23 can be selected by means of a dial.

- Wind turbine: its corresponding block gives a better understanding of how the DFIG scheme works, by providing different measures of active and reactive power in different points of the circuit. References for the reactive power in both the stator and rotor can be set with sliders. A turbine fault sub-block is also included, mainly dedicated to the crowbar control and with the possibility of applying short faults with push-buttons.
- Diesel generator: the diesel generator block provides values of the inputs/outputs of the electric machine model (E_{field} , V_{pu} , W and T_m) in real time. It also gives the user the option of acting on the power system stabilizer's mode of operation, as well as choosing between droop or asynchronous control for the generator.

Loads

The loads included in the general overview have a representative character, as they consist on different meters accounting for their power consumption. When modifications are to be made in their active and reactive power requirements, the "Loads" block shall be utilized. It implements two sliders for every load, where the user can modify the P and Q values.

Furthermore, the general overview presents two different meters allowing for a quick comparison between the total amount of power generated and consumed within the microgrid.

Islanded mode

The switch of functioning between grid-connected and islanded mode of operation can be done by simply making use of the "Island Mode" push button. It is directly connected to the circuit-breaker of figure 5.1, allowing for a quick transition.

When the situation requiring islanded functioning of the microgrid has ended, we can go back to grid-connected mode of operation with the push button next to it. It will check whether the implemented synchronization criteria is met at both sides of the circuit breaker, and when this is the case, switching of the mode of operation will be done.

Event simulation

The Draft module allows the implementation of "sequencers", used to create a series of events which will occur at certain points in time during a simulation. These events include:

- Opening and closing of circuit breakers, which can be used to simulate failure in transmission lines.
- Applying and clearing of faults.
- Modification of variables, allowing to change the values of wind speed and solar irradiance among others.

Another way of simulating how different meteorological conditions affect the model is with schedulers. This pre-defined block has already been explained (section 5.3.2), and it gives the option of reading data from a file and outputting it every selected fraction of time (seconds, minutes or hours). This data can be fed in the model, varying the circumstances under which the model is operating.

6.2. Microgrid operation

Once the RunTime implementation of the model has been explained, this section will test its functioning, validating the theoretical models implemented in chapter 4. In order to do so, a normal situation where the microgrid is working grid-connected will be deployed, providing information of the conditions applied and the results obtained throughout the process.

In order to do so, the simulation of a normal day in the functioning of the microgrid will be performed. To that end, 24 hours of uninterrupted grid-connected operation will be simulated, where the PV system and the wind turbine will work at their maximum power of operation given the meteorological conditions. Ancillary services of the microgrid (Diesel generator and BESS) will not provide power supply to the system during this simulation, given that the main grid is the one conducting load-following strategies.

The variation of meteorological conditions will be implemented by providing to the model different values of wind speeds and solar irradiances (the temperature of the solar cells is considered fixed at 25°C). The data is purely fictional, and represents a sunny day with medium-speed winds. The chosen values can be easily modified by the user in order to represent any scenario. This is done by editing two text files within the project, "insol" and "windspeed".

Hour	Irradiance(W / m ²)	Wind speed (m/s)
00:00	0	12
01:00	0	12
02:00	0	12
03:00	0	10
04:00	0	11
05:00	0	12
06:00	100	12
07:00	300	12
08:00	500	11
09:00	750	10
10:00	900	11
11:00	1000	11
12:00	1000	9
13:00	1000	8
14:00	1000	8
15:00	1000	9
16:00	1000	10
17:00	900	11
18:00	800	9
19:00	600	11
20:00	450	12
21:00	250	12
22:00	100	11
23:00	0	12

Table 6.1: Solar irradiance and wind speed inputs.

These values will be inputted to the model every two seconds, representing one hour each. As it can be seen, more power from the main grid will be required during night hours, where the photovoltaic panels provide no power to the system. The following figure plots the active power contribution of the four DERs implemented in the microgrid, as well as the power provided by the main grid. The four loads have been set to a fixed value, which is supposed not to change during the course of the day. However, the user can modify these values upon desire, using sliders.

- PHospital = 1.3 MW

- PStation = 1.4 MW
- PNeighborhood = 1.2 MW
- PSchool = 0.6 MW

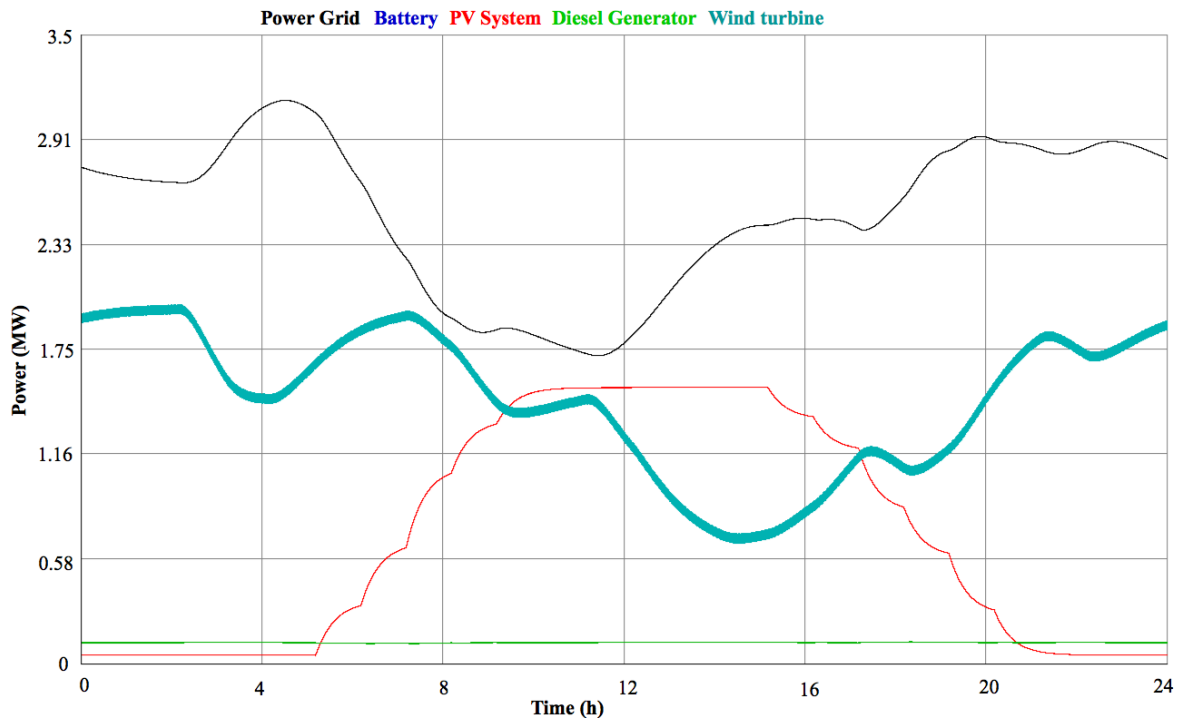


Figure 6.2: Active power contribution of each DER and main grid during a normal-day simulation.

As it can be observed, the PV system mainly provides power during central hours of the day, presenting good rapport with the Wind Energy system. The latter is functioning non-stop during the whole day, providing key support during night hours.

The battery has no role in this simulation, since its active power reference value has been set to zero. This means that no power will be offered or required by it, given the normal operation which the microgrid is undergoing. The other ancillary service, the Diesel generator, also plays a minor part in this situation. Since the microgrid's power needs that exceed the generation offered by the renewable DERs can be fulfilled by the main grid, the diesel generator remains operating at a low level, waiting to provide a quick response when its services are needed.

Islanded mode of operation

The main purpose of the previous simulation was to validate the model from a purely theoretical perspective. We can now conclude that we have successfully developed a microgrid model within the RTDS simulator, which can be used to represent its behaviour under normal circumstances¹

However, and taking the resilience perspective that characterizes this project, we must stress these operating conditions in order to see how the system responds. One of the main features implemented by the microgrid, and widely discussed in section 3.1, is the ability to switch its mode of operation from grid-connected to islanded. It has a great impact in both the system's survival throughout extreme

¹Grid-connected microgrid, where the PV system and the wind energy system work by providing the maximum power given the meteorological conditions, the BESS is not required to ensure the functioning of the system, and the diesel generator's load-following functions are taken by the main grid.

weather events and its posterior restoration. Thus, widespread failure in the main grid, triggering the necessity of operating in islanded mode, will be simulated. This is simply done by making use of the push-button named "Island mode", next to the grid representation in figure 6.1. This action triggers the "GridDisconnection" circuit breaker installed in the connection line between the main grid and the microgrid (figure 5.1), changing its state to open. The following figure will illustrate the change in the power generation within the microgrid, once the main grid is no longer able to provide load-following services.

Prior to triggering the switch in the mode of operation, the microgrid is simulated to be operating with $1000 \text{ (W / m}^2\text{)}$ and winds at the rated speed of 12 m/s . The reference point for the active power contribution of the BESS is still zero and the diesel generator's aid is not required. The values of the four dynamic loads are set according to the fixed quantities utilized in the previous section.

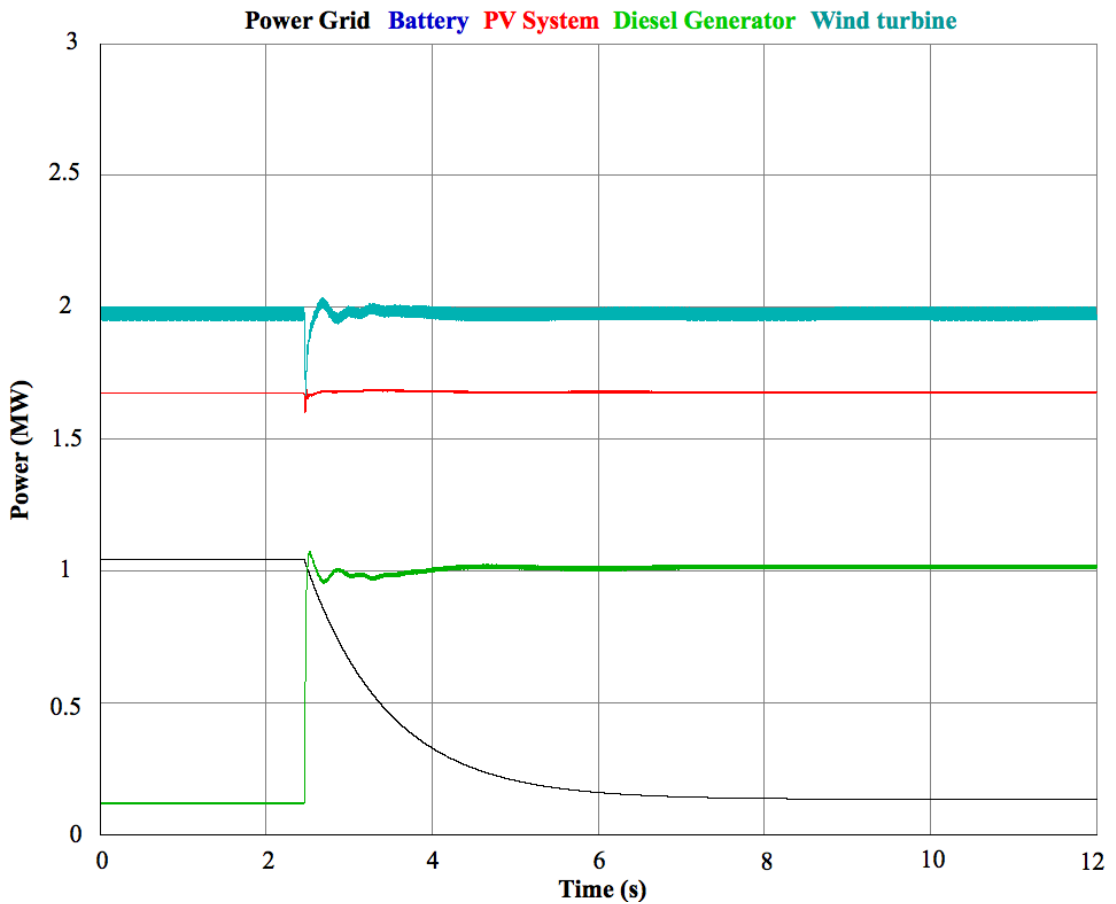


Figure 6.3: Switch of mode of operation to islanded mode.

This simulation, which runs during a time-span of 12 seconds, shows how the transition affects the power outputs of the DERs. The output of the PV and Wind energy systems present a little ripple during the shift, but they recover normality relatively fast.

Regarding the diesel generator, its power output quickly spikes in order to achieve the previous level of power supplied by the main grid. From this point on, and until the microgrid can go back to grid-connected operation again, the functions of the main grid will be taken over by the diesel generator. These functions include the load-following previously performed by the main grid, which now has an upper limit of 3MW, reducing the flexibility of the microgrid's operation.

Supposing the conditions prompting the islanded operation of the microgrid have been dealt with, we would like to go back to grid-connected mode of operation. In order to do so, the push-button marked as "Reconnect to Grid" in figure 6.1 must be pressed. This will start a procedure which will end up with a successfully re-connection to the main grid under two conditions:

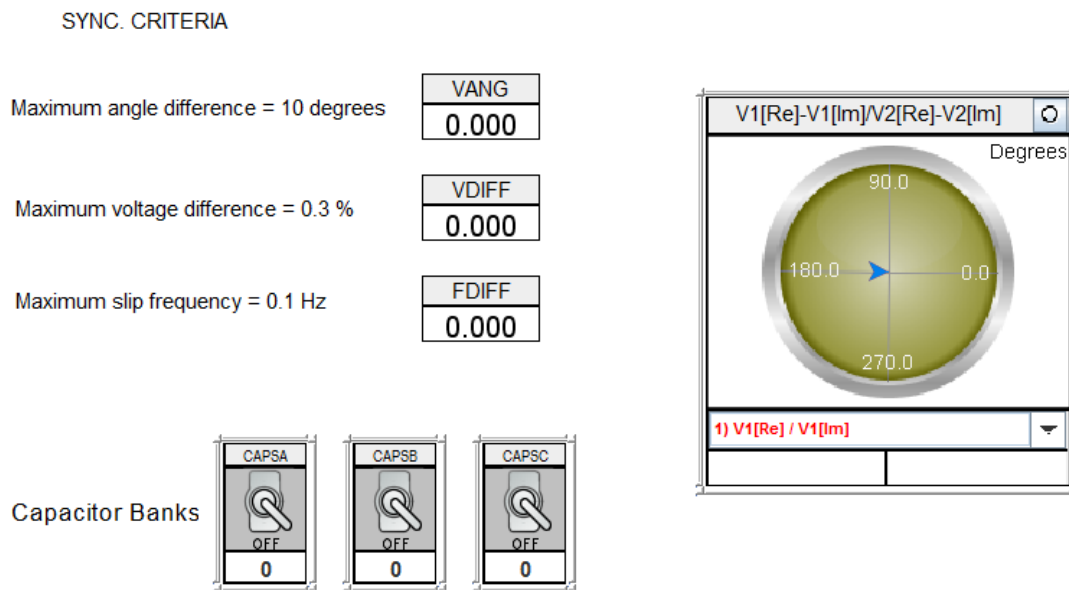
- The re-connection criteria is met. The voltages at both sides of the circuit breaker are checked to be within set limits of magnitude, angle and frequency differences. These differences are calculated and compared to the following pre-defined values, and must be in the desired range in order to continue with the re-connection.

Maximum angle difference (°)	Maximum slip frequency (Hz)	Maximum voltage difference (%)
10	0.1	0.3

Table 6.2: Synchronization criteria.

- Alignment between the microgrid's voltage phasor and the main grid phasor.

When this three-step process (requiring re-connection, meeting pre-defined criteria and alignment of phasors) is successfully conducted, the re-connection will be achieved. In order to perform it with an overview of the situation, and the possibility of modifying parameters, a synchronization block has been implemented.



After attempting to reconnect, while meeting the synchronization criteria, wait for alignment of vectors.

Figure 6.4: Synchronization block in the RunTime canvas.

It implements three meters, accounting for the three magnitude differences where criteria has been applied. Furthermore, switches allowing the user to connect three different capacitor banks to the microgrid are offered. Their objective is to help reducing the voltage difference at both sides of the circuit breaker, prompting the meeting of the set limit. The visual representation of both phasors, by means of the vector display tool, helps checking when their alignment takes place.

To end up with this islanded mode of operation section, we will conduct a similar simulation to the one plotted in figure 6.3, showing the power generation distribution upon re-connection. As predicted, and given that the PV system and the Wind energy system remain outputting a fixed active power value, the distribution of power generation is the inverse of figure 6.3. However, a steeper ripple can be seen in the diesel generator's output when performing the transition.

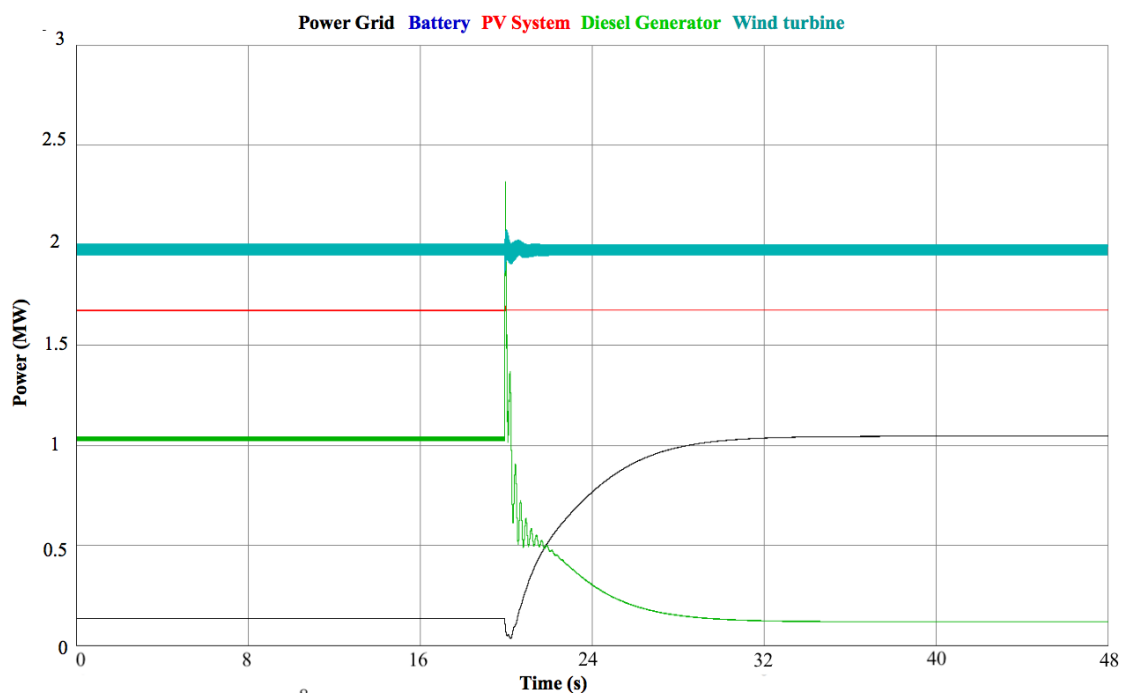
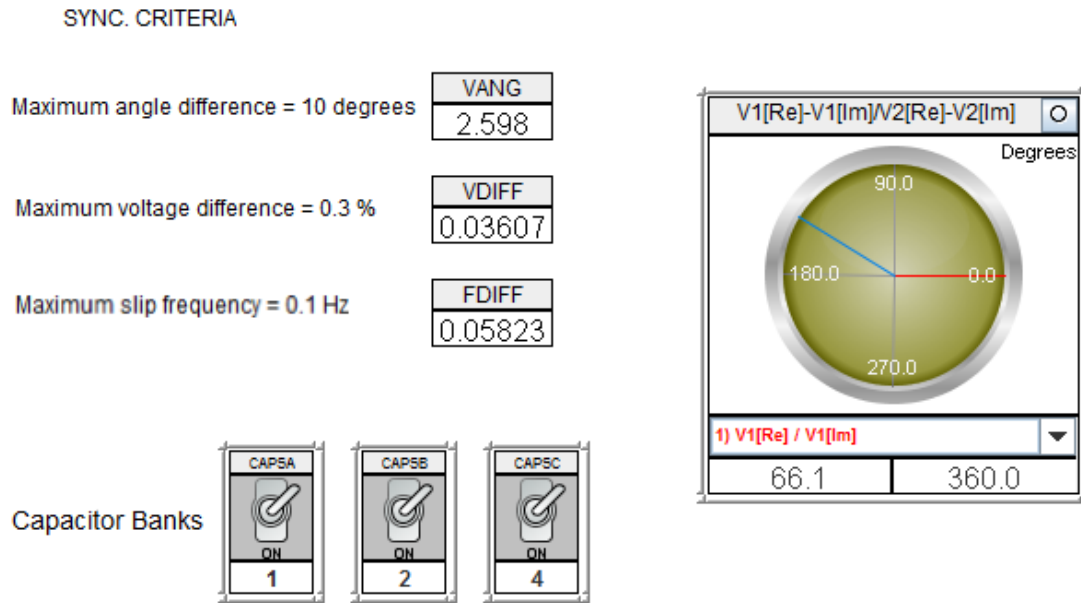


Figure 6.5: Re-connection to the main grid.

In this case the time-span of the simulation is wider, 48 seconds. This is due to the fact that the re-connection procedure is not as fast as switching to islanded mode, and requires a few seconds. As previously explained, it is started by the user (or master controller) once the situation is optimal for the microgrid to operate connected to the main grid. The following figure will give an insight on what were the actions followed after pressing the re-connection push button and prior to the confirmed re-connection.



After attempting to reconnect, while meeting the synchronization criteria, wait for alignment of vectors.

Figure 6.6: Synchronization block during re-connection procedure.

As it can be seen in figure 6.6, the user is getting information on the angle difference, frequency slip and voltage difference between the main grid and the microgrid in real time. Based on this information, the capacitor banks can be dis/connected to the microgrid (in the example they were connected in order to meet the criteria). The vector display is providing information on the main grid’s phasor (red one) and the microgrid’s phasor (blue one), which will be rotating until both coincide. When this happens, and if the criteria is met at the same time, the transition shown in figure 6.5 will be conducted.

6.3. Simulating weather events during islanded mode of operation

A normal situation where the meteorological conditions are varying during the day, as well as two different simulations regarding grid-connected to islanded and islanded to grid-connected transitions have been conducted. This section will start with a combination of the two, as we would like to analyze how is our system’s response to non-ideal situations where the microgrid is working without a connection to the main grid. To that end, previously defined inputs of table 6.1 will be fed again to the microgrid, which will be working in islanded mode of operation.

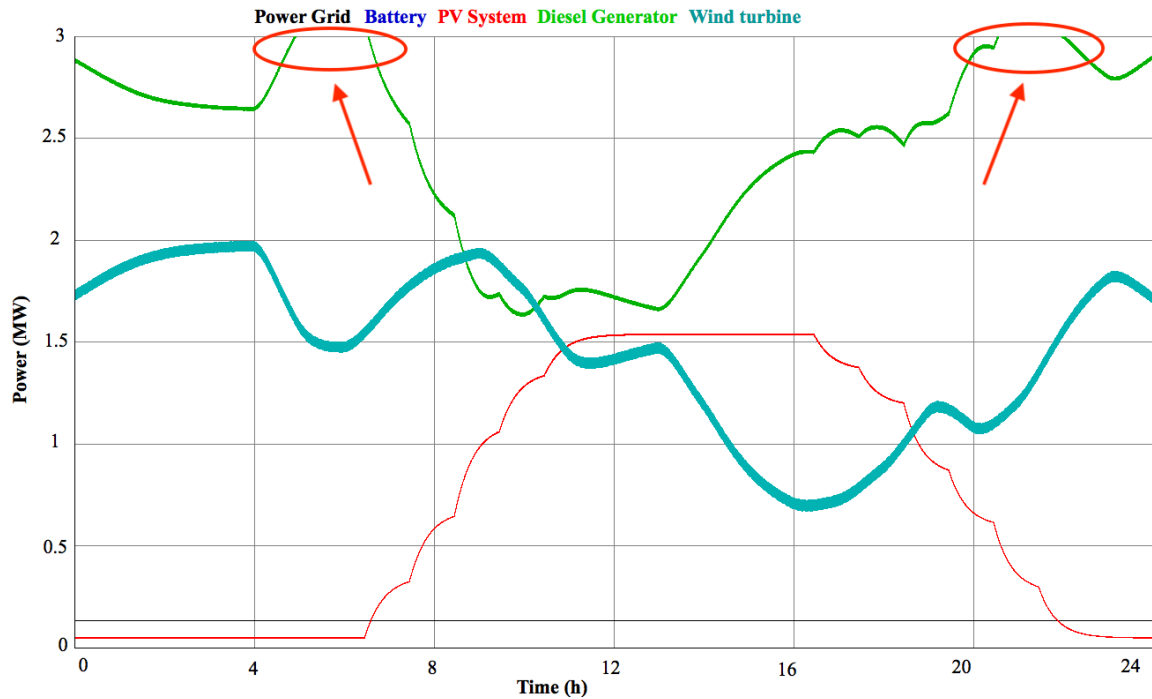


Figure 6.7: Microgrid's response to varying meteorological conditions under islanded mode of operation.

This simulation, accounting for varying conditions of wind speed and solar irradiance during a day, shows how under islanded mode of operation the microgrid struggles to supply every load.

Before the dawn, approximately between 5 and 7 am, the lack of sun irradiance combined with a variation in the wind speed force the Diesel Generator to work above its rated power output in order to ensure the supply. Furthermore, and towards the end of the simulation, between 8 pm and 10 pm, low wind combined with a declining solar irradiance cause the diesel generator to face the same situation. Both these situation have been highlighted in the figure above, given that the situation would be untenable. In order to help the microgrid deal with these edge situations, the Battery Energy Storage System must provide power support. To that end, another scheduler is deployed to set the power reference of the battery at 0.5 MW during peaks in the power needs of the diesel generator.

The following plot of figure 6.8 shows the same situation, but with the battery playing an active role in ensuring full functionality of the microgrid.

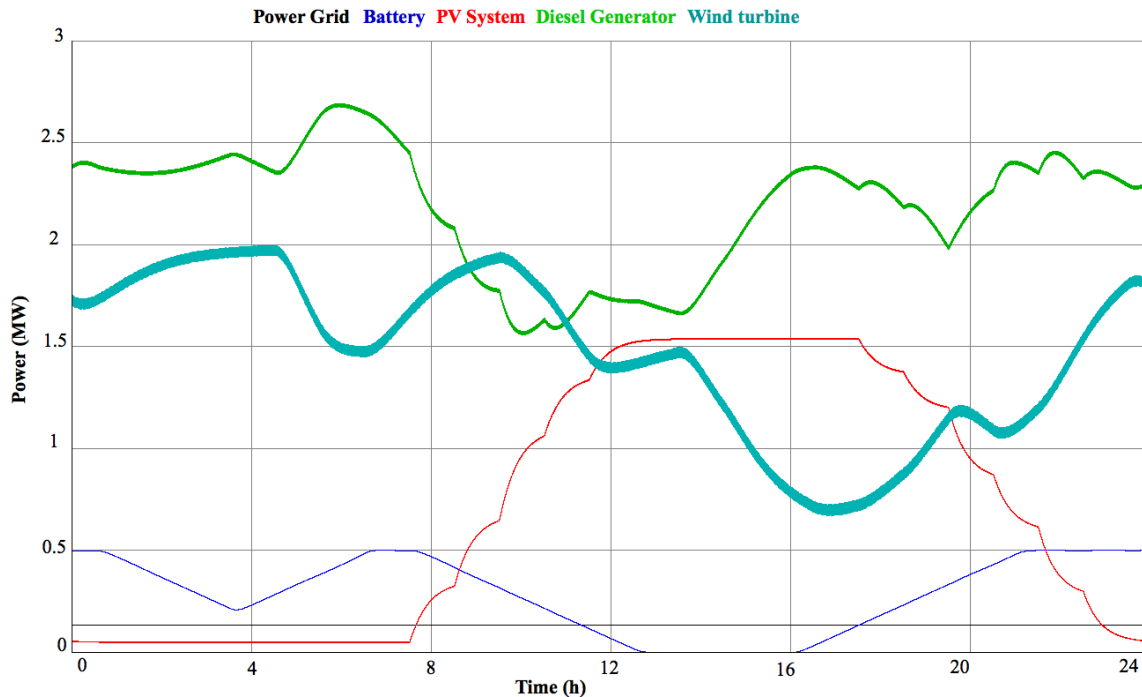


Figure 6.8: BESS support to microgrid's islanded mode of operation.

From a quick analysis, it can be observed that now the diesel generator does not need to go above its rated active power capabilities. The power contribution of the battery is plotted in blue, and the battery dynamics influence the time that it needs to achieve the set reference of 0.5 MW. Therefore, the BESS helps extending the range of circumstances under which the microgrid is able to fully function. However, and aiming to stress even more the situation under which the microgrid must perform its power supply responsibilities, the next subsection will push the limits until the microgrid is no longer able to maintain every load functional.

6.3.1. Load shedding

Previous situations have been simulated under the assumption that the amount of generation power exceeds the amount of power required by the loads within the microgrid. However, this is not always the case, as several situations may arise during islanded mode of operation where this assumption does not hold.

- When meteorological circumstances are rough, both DERs based on renewable energies (PV and Wind energy system) will not be able to provide their maximum active power values. This may result in the system making use of both ancillary services at full capacity, and still not being able to fulfill power demand, leading to the necessity of performing load shedding.
- Supposing our microgrid is taking part of the meshed set of loop-based microgrid described in section 3.3, a hierarchical arrange of loads is to be displayed. When a microgrid is having trouble supplying a critical load, it may require help from near-by microgrids, which could be asked to provide power even at the expense of disconnecting low-priority loads.
- Failure in the distributed energy resources would imply a significant drop in the power capacities of the microgrid, causing the master controller to disconnect a variety of loads.

Next simulations will work in a critical environment, where the power generation is not sufficient to supply all the loads within the microgrid. A load shedding strategy will be implemented, and two loads will be eligible to be disconnected upon necessity: the school and the neighborhood. The hospital and the train station are considered of high priority, and therefore their supply must be ensured throughout

any kind of situation.

The first simulation will apply conditions that could arise during the starting of a hurricane: decrease in solar irradiance due to formation of clouds and high-speed winds. These winds will take the wind turbine to its limit, exceeding the cut-out speed and thus, prompting its disconnection from the microgrid. Consequently, the amount of power generated will not be enough to satisfy every load and load shedding will be applied. Ordered by amount of importance to the community, the first disconnected load will be the school and then, if needed, the neighborhood will be induced a blackout.

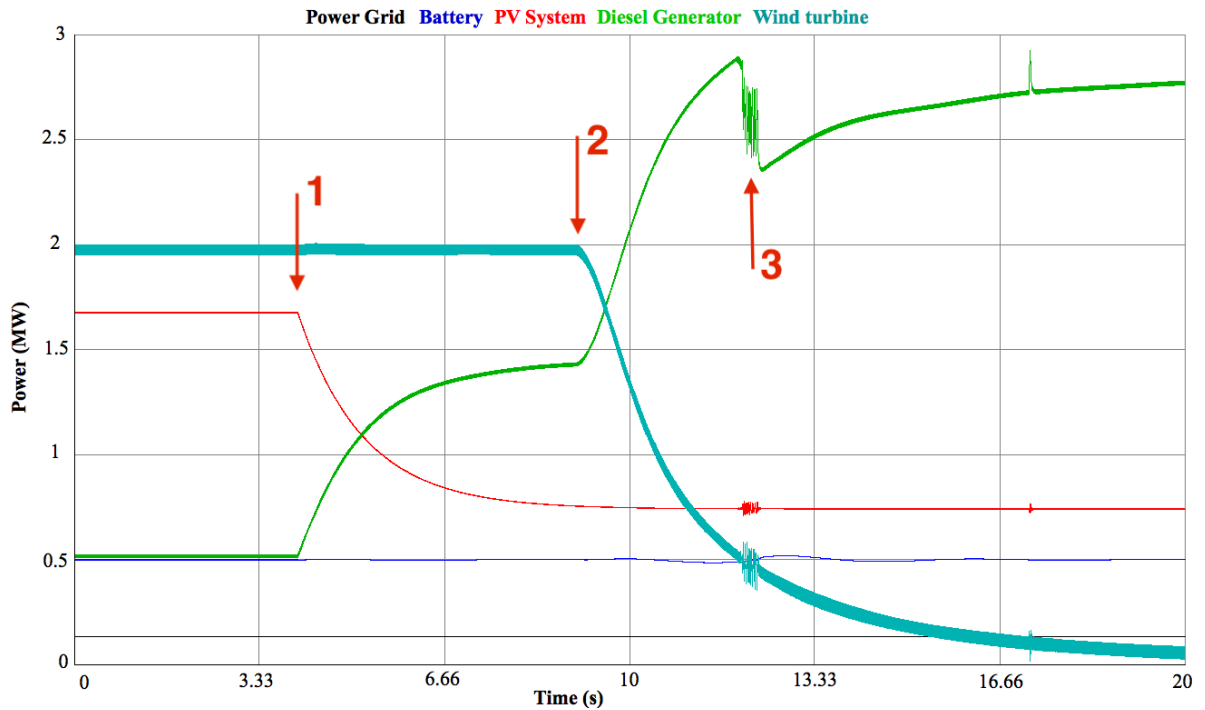


Figure 6.9: Load shedding applied during hurricane-like meteorological conditions.

Figure 6.9 can be explained by differentiating three main changes in the system's tendency. First point represents the user triggering the "Hurricane" button present in figure 6.1, which starts a sequence whose first step is the progressive declining of solar irradiance from $1000 \text{ W} / \text{m}^2$ to $500 \text{ W} / \text{m}^2$. The diesel generator is in charge of compensating this decrease of the PV system's power generation. The second point corresponds to the second step of the sequence, which represents the wind turbine receiving winds with a speed above the cut-out threshold, and stopping its functioning. This situation results in the diesel generator having to offset this power loss, which leads to the diesel generator approaching its maximum rated active power generation.

Finally, the third point represents the master controller triggering disconnection of the school load, when facing the sudden spike in the power required to the diesel generator. By stopping the supply to the school load, the microgrid manages to keep the other three loads functioning at full capacity, with the diesel generator working under its rated active power. If the situation would worsen, the next load in the priority ranking would face disconnection in order to maintain the critical loads functioning.

6.3.2. Failure in transmission lines

Continuing with the hurricane simulation, the developed RunTime GUI offers the opportunity of simulating failure in the transmission lines of the microgrid. This can be done with the push-buttons implemented in figure 6.1, under the name of "LineFailure1" and "LineFailure2". The first one triggers

the opening of a circuit breaker placed between the hospital and the PV system, and the second one does the same with the line that connects the Wind energy system and the neighborhood load.

This type of failures in transmission lines are common during hurricanes, mainly because of high-speed winds and trees falling onto the aforementioned lines. The effects that these situations could have on the microgrid are shown hereafter. First, we will simulate failure in the line connecting the wind energy system and the neighborhood load. This induced situation will not have any effect in our microgrid's functionality, as we predicted in the topology section of the chapter "Fields of improvement" (figure 3.3). This is one of the main advantages of loop-based microgrids, and the simulation results are shown in figure 6.10.

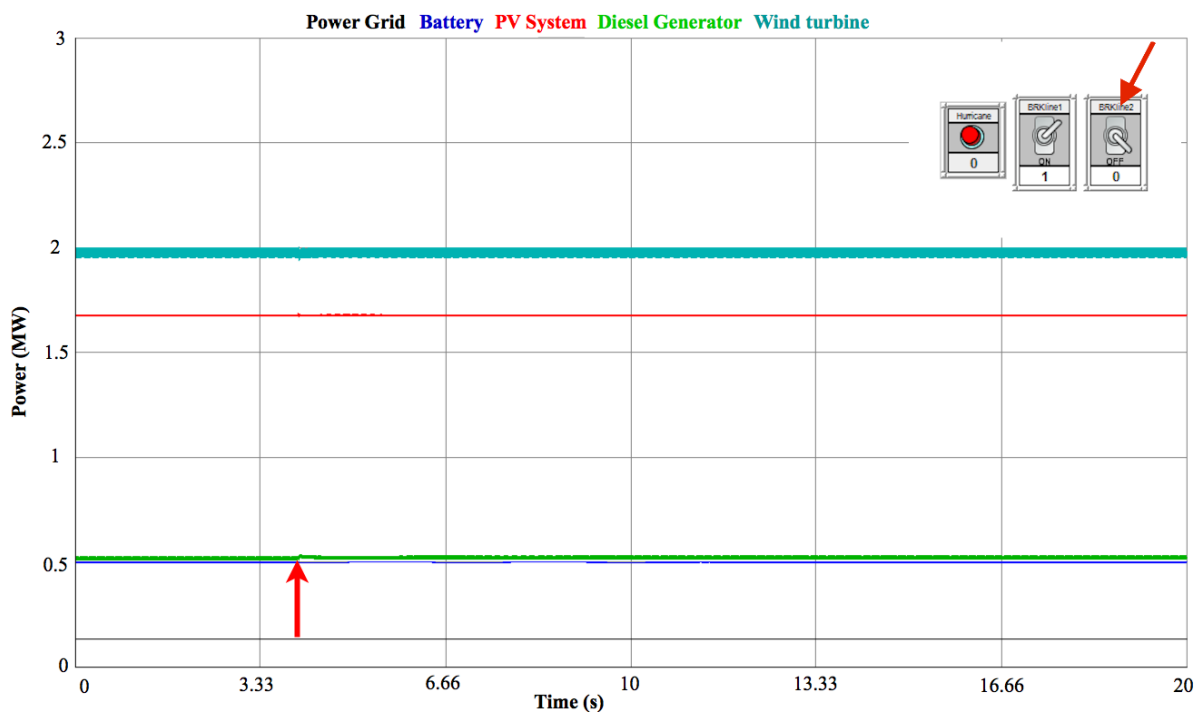


Figure 6.10: Single failure in transmission lines.

As it can be observed, only a slightly ripple in the power generation distribution is produced when the microgrid faces failure in a single transmission line. The next simulation is a follow-up of the current one, and accounts for the user triggering a fault in the line connecting the hospital and the PV system.



Figure 6.11: Division of the microgrid in two separated sub-microgrids.

This type of N+2 contingency exceeds the microgrid's redundancy, separating it into two different ones:

- First sub-microgrid: which comprises the wind energy system, the diesel generator (still able to perform load following functions) and two loads, the hospital and the station. This improvised microgrid still presents high functionality, given that it is connected to the master controller, there is complete observability of its components and the diesel generator is fully functional.
- Second sub-microgrid: situated between the two failures, with no connection to the master controller. It is composed of the BESS, the PV system and two loads, the neighborhood and the school. There is no observability of this sub-system, which is not able to perform load following. After extreme disturbances, it will not succeed in supplying its loads, which will remain disengaged.

After the user has triggered the second failure, the subsequent response of the system is plotted in figure 6.12.

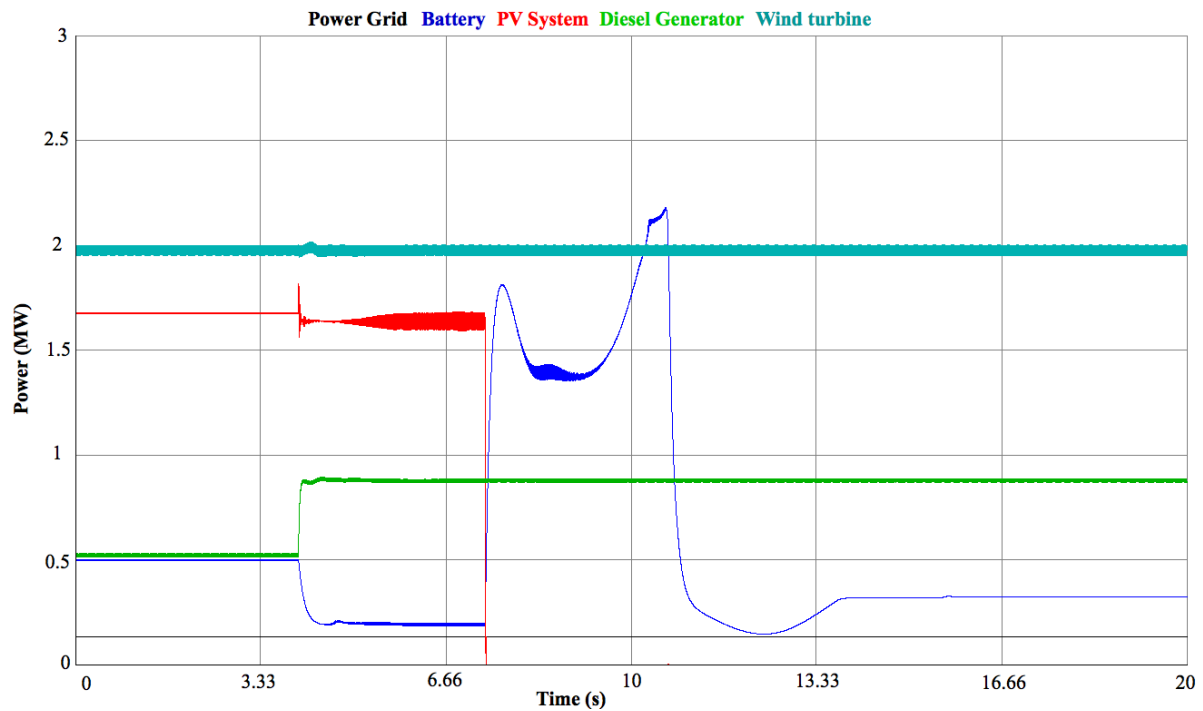


Figure 6.12: Response of the system to the second line failure.

We can observe how the DERs which are part of the first “sub-microgrid” behave normally by adapting to the power requirements of the two loads within their electrical boundaries. After a quick transition, they reach steady operation, which is maintained until the end of the simulation.

Opposite to this, the PV system crashes almost immediately after failure and the BESS presents great fluctuations when trying to supply the loads, reaching a steady state under its set active power reference. This part of the microgrid can be considered as non-functional, and will need restoration. Once the simulation is ended, the RunTime GUI provides the following information to the user, by means of the implemented meters and switches.

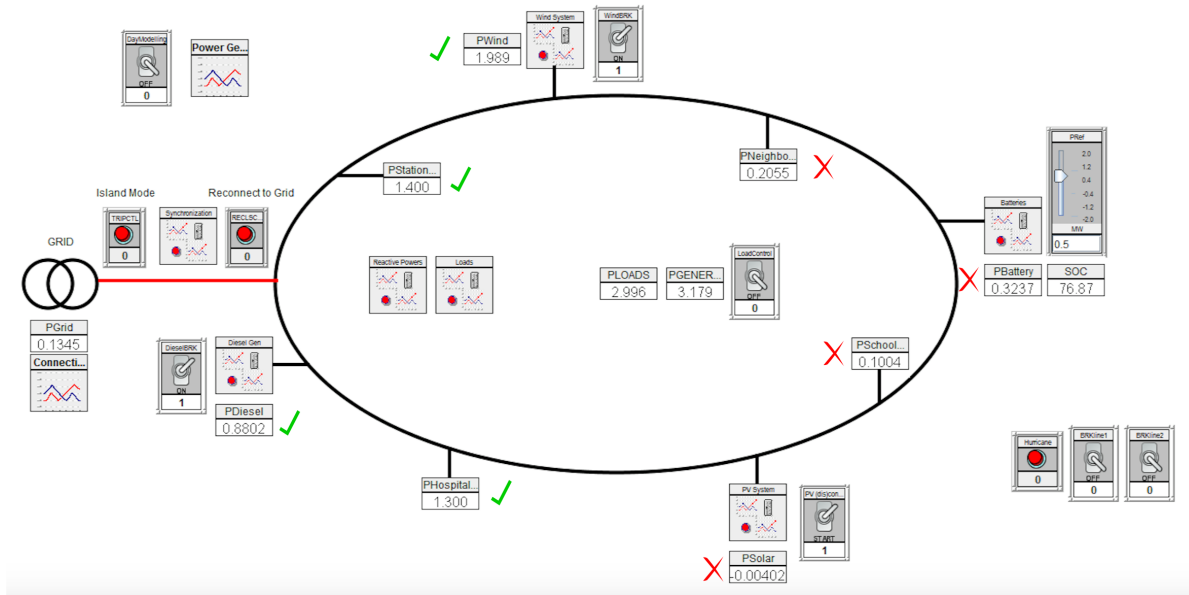


Figure 6.13: RunTime canvas after performing the second simulation.

6.4. Meshed set of loop-based microgrids

The implementation of a complete microgrid in the RTDS simulator is already challenging in terms of computational burden and amount of hardware required. In fact, the microgrid model which has been used for the previous simulations makes use of 90 nodes, exceeding the node limit set for PB5 network processors (72 single phase nodes). In order to be able to simulate our system, one of the NovaCor cores (section 5.1) owned by the TU Delft must be used.

The last simulation performed, where the loop-based microgrid is no longer able to continue functioning within the required parameters, accounts for a situation that would need the concept developed in the fields of improvement's section 3.3. By working with a meshed set of loop-based microgrids, and implementing a logic that takes into consideration the hierarchy of different loads in order to always maintain the supply to the critical ones, this situation could be dealt with. However, the performance of these simulations would need a significant amount of hardware exclusively dedicated to them, and thus, it shall be left for future lines of work.

7

Conclusions

Although the previous chapter was the culmination of the developed dissertation within this project, this last chapter will conclude the thesis, by providing answers to the research questions formulated in chapter 1. Overall, contributions to the grid-resilience field have been made, both theoretical and with the development of a functional microgrid model. The following sub-sections will provide specific answers based on the degree of fulfillment achieved.

What are the state-of-the-art guidelines that shall lead the design of smart microgrids in order to enhance its resilience?

After extensive analysis of the state-of-the-art trends regarding Smart Microgrids and their influence in resilience, the number of areas that should be considered when designing a microgrid have been narrowed down to five:

- **Island mode of operation.** The transition between grid-connected and island mode of operation must be optimized in terms of feasibility and power generation. Quick disconnection from the main grid upon facing critical conditions, resulting in an autonomous functioning of the microgrid must be ensured in order to enhance system's resilience. Restoration procedures must be started from the distribution grid, combining these efforts with the traditional down-stream procedures.
- **Redundancy.** The amount of redundancy implemented in the microgrid must be studied before its design. A compromise must be selected between economic expenditure and level of resilience achieved. Taking a N+X redundancy approach can be useful, differentiating between standby and active-active components.
- **Topology.** Loop-based has been found to be the optimal topology for the deployment of Smart Microgrids. Along these lines, the concept of *Meshed set of loop-based Smart Microgrids* has been introduced, implementing a different topology for the microgrids and for the overall system, loop-based and meshed. The benefits of this idea have been discussed, and its positive impact in the system resilience is believed to be significant.
- **Advanced metering infrastructure.** It is one of the key points of systems resilience, when it comes to improve the observability of the system. Having real-time information regarding the state of every component of the microgrid helps improving the response to critical situations, in addition to facilitate policy-making. The ability of gauging the extent of failures is vital when deploying the restoration procedures.
- **Self-healing.** Approached along with the previous point, can be performed by adding distributed automation to the AMI. The proposed procedure is called FLISR (Fault Location, Isolation and Service Restoration) and by making some adjustments to the original idea, the grid-resilience can present major enhancements by means of deploying a set of Smart Microgrids

Considering the theoretical analysis, can we provide a versatile model in accordance with it, aiming to offer a benchmark scenario to study grid resilience by means of Smart Microgrids implementation?

The objective of developing an accurate microgrid model has been reached within chapters 4 and 5. The represented microgrid has been deployed in the vicinity of Delft, and comprises four distributed energy resources (PV system, Wind energy system, Battery energy storage service, Diesel Generator) and four loads accounting for important facilities.

The achieved model, while having a strong theoretical background, presents a great versatility. Thus, the user is able to modify not only the inputs fed into it (such wind speed or solar irradiance) but also the selected control strategy for some of the DERs. It comes with an user-friendly GUI, which facilitates simulation and displaying of results.

Once simulations are run in the model, do the results validate the model itself and the theoretical resilience-related assumptions?

The versatility of the model allows the user to perform a wide variety of situations that the microgrid could encounter in real life. In order to provide validation of the model, as well as to analyze the response of the resilience-enhanced modelled microgrid, the following simulations have been successfully deployed.

- Grid-connected operation under fluctuating weather conditions.
- Transition to island mode of operation.
- Re-synchronization with the main grid by switching from island mode of operation to grid-connected.
- Island mode of operation response to fluctuating weather conditions.
- Support of the BESS during island mode of operation.
- Load-shedding policies when facing extreme weather events.
- Response to failure in the transmission lines during island mode of operation.

Future lines of work

Due to the wide topic that has been chosen and developed throughout the thesis, it could serve as a starting ground for a large number of possible research. Hereafter, two different possible lines of future work are briefly overviewed.

- The guidelines selected in the third chapter could serve as starting point for future projects developing them further. The possibility of analyzing their impact in system's resilience, by making use of data from real installations, could result in a more accurate study. Along these lines, extensive literature can be found on several U.S. microgrid-related projects, which share their results publicly.
- The model could be improved in order to fully implement the *Meshed set of loop-based microgrids* concept. One of the main challenges is the development of a master controller, which would be in charge of regulating the power exchanges between microgrids, in addition to provide accurate gauging of failures within the system. Furthermore, the amount of hardware needed and the computational burden of modelling such an large system would arise as a problem. One option could be to implement some microgrids in different types of software with less computational requirements, and then interconnect the whole system.

Appendices

A

PV system control

The content of this appendix are six different figures, accounting for the circuitry of the phase lock loop (PLL) and the PI control blocks of the PV control. Their circuitry, which was over-viewed in section 5.3.3, will be exposed hereafter.

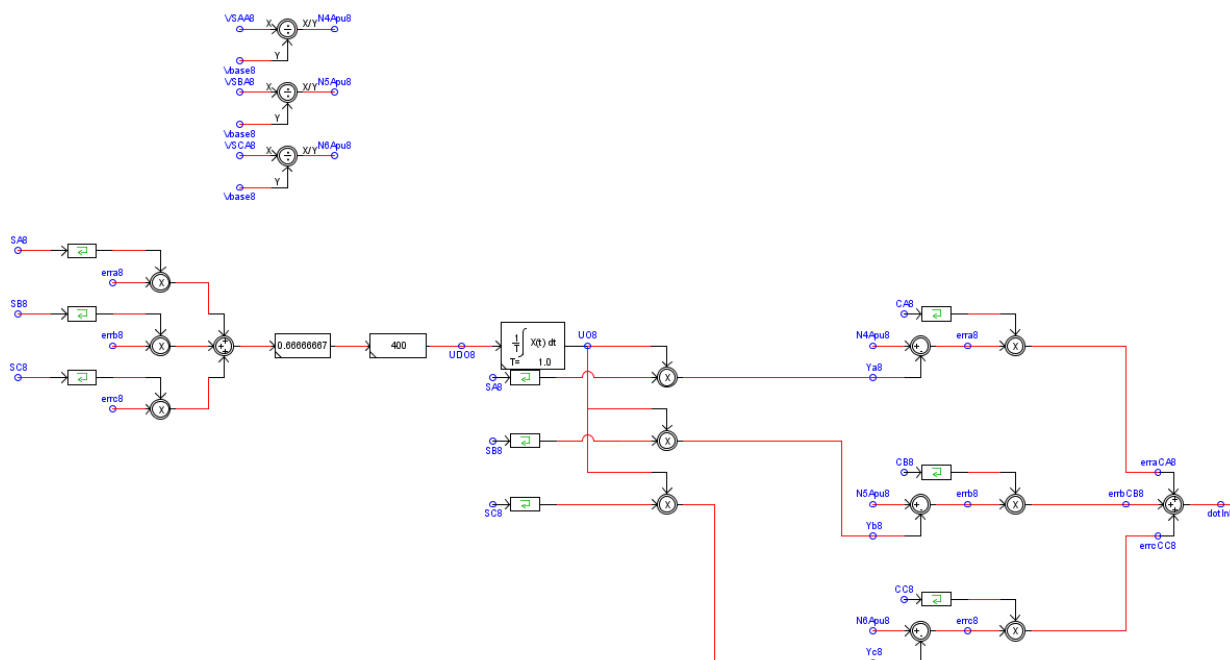


Figure A.1: Phase Lock Loop circuitry (A).

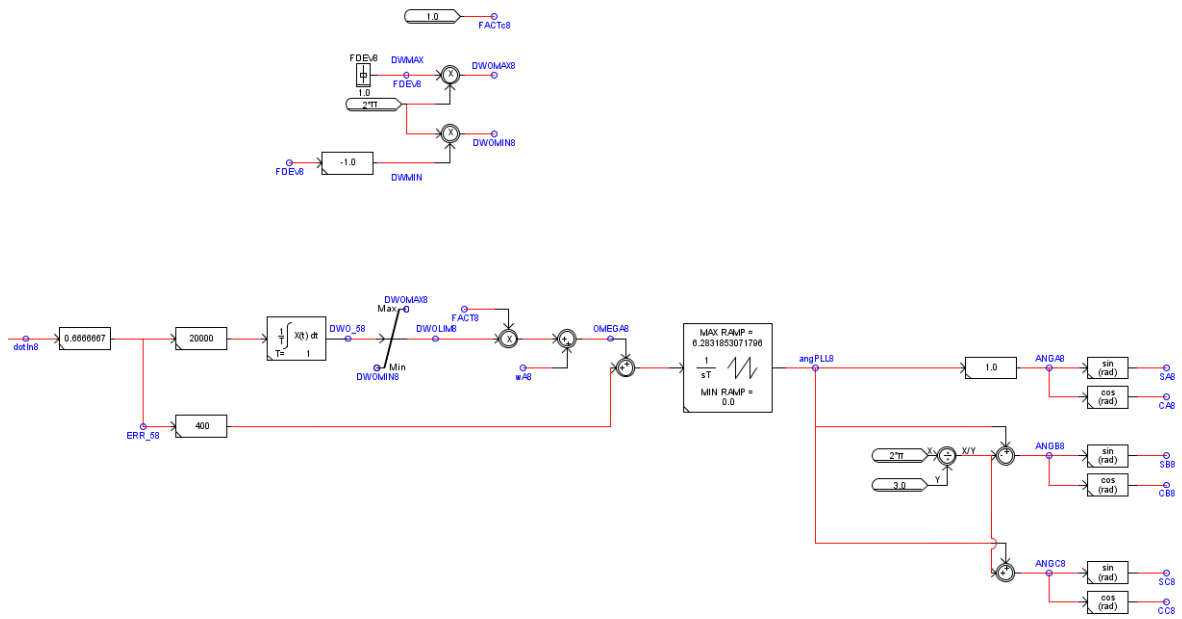


Figure A.2: Phase Lock Loop circuitry (B).

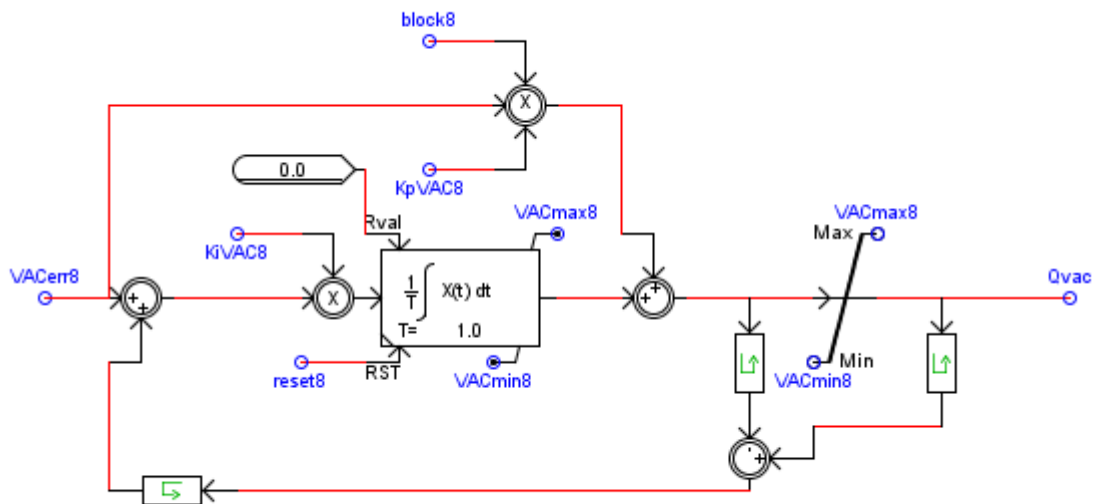


Figure A.3: Outer loop PI control (VAC) circuitry.

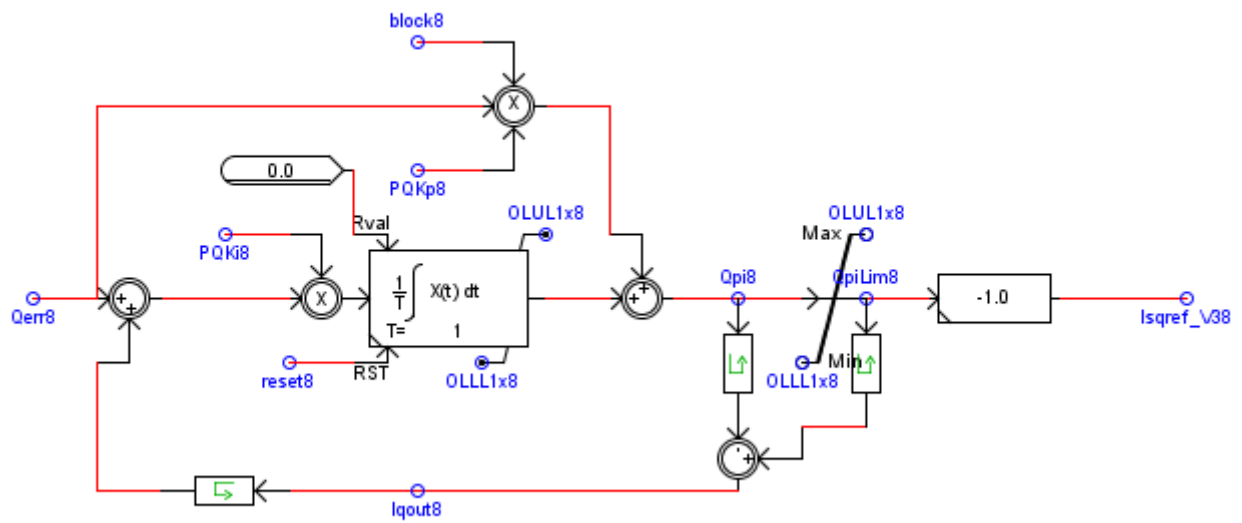


Figure A.4: Outer loop PI control Q circuitry.

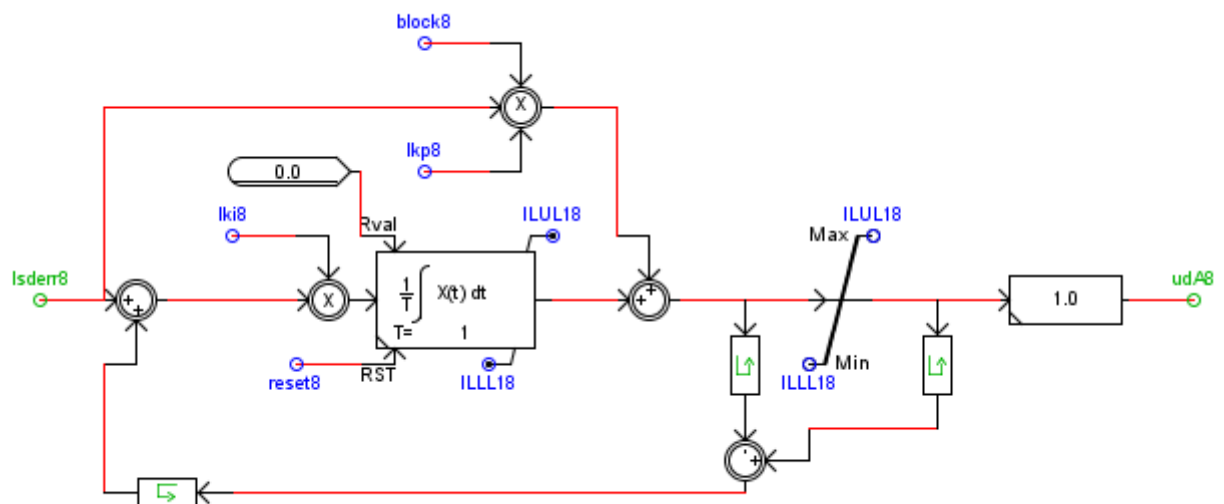


Figure A.5: Inner loop PI control for id circuitry.

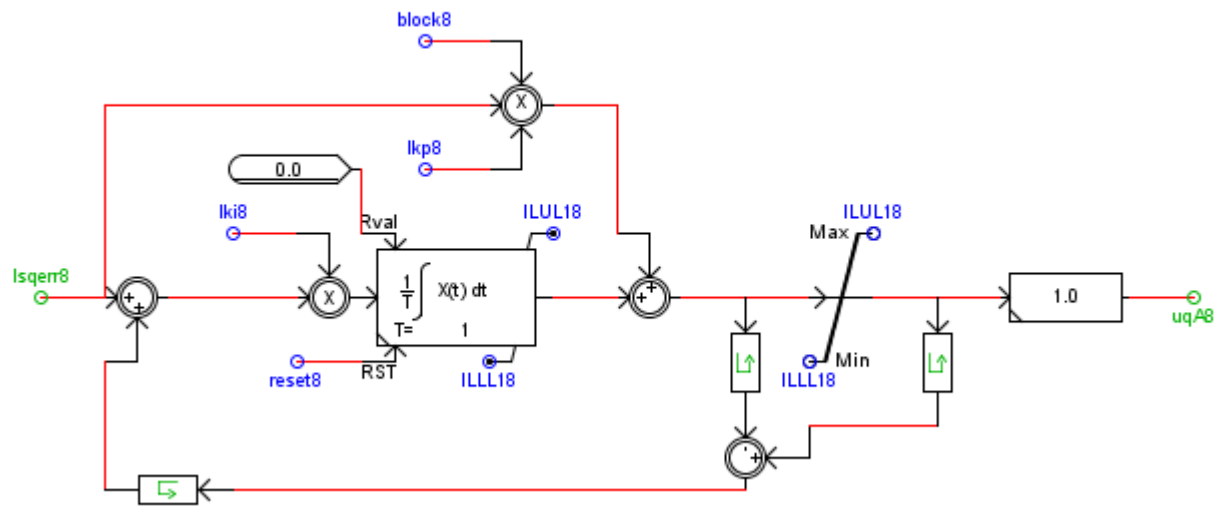


Figure A.6: Inner loop PI control for i_q circuitry.

B

BESS control

The content of this appendix are four different figures, accounting for the circuitry of the PI control blocks of the BESS control. Their circuitry, which was over-viewed in section 5.4.3, will be exposed hereafter.

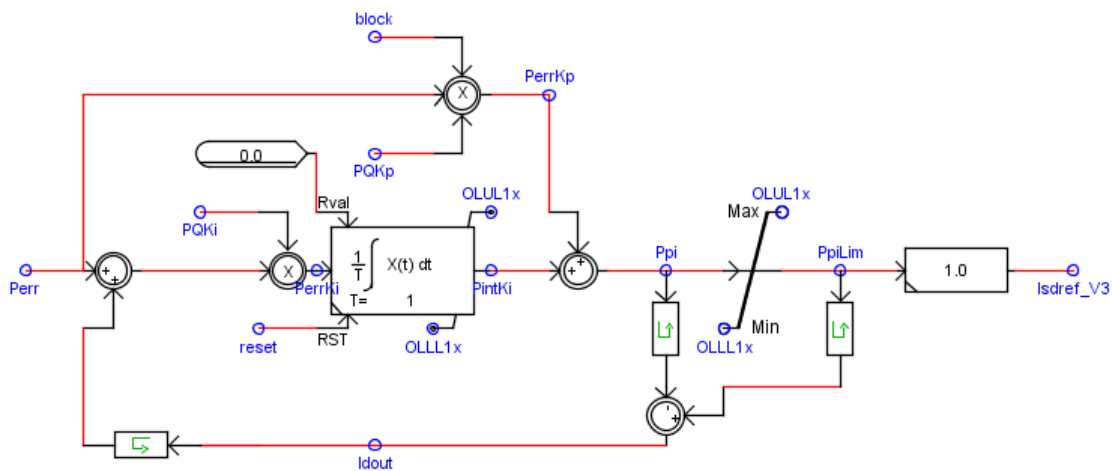


Figure B.1: BESS PI control for active power (P) circuitry.

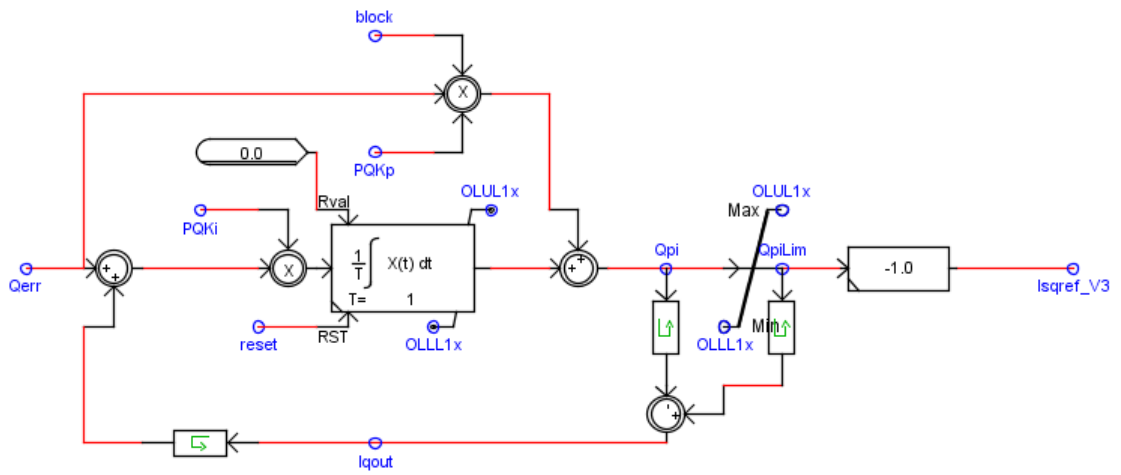


Figure B.2: BESS PI control for reactive power (Q) circuitry.

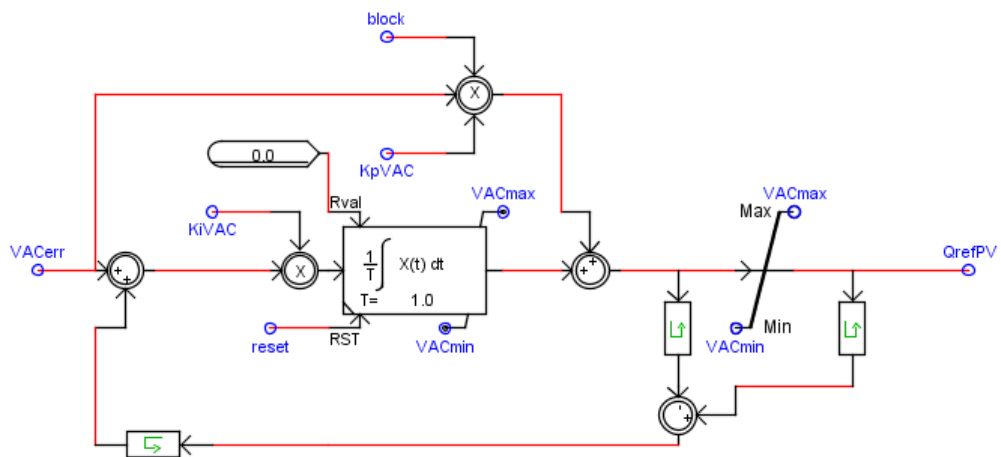


Figure B.3: BESS PI control (VAC) for q axis reference circuitry.

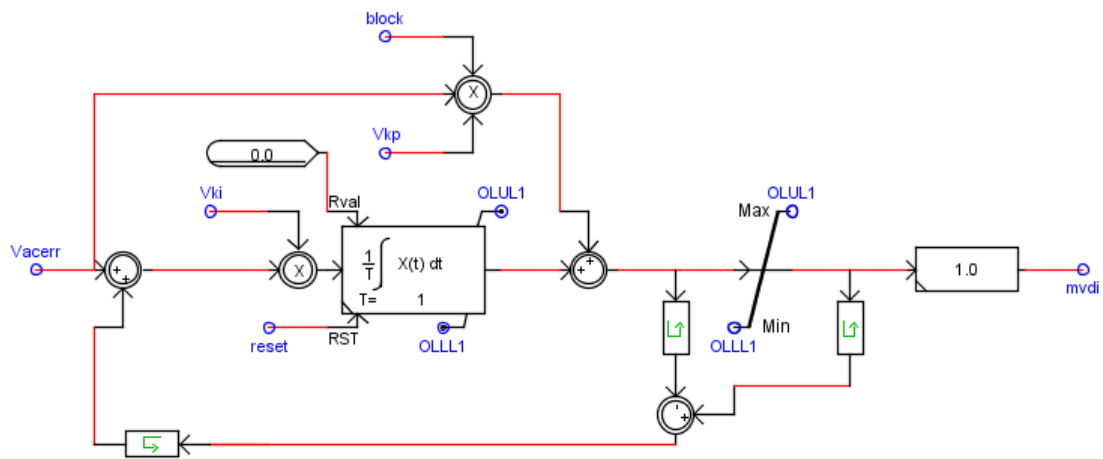


Figure B.4: BESS PI control (VAC) for islanded mode of operation circuitry.

C

User Manual

The content of this appendix includes a brief manual, which shall be followed by the user when performing simulations with the provided microgrid model. We aim to offer an use guide to facilitate a quick understanding of how to manipulate the model, with the following two objectives:

1. The user will get an insight on how to manipulate the predefined model, making use of every feature implemented within it.
2. The user will be able to modify certain characteristics of the predefined model, so that the model can provide a better simulation of the specific required scenario.

C.1. Compiling the circuit

This first step takes place in the Draft module, which can be accessed from the RSCAD main window by clicking on the .dft file. (Further information regarding the different modules of the RSCAD software can be found in Section 5.1).

In our specific case, the complete name of the file is **Delft.dft** and it contains the entire circuitry developed for the microgrid model. Given that the model has been properly developed, implemented and validated in the previous three chapters (4, 5 and 6) it is not the scope of this user manual to further extend it, and thus we assume that the model is up to date and working. From this point, two simple actions must be carried out by the user in order to perform the compiling of the circuit.

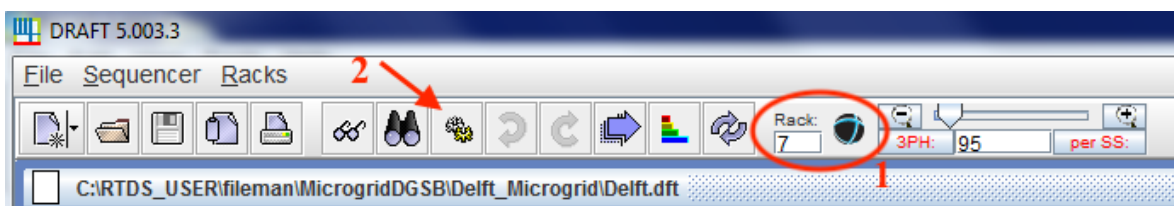


Figure C.1: Draft compiling process.

The first action is to select the rack in which the file must be compiled. Currently, the equipment of the IEPG group's RTDS simulator consists in eight different racks, two of them being NovaCor cores (further information can be found in section 5.1). The complexity of the model results in the necessity of assigning 90 nodes to it, which cannot be dealt with by normal PB5 network processors (limit of 72 single phase nodes). Therefore, one of the two Novacor cores must be selected in order to perform the compiling and posterior simulation. At present time, these two cores are situated in racks 7 and 8.

The second action, highlighted with number two in figure C.2, consists in pushing the compiling button, which will generate a simple message when the compilation is successful and a warning pop-up window when warnings or errors are encountered.

C.2. RunTime canvas

The RunTime module, which runs in the host computer, presents a canvas where the graphical user interface has been developed. Its function is to run and control the simulation of the circuit previously designed and compiled.

Although this GUI has already been explained (Section 6.1) in relation to the theoretical guidelines and the model implementation of the Smart Microgrid, this manual will provide explanations from a functional perspective. To that end, the different parts of the interface have been highlighted, and its purpose shall be explained hereafter. It must be noted that some parts of the canvas, the ones related to the performance of simulations, are left out of this section and will be explained in section C.3.

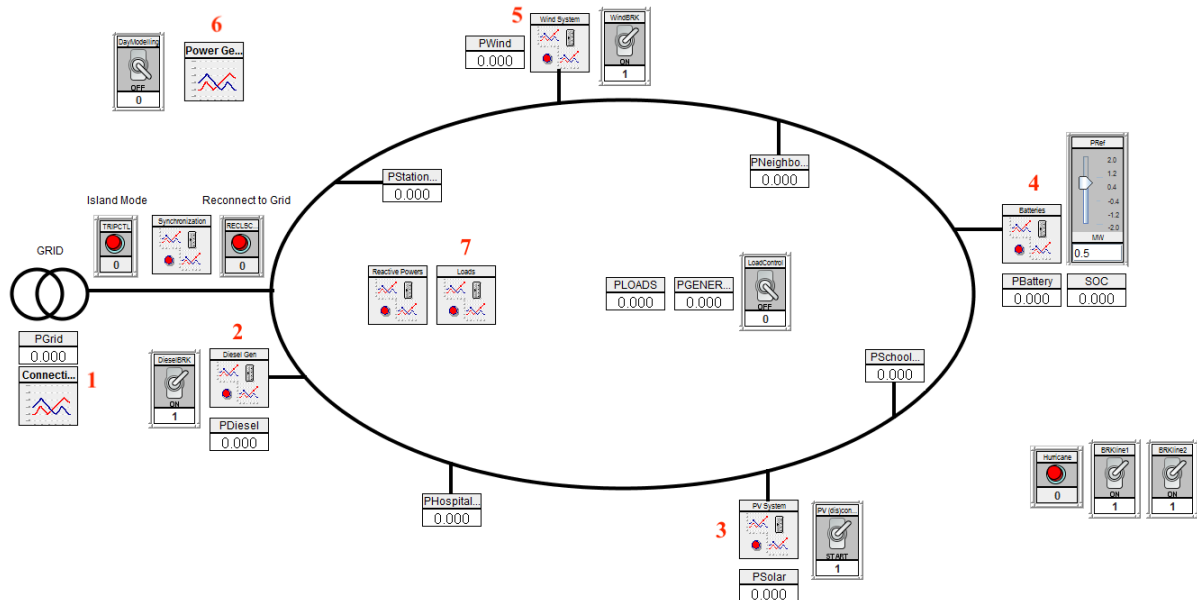


Figure C.2: RunTime canvas functionality.

An enumeration has been chosen to highlight the different components. The function of every part of the model, as well as the opportunities given to the user to modify parameters in order to adequate the simulation, will be explained.

1. Connection to the main grid: characterized by an active power meter and a plot representing the three-phase current of the main grid. This plot, as well as the rest of plots within this canvas, are updated every time the user performs an action on the model or updates it.
2. Diesel Generator: in addition to the active power meter (present in every generator of the system), a sub-block allowing the user to directly modify its functioning has been implemented.

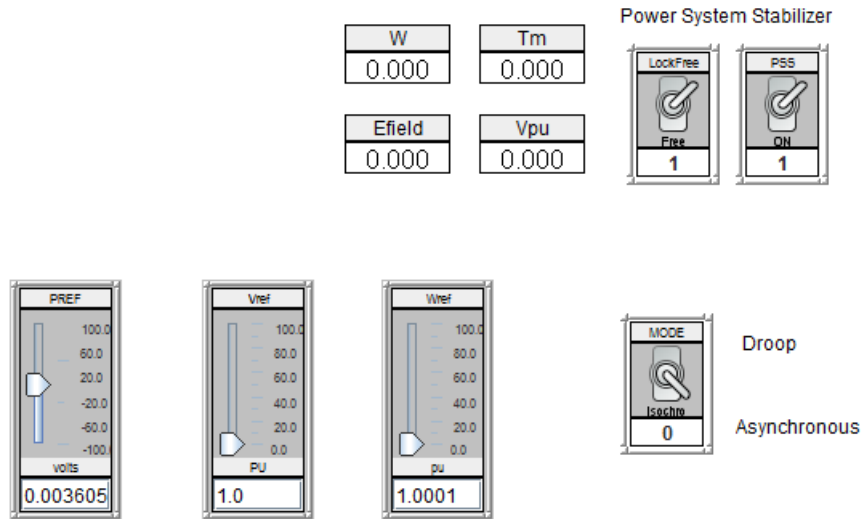


Figure C.3: Diesel generator sub-block.

It serves a double function, as it shows several variable values and provides the user the means to choose the power system stabilizer’s mode of operation, as well as the option of selecting droop or asynchronous control for the generator. Values for the active power, voltage and speed references used in the control can be set with sliders.

3. **PV system**: a visual representation of the PV array connection to the microgrid is provided in the PV system’s sub-block. Furthermore the DC source power calculation is given, alongside with the option of setting the solar cell temperature and the irradiance received by the PV array. This two values, which have a direct effect on the output of the system can be manually set by the user.

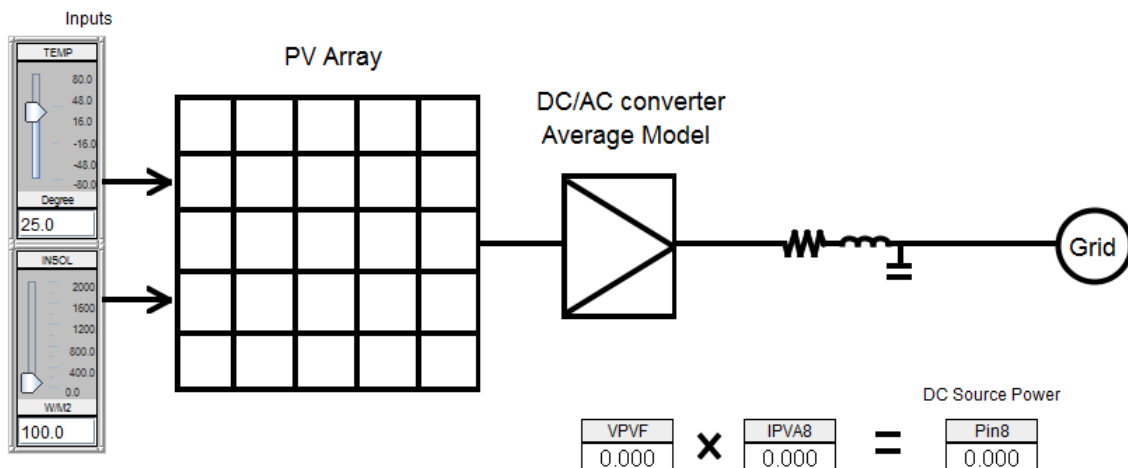


Figure C.4: PV system sub-block.

4. **BESS (Battery Energy Storage System)**: the battery distributed energy resource comes with another meter referred to the SOC (state of charge) and a slider allowing the user to determine the flow of power. When selecting a positive value, the direction will be DC-AC, working as a

power generator. When selecting a negative value, the BESS will require that amount of power, charging itself (increasing its SOC) by working as a load.

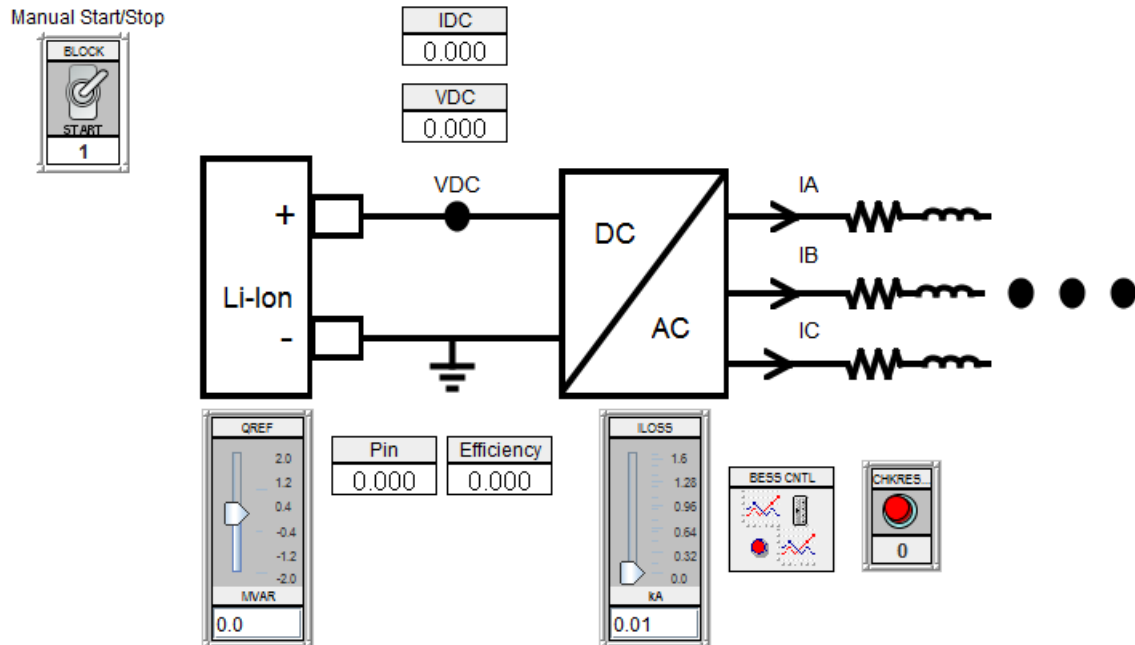


Figure C.5: Battery energy storage system sub-block.

The sub-block attached to the aforementioned meters and slider follows the same structure of the PV system's one. It provides a graphical representation of the BESS connection to the microgrid with some meters, as well as the opportunity of setting control parameters via sliders. Further information can be found in section 6.1.

5. Wind system: the content of the sub-block accounts for a representation of the DFIG structure, with meters giving information about different sections of it. Several control parameters can be modified by the user, and another sub-block regarding the faults in the turbine is included, mainly dedicated to the crowbar control and the possibility of applying short faults by means of push buttons.

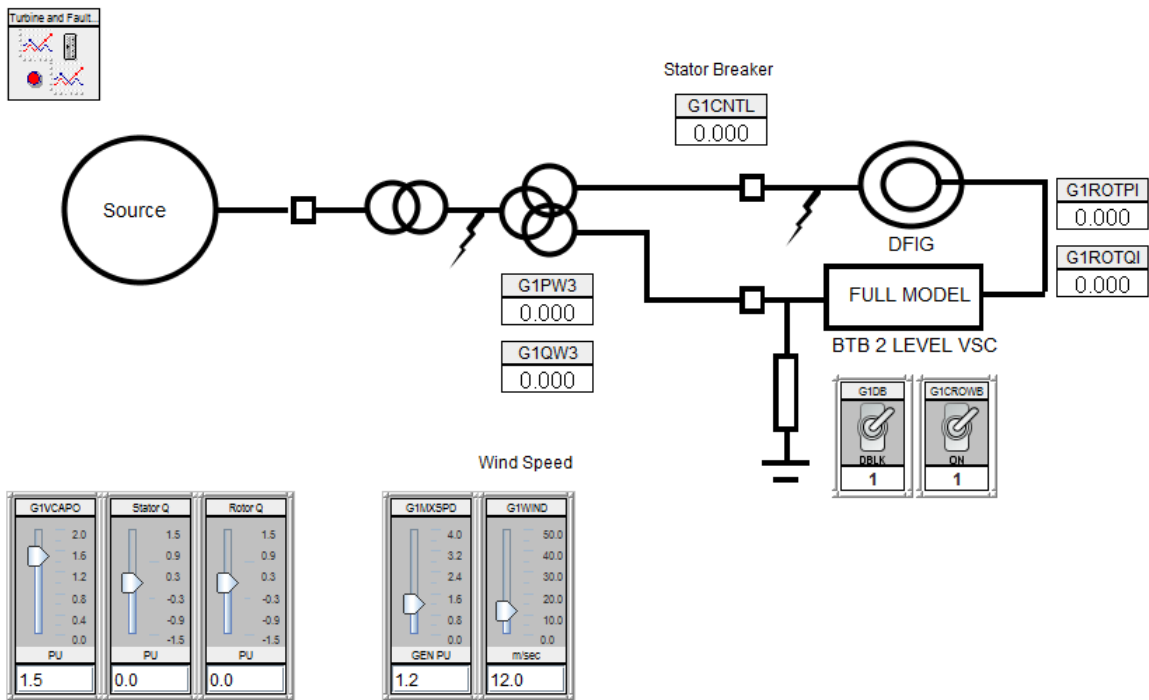


Figure C.6: Wind system sub-block.

6. Power generation plot: following the same updating policy explained in the first item of this enumeration, it accounts for the power contribution of the different generators within the microgrid: wind turbine, diesel generator, PV system, battery and the power grid. Figures 6.2, 6.3, 6.5, 6.7, 6.8, 6.9, 6.10 and 6.12 from the Simulations chapter have been obtained from this tool.
7. Loads: in order to set the active and reactive power requirements of the loads within the system, different sliders are made available for the user.



Figure C.7: Loads' P and Q sliders.

As a final remark for this section, it must be noted that the island mode / re-connection to grid functionalities of the model will not be revised. This is due to the fact that chapter 6 includes a subsection 6.2 which deals in great detail with this issue.

C.3. Simulations

Based on the different opportunities to influence the model offered in the previous section C.2, it is clear that the user can start the simulation and then modify different values in order to achieve desired scenarios. Each modification / general-refresh triggered by the user will update the different plots of the RunTime canvas. This can make the simulation process longer than necessary, and this section will deal with the opportunity of achieving different modelling conditions with pre-defined sequences or by automating the triggering of actions.

Draft simulation block

To that end, we must make use of the opportunities that the Draft module offers regarding the automation of simulation procedures. Along those lines, a block under the name of "Simulation" has been introduced in the Draft model, and it can be seen in figure 5.1. The internal circuitry can be divided in four different strategies, that will be displayed and explained hereafter.

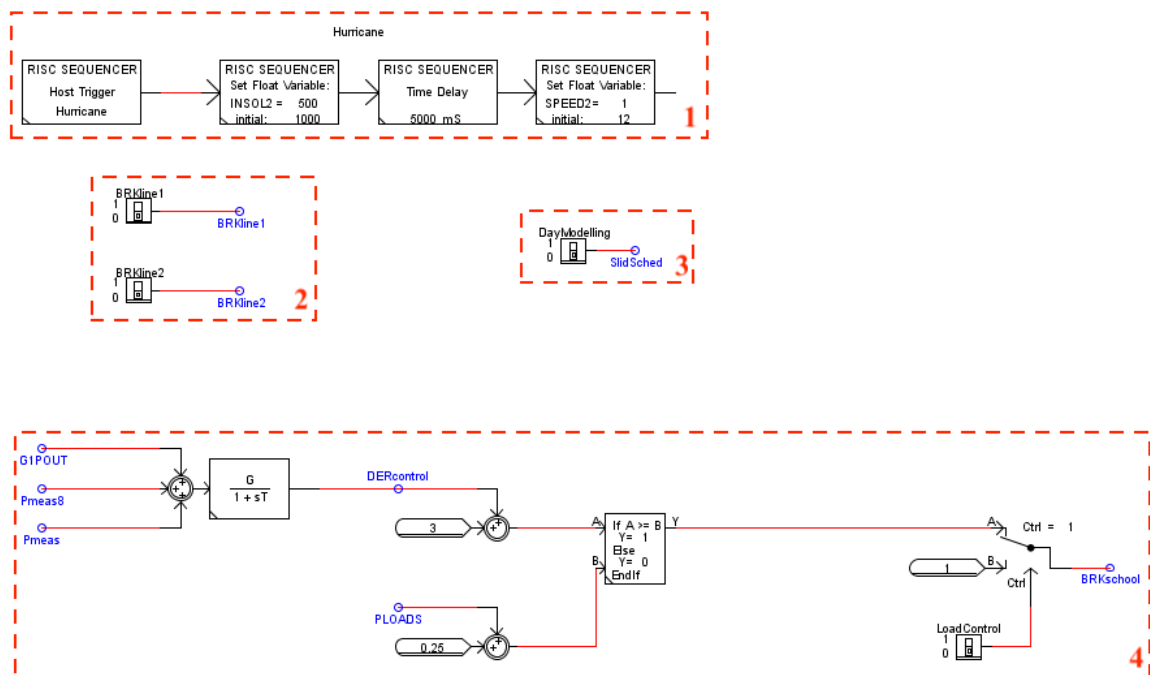


Figure C.8: Simulation block in the Draft module.

Again, an enumeration of the different features will be used so that every possibility is explained. These four different simulation techniques of figure C.8 are closely related to the RunTime canvas. In order to make that relation clear, the numbers assigned to each one of them will be written near the blocks implementing these functionalities in the GUI.

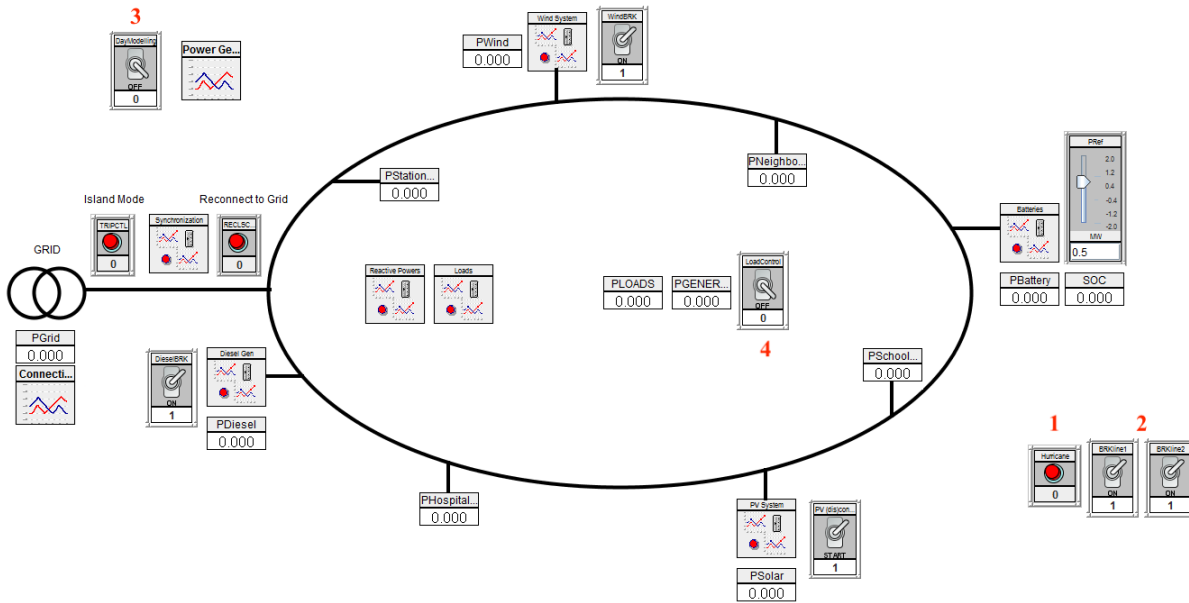


Figure C.9: Simulation block in the RunTime module.

1. Sequencer: upon triggering the push-button under number 1 of figure C.9, three concatenated events (the number can be indefinitely extended) are performed. First, the irradiance goes from 1000 to 500 W/m^2 , simulating the appearance of clouds. Then, a time delay of 5 seconds is applied and the wind speed drops to 1, simulating the wind-turbine stopping its functioning (for instance, upon facing winds over the cut-out speed). This sequencer block is really versatile, as it allows the representation of a wide variety of events: trigger, cross, delay, brk, fault, init or var (figure C.10).

CONFIGURATION		SET VARIABLE			
Name	Description	Value	Unit	Min	Max
type	Sequencer component type	Var			
Proc	Processor	Trigger		1	
Pri	Priority Level	Cross		1	
		Delay			
		Brk			
		Fault			
		Init			
		Var			

Figure C.10: Sequencer block component types.

2. Transmission lines failure: by making use of the switches shown in figure C.9 under the number 2, we trigger the signals BRKline1 and BRKline2 of figure C.8. These signals open the two circuit breakers that can be observed in figure 5.5 between the wind system-neighborhood and between the hospital-PV system. By making use of both of these circuit breakers, the situations simulated in section 6.3.2 would be achieved.
3. Daily Modelling: the switch under number 3 triggers a daily-modelling simulation, which makes use of schedulers for the battery, the wind and the PV system. These schedulers take values

from three different .txt files, and feed them to the corresponding DER references every chosen unit of time (second, minute or hour). The circuitry implemented in order to achieve this can be found in figure C.11.

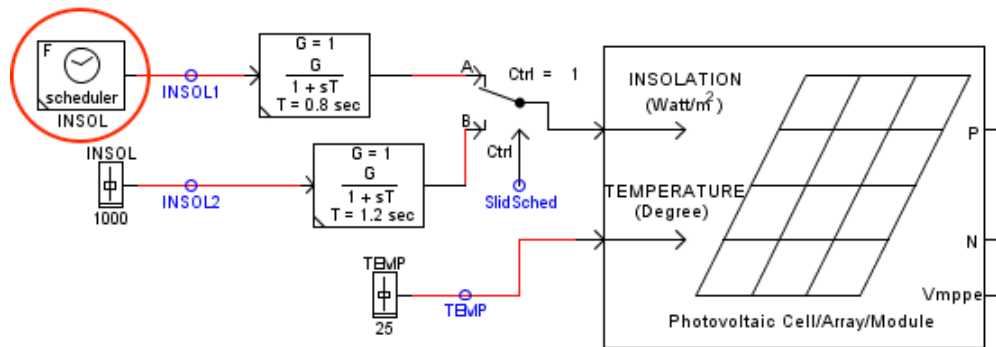


Figure C.11: Scheduler implementation in the PV system.

The user can decide which values to feed to the model by simply modifying these .txt files, that are included in the project under the names: INSOL, WINDSPEED and BATT.

4. Load-shedding: a simple load-shedding strategy has been implemented in the draft circuitry with the logic shown in the square number 4 of figure C.8. The user can choose if the school load is subject of disconnection upon facing critical situations by means of the switch under the name of "LoadControl".

And with these four simulation techniques we conclude the user manual of our microgrid model. It must be noted that these explanations represent the basic features that can be made use of when performing simulations. By combining them, we can achieve high-complexity scenarios, accounting for a great variety of possibilities.

Bibliography

- [1] S. G. I. G. Program, *Smart Grid Investments Improve Grid Reliability, Resilience and Storm Responses*, Tech. Rep. (US Department of Energy, 2014).
- [2] *Energy transition outlook* (DNV GL, 2017).
- [3] N. Phuangpornpitak and S. Tia, *Opportunities and challenges of integrating renewable energy in smart grid system*, *Energy Procedia* **34**, 282 (2013).
- [4] C. W. Potter, A. Archambault, and K. Westrick, *Building a smarter smart grid through better renewable energy information*, in *Power Systems Conference and Exposition, 2009. PSCE'09. IEEE/PES (IEEE, 2009)* pp. 1–5.
- [5] F. Mwasilu, J. J. Justo, E.-K. Kim, T. D. Do, and J.-W. Jung, *Electric vehicles and smart grid interaction: A review on vehicle to grid and renewable energy sources integration*, *Renewable and Sustainable Energy Reviews* **34**, 501 (2014).
- [6] F. Sissine, *Energy independence and security act of 2007: a summary of major provisions*, (Library of Congress Washington DC Congressional Research Service, 2007).
- [7] K. Moslehi and R. Kumar, *A reliability perspective of the smart grid*, *IEEE Transactions on Smart Grid* **1**, 57 (2010).
- [8] L. E. T. Stephen M. Folga, Michael R. McLamore and A. M. Tompkins, *National Electricity Emergency Response Capabilities*, Tech. Rep. (Argonne National Laboratory, 2016).
- [9] W. House, *Economic benefits of increasing electric grid resilience to weather outages*, Washington, DC: Executive Office of the President (2013).
- [10] R. Manual, *Rtds technologies*, Winnipeg, Manitoba, Canada (2009).
- [11] C. Schwaegerl and L. Tao, *Microgrids: Architectures and Control*, edited by N. Hatziaargyriou (John Wiley and Sons Ltd. online, 2013).
- [12] D. T. Ton and M. A. Smith, *The U.S. department of energy's microgrid initiative*, *The Electricity Journal* (2012).
- [13] C. Cecati, G. Mokryani, A. Piccolo, and P. Siano, *An overview on the smart grid concept*, in *IECON 2010-36th Annual Conference on IEEE Industrial Electronics Society (IEEE, 2010)* pp. 3322–3327.
- [14] E. SmartGrids, *Strategic deployment document for europe's electricity networks of the future*, European Technology Platform SmartGrids. Brussels (2008).
- [15] H. Farhangi, *The path of the smart grid*, *IEEE power and energy magazine* **8** (2010).
- [16] N. Liu, J. Chen, L. Zhu, J. Zhang, and Y. He, *A key management scheme for secure communications of advanced metering infrastructure in smart grid*, *IEEE Transactions on Industrial Electronics* **60**, 4746 (2013).
- [17] *New Oxford American Dictionary* (Oxford University Press, USA, 2010).
- [18] *ISO 31000. Risk Management* (International Organization for Standardization, 2009).
- [19] P. Hines, J. Veneman, and B. Tivnan, *Smart grid: Reliability, security, and resiliency*, (2014).
- [20] M. N. Albasrawi, N. Jarus, K. A. Joshi, and S. S. Sarvestani, *Analysis of reliability and resilience for smart grids*, in *Computer Software and Applications Conference (COMPSAC), 2014 IEEE 38th Annual (IEEE, 2014)* pp. 529–534.

- [21] H. F. Lipson and D. A. Fisher, *Survivability—a new technical and business perspective on security*, in *Proceedings of the 1999 workshop on New security paradigms* (ACM, 1999) pp. 33–39.
- [22] H. Goldman, R. McQuaid, and J. Picciotto, *Cyber resilience for mission assurance*, in *Technologies for Homeland Security (HST), 2011 IEEE International Conference on* (IEEE, 2011) pp. 236–241.
- [23] S. Grijalva and M. U. Tariq, *Prosumer-based smart grid architecture enables a flat, sustainable electricity industry*, in *Innovative Smart Grid Technologies (ISGT), 2011 IEEE PES* (IEEE, 2011) pp. 1–6.
- [24] Z. Li, M. Shahidehpour, F. Aminifar, A. Alabdulwahab, and Y. Al-Turki, *Networked microgrids for enhancing the power system resilience*, *Proceedings of the IEEE* (2017).
- [25] A. Nocoń and S. Paszek, *Transient states and island mode operation of industrial electricity networks*, in *Selected Issues of Electrical Engineering and Electronics (WZEE), 2016 13th* (IEEE, 2016) pp. 1–6.
- [26] A. Gholami, F. Aminifar, and M. Shahidehpour, *Front lines against the darkness: Enhancing the resilience of the electricity grid through microgrid facilities*, *IEEE Electrification Magazine* **4**, 18 (2016).
- [27] C. Abbey, D. Cornforth, N. Hatziaargyriou, K. Hirose, A. Kwasinski, E. Kyriakides, G. Platt, L. Reyes, and S. Suryanarayanan, *Powering through the storm: Microgrids operation for more efficient disaster recovery*, *IEEE power and energy magazine* **12**, 67 (2014).
- [28] [Case Study - White Oak Microgrid](#), Tech. Rep. (Honeywell Microgrid and Enabling Technologies, 2013).
- [29] K. Hirose, J. Reilly, and H. Irie, *The sendai microgrid operational experience in the aftermath of the tohoku earthquake: a case study*, *New Energy and Industrial Technology Development Organization* **308** (2013).
- [30] V. R. Yerravalli and A. Tharigonda, *High availability cluster failover mechanism using artificial neural networks*, in *Cloud Computing in Emerging Markets (CCEM), 2015 IEEE International Conference on* (IEEE, 2015) pp. 81–84.
- [31] E. Sortomme, S. Venkata, and J. Mitra, *Microgrid protection using communication-assisted digital relays*, *IEEE Transactions on Power Delivery* **25**, 2789 (2010).
- [32] J. P. Lopes, C. Moreira, and A. G. Madureira, *Defining control strategies for microgrids islanded operation*, *IEEE Transactions on power systems* **21**, 916 (2006).
- [33] J.-Y. Kim, J.-H. Jeon, S.-K. Kim, C. Cho, J. H. Park, H.-M. Kim, and K.-Y. Nam, *Cooperative control strategy of energy storage system and microsourses for stabilizing the microgrid during islanded operation*, *IEEE Transactions on Power Electronics* **25**, 3037 (2010).
- [34] J. M. Guerrero, J. C. Vasquez, J. Matas, M. Castilla, and L. G. de Vicuna, *Control strategy for flexible microgrid based on parallel line-interactive ups systems*, *IEEE Transactions on Industrial Electronics* **56**, 726 (2009).
- [35] L. Che, X. Zhang, M. Shahidehpour, A. Alabdulwahab, and Y. Al-Turki, *Optimal planning of loop-based microgrid topology*, *IEEE Transactions on Smart Grid* **8**, 1771 (2017).
- [36] A. Prasai, Y. Du, A. Paquette, E. Buck, R. Harley, and D. Divan, *Protection of meshed microgrids with communication overlay*, in *Energy Conversion Congress and Exposition (ECCE), 2010 IEEE* (IEEE, 2010) pp. 64–71.
- [37] S. S. Paulo Alexandre Regis, *Distributed split-path routing strategy for multi-hop mesh networks*, (2017).
- [38] K. P. Vijayaragavan, *Feasibility of DC Microgrids for Rural Electrification*, Master's thesis, European Solar Engineering School (2017).

- [39] L. Che, M. Shahidehpour, A. Alabdulwahab, and Y. Al-Turki, *Hierarchical coordination of a community microgrid with ac and dc microgrids*, IEEE Transactions on smart grid **6**, 3042 (2015).
- [40] P. Siano, *Demand response and smart grids—a survey*, Renewable and Sustainable Energy Reviews **30**, 461 (2014).
- [41] J. Zhou, R. Q. Hu, and Y. Qian, *Scalable distributed communication architectures to support advanced metering infrastructure in smart grid*, IEEE Transactions on Parallel and Distributed Systems **23**, 1632 (2012).
- [42] Z. Wang and J. Wang, *Self-healing resilient distribution systems based on sectionalization into microgrids*, IEEE Transactions on Power Systems **30**, 3139 (2015).
- [43] *Distribution automation, results from the smart grid investment grant program*, Tech. Rep. (US Department of Energy, 2016).
- [44] [Tennet corporate website - tennet](#), (2018).
- [45] P. IEA-PVPS, *Report snapshot of global pv 1992-2014*, Report IEA-PVPS T1-26 (2015).
- [46] *ALLMAXm Plus, framed 60cell module*, Trina Solar (2018).
- [47] M. Chen and G. A. Rincon-Mora, *Accurate electrical battery model capable of predicting runtime and iv performance*, IEEE transactions on energy conversion **21**, 504 (2006).
- [48] *Polymer Lithium Ion Battery (PL-383562)*, Tech. Rep. (TCL Hyperpower Batteries Inc, 2003).
- [49] K. S. Ng, C.-S. Moo, Y.-P. Chen, and Y.-C. Hsieh, *Enhanced coulomb counting method for estimating state-of-charge and state-of-health of lithium-ion batteries*, Applied energy **86**, 1506 (2009).
- [50] L. Xu and P. Cartwright, *Direct active and reactive power control of dfig for wind energy generation*, IEEE Transactions on energy conversion **21**, 750 (2006).
- [51] D. Meulenbroeks, *Aluminum versus Copper Conductors*, Tech. Rep. (Siemens, 2014).
- [52] C. Spanish Industry and T. Ministry, *Royal decree 223/08, "regulation on technical conditions and safety guarantees in high voltage power lines and their complementary technical instructions itc-lat 01 to 09."*, (19th March 2008).
- [53] *Complementary technical instruction ITC-LAT 06*, Spanish Industry, Tourism and Commerce Ministry (2008).
- [54] *UNE 21144. "Electrical cables: calculation of admissible current"*, Tech. Rep. (AENOR, 1997).
- [55] E. Csanyi, *Characteristics of XLPE insulated cables*, Tech. Rep. (Electrical Engineering Portal (EEP), 2014).
- [56] S. Science and T. Ministry, *Technical guide of application of the low voltage regulation (royal decree 842/2002)*, 2nd ed. (Thomson Paraninfo, 2009).
- [57] *Real time digital simulation for the power industry*, RTDS technologies (2018).